UNIVERSITÉ DU QUÉBEC À MONTRÉAL

DYNAMIQUE GLACIAIRE ET GÉOCHRONOLOGIE DU SECTEUR LABRADOR DE L'INLANDSIS LAURENTIDIEN ET ÉVOLUTION DU LAC NASKAUPI AU COURS DE LA DERNIÈRE DÉGLACIATION

THÈSE

PRÉSENTÉE

COMME EXIGENCE PARTIELLE

DU DOCTORAT EN SCIENCES DE LA TERRE ET DE L'ATMOSPHÈRE

PAR

HUGO DUBÉ-LOUBERT

JUIN 2019

REMERCIEMENTS

J'ai longtemps et souvent pensé à l'écriture des remerciements de cette thèse comme d'une lointaine et inaccessible étape. M'y voici...

Mes premiers mots seront bien évidemment dirigés vers Martin Roy, directeur de ce projet de doctorat. Après maintenant près de 10 ans de collaboration, à travers maîtrise et projet de thèse, campagnes de terrain parfois précaires, des basses terres de la baie James à celles de l'Ungava, ton rôle a transcendé celui de professeur pour devenir également un ami. Je n'aurais jamais entrepris l'aventure doctorale avec une autre personne et devant ta disponibilité et ton dévouement dans la réalisation de cette thèse, je ne peux que simplement et sincèrement te remercier.

Je me dois aussi de souligner et remercier la participation de Mme Isabelle McMartin, M. Robert-André Daigneault et M. Michel Allard en tant que jury de cette thèse. Un merci particulier à Joerg Schaefer pour la réalisation des analyses cosmogéniques ainsi qu'à Peter U. Clark pour les discussions et commentaires dans l'interprétation et la rédaction de certains aspects de cette thèse.

Je m'en voudrais de ne pas témoigner ma reconnaissance à Patrice Roy qui m'a ouvert les portes du Bureau de la Connaissance Géoscientifique du Québec à Val-d'Or et qui a permis que je réalise ce projet d'étude en parallèle de mon boulot de géologue. Ce projet n'aurait pu se réaliser sans le soutien logistique et financier du Ministère de l'Énergie et des Ressources naturelles à qui je suis grandement redevable. L'aboutissement de ce projet et mon aventure abitibienne laisseront des marques inaltérables sur la personne que je suis. Un clin d'œil à tous mes amis, collègues quaternaristes et géologues du MERN qui, de différentes façons, ont contribué de près ou de loin à ce projet. Aux gens de l'UQAM, croisés au détour d'un cours, d'une excursion, d'une pinte ou d'un ièneme café; merci pour tout!

Ce projet de doctorat comportait un important volet de terrain au cœur du Nunavik, région à la fois hostile et d'une hypnotisante beauté, vulnérable et figée dans le temps. J'y ai séjourné à plusieurs reprises dans le cadre de ce projet entre 2012 et 2015 pour un séjour équivalent à plus d'une année. Il est difficile, pour ne pas dire impossible, de traduire en quelques mots les innombrables souvenirs qu'ils me restent de la vallée de la George, de la vie en camp isolé et des gens croisés. Ils prennent la forme de moments singuliers, de paysages rudes et grandioses et de découvertes grisantes. C'est une chance inouïe que d'avoir pu travailler et étudier sur et en ces lieux. J'ai une profonde admiration pour les pionniers ayant parcouru et investigué ce territoire des décennies auparavant, et ce dans des conditions parfois extrêmes. Nos travaux ne sont souvent qu'une humble extension de ce qui précède ou une petite pierre de plus ajoutée à l'édifice de la connaissance. À Mme Pauline et M. Jack Ives, merci pour ces échanges et ces souvenirs partagés. Je vous transmets mes sincères salutations!

À ma famille, que dire de plus sinon que je vous apprécie plus que tout et qu'il est salvateur de pouvoir compter sur des gens comme vous. Merci d'avoir été et d'être toujours là.

Finalement, au-delà de tout, « mamzelle » Beauchamp. Merci de faire partie de ma vie. Et merci surtout pour ta patience et ton appui dans mes nombreux moments de doute et de vacillement... Ceci est la fin d'une certaine étape, mais le début d'une toute nouvelle à tes côtés. À toi, qui que tu sois, vivement ta venue petite crevette!

AVANT PROPOS

La présente recherche est composée de trois articles rédigés en langue anglaise qui forment les principaux chapitres de cette thèse. Les autres sections (Introduction, Conclusion, etc.) ont été écrites en français selon les exigences de l'Université du Québec à Montréal (UQAM). Ces articles sont issus de collaborations entre chercheurs agissant à titre de coauteurs. Pour chacun des articles de la thèse, la version intiale des articles a été écrite par le candidat. L'étudiant a également été responsable des campagnes de terrain, de l'échantillonnage, de l'interprétation des résultats et des calculs subséquents. Le professeur Martin Roy (UQAM) a encadré les travaux à titre de directeur de thèse. Les analyses des données géochronologiques et cosmogéniques ont été réalisées en collaboration avec le Dr Joerg M. Schaefer du *Lamont-Doherty Earth Observatory* de l'Université Columbia à New-York ainsi qu'avec la Dr Hella Wittmann du *GFZ Laboratory* de Postdam en Allemagne. Ces chercheurs, de même que le Dr Jean Veillette de la Commission Géologique du Canada, ont contribué à la rédaction de ces manuscrits via des commentaires et suggestions. La nomination des coauteurs a respecté les règles en vigueur à l'Université du Québec à Montréal.

TABLE DES MATIÈRES

LISTE DES FIGURES

LISTE DES TABLEAUX

LISTE DES ABRÉVIATIONS ET ACRONYMES

^{10}Be et ^{26}Al	Isotopes cosmogéniques
µm	micromètre
A	« cross-sectional area of the channel (m^2)
AMOC	« Atlantic meridional overturning circulation »
asl	« Above sea level »
BCGQ	Bureau de la Connaissance Géoscientifique du Québec
cal a BP	Années calibrées avant aujourd'hui (1950)
CIA	« Chemical index of alteration »
DEM	« Digital elevation model »
Ft	« feet »
GMSL	« Global mean sea level »
GRV	« George River valley »
HF	Haute Falaise
ICP-OES	« Inductively coupled plasma optical emission spectrometry »
ICE-5G (VM2)	« Global glacial isostasy and age surface model »

IHL	« Indian House Lake »
LDEO	« Lamonth-Doherty Earth Observatory »
LIS	« Laurentide Ice Sheet »
LQ	Labrador-Québec
LSDn	« Lifton-Sato-Dunai scaling model »
MENRQ	« Ministry of Energy and Natural Resources of Quebec »
NSERC	« Natural Sciences and Engineering Research Council of Canada »
PH	« Pyramid Hills »
Q	« Discharge (m^3 s^{-1})
SNRC	Système National de référence cartographique
V	velocity (m s^{-1})
WH	« Wedge Hills »

RÉSUMÉ

Les grandes glaciations qui ont marqué la période du Quaternaire ont laissé un vaste héritage de formes de terrain et de dépôts glaciaires qui renseignent sur l'étendue et la configuration des inlandsis ayant recouvert le territoire, en plus d'enregistrer le retrait de ces calottes d'envergure continentale. La déglaciation a d'ailleurs été marqué par le développement aux marges de ces masses de glace de grands lacs glaciaires. Le drainage abrupt de ces plans d'eau s'est traduit par des décharges massives d'eau de fonte qui ont présumément perturbé la circulation océanique, causant de nombreuses fluctuations climatiques au cours de l'intervalle de temps compris entre 15 et 7 ka. L'évaluation précise de l'impact de ces apports d'eaux de fonte sur le système climatique est cependant limitée par le peu de données sur l'étendue, le volume, et la chronologie de ces lacs glaciaires. Ces incertitudes sont principalement liées au manque de connaissance sur l'évolution temporelle des patrons de retrait de la marge glaciaire, laquelle contrôlait en grande partie la configuration de ces plans d'eau.

L'empreinte géomorphologique du Secteur Labrador de l'Inlandsis laurentidien est unique, avec des assemblages singuliers de formes glaciaires qui traduisent la complexité de l'évolution de ce secteur au cours du dernier cycle glaciaire et de la déglaciation subséquente. Ces archives géomorphologiques et sédimentaires ont également enregistré le développement et l'évolution de grands lacs de barrage glaciaire qui ont occupé les principales vallées des rivières de l'Ungava. Ces lacs se sont drainés dans la Mer du Labrador, un secteur critique où se forment les masses d'eau profondes de l'Atlantique Nord et qui gouvernent la circulation thermohaline, faisant de ces plans d'eau des candidats importants pour certains forçages climatiques de la dernière déglaciation. Malgré l'importance potentielle du rôle joué par le drainage des lacs de l'Ungava dans les fluctuations climatiques holocènes, l'évolution et le

drainage de ces plans d'eau sont encore très mal documentés et contraints dans le temps. Ceci découle en partie du fait que le schéma global de la déglaciation régionale est inadéquatement connu pour cette partie de l'Inlandsis; la plupart de ces lacs étant difficiles à intégrer dans les modèles paléogéographiques existants. En effet, plusieurs questions fondamentales demeurent quant à la paléogéographie quaternaire du Nord québécois et du Labrador, notamment en ce qui a trait à la répartition spatiale et à l'âge des grands ensembles géomorphologiques, mais également par rapport à la signification d'une zone étroite arquée qui départage les grands ensembles morpho-sédimentaires de l'Ungava, et communément appelée la *Horseshoe Unconformity*.

L'objectif principal de cette thèse est de contribuer à la compréhension de l'évolution spatio-temporelle de l'un des plus importants lacs glaciaires de l'Ungava – le Lac Naskaupi – et d'intégrer le développement de ce lac, et des plans d'eau attenants, dans le schéma paléogéographique de la dernière déglaciation. Pour ce faire, une campagne exhaustive de cartographie de détails a été menée sur un vaste territoire de l'Ungava. Des mesures d'élévation sur des rivages surélevés du Lac Naskaupi ont permis de caractériser l'extension du plan d'eau, ainsi que de dénombrer les différentes phases et leurs volumes, en plus d'identifier les secteurs associés aux épisodes de vidange. Des datations cosmogéniques sur des lignes de rivage ont permis d'apporter des contraintes sur le développement et le drainage du lac et d'évaluer le rôle des plans d'eau de l'Ungava dans les changements climatiques holocènes. Finalement, le contexte du dernier cycle glaciaire et de la déglaciation ont été raffinés par un inventaire exhaustif des marques d'érosion glaciaire, par la cartographie détaillée des formes de terrain et par des datations cosmogéniques sur des constructions glaciomarines et des terrains de nature variée. L'intégration de ces données a permis de délimiter les principaux ensembles géomorphologiques en fonction de leur nature et de leur âge. Ces travaux ont également servis à documenter la séquence et la chronologie relative entre les différents écoulements glaciaires qui délimite la branche est du *Horseshoe Unconformity*. De plus, la séquence d'écoulements documentée a enregistré la migration des lignes de partage glaciaire et l'activité des courants de glace de ce secteur de l'Inlandsis laurentidien.

Les principaux résultats ont permis de montrer que :

i) le Lac Naskaupi a été caractérisé par une configuration centrée autour de deux bassins qui sont demeurés indépendants pour une bonne partie de son existence. Les nombreux rivages identifiés témoignent d'une évolution complexe marquée par au moins cinq phases majeures et des épisodes importants de drainage. La reconstruction de ce lac indique que le volume d'eau de fonte maximale se situait autour de 600 km^3. Le développement du lac et son évolution ont été en partie contrôlés par la présence de conditions de glace à base froide au cours de la déglaciation.

ii) Les âges ^{10}Be obtenus sur des rivages surélevés démontrent que le développement et le drainage du Lac Naskaupi se sont déroulés dans un court laps de temps centré autour de 8,300 ± 300 a. Conséquemment, la décharge d'eau de fonte du Lac Naskaupi a pu participer à l'événement de 8,2 ka, l'un des refroidissements le plus marqué de l'Holocène. Ces résultats soulignent du même coup le potentiel des autres lacs de l'Ungava comme mécanisme de forçages climatiques. De plus, ces données permettent de raffiner le cadre géochronologique de la déglaciation en contraignant la position d'un long flanc de la marge nord-est du Secteur Labrador.

iii) La nature et la distribution des formes glaciaires et de déglaciation suggèrent une mosaïque complexe de conditions sous-glaciaires, caractérisée par une couverture polythermale de la glace depuis le dernier maximum glaciaire jusqu'à la fin de la déglaciation. De plus, nos travaux montrent que les formes convergentes au nord du *Horseshoe Unconformity* seraient le résultat d'une succession d'événements glaciaires d'âges probablement rapprochés, mais distincts. Des âges ^{10}Be de 8,400 ± 300 sur des deltas glaciomarins nourris par des eskers montrent que l'ensemble de formes glaciaires convergeant vers la baie d'Ungava, et situé au nord-ouest de la limite du

Horseshoe Unconformity, est d'âge tardi-glaciaire. Cet ensemble découlerait de l'activité de courants de glace entre 8 et 10 ka. Ces résultats rejettent tous modèles invoquant la présence d'une masse de glace à base froide centrée sur la baie d'Ungava. Nos travaux indiquent que ce qui est communément décrit comme la limite orientale de la zone du *Horseshoe Unconformity* traduit plutôt l'activité de la ligne de partage glaciaire du Labrador au dernier maximum glaciaire dont les terrains ont été subséquemment recoupés par l'activité de courants de glace convergeant vers la baie d'Ungava. De plus, l'étroitesse de la zone de rencontre du *Horseshoe Unconformity* peut être expliquée par un modèle de capture de l'ensemble morphologique divergent de direction sud par la migration de la tête de deux courants de glace qui convergent vers la baie d'Ungava, supportant ainsi certaines reconstructions antérieures. La forme arquée du *Horseshoe* et les caractéristiques suggérant la position d'une ligne de partage glaciaire ne sont que des artefacts associés à la génération/préservation des ensembles morpho-sédimentaires à travers le temps. La position de cette limite serait plutôt contrôlée par des aspects topographiques locales, tel que la limite sud du bassin versant de la baie d'Ungava, plutôt qu'exclusivement par la configuration de la calotte glaciaire.

En somme, cette thèse apporte de nouvelles informations sur l'importance des lacs glaciaires de l'Ungava dans les changements climatiques récents reconnus pour la dernière déglaciation. De plus, les travaux de cartographie permettent en outre de raffiner la compréhension de l'architecture et de l'âge des ensembles morpho-sédimentaires du Secteur Labrador de l'Inlandsis laurentidien, contribuant ainsi à l'amélioration des cadres paléogéographiques quaternaires.

ABSTRACT

The glaciations that marked the Quaternary Period have left a vast record of landforms and glacial deposits that provide information on the extent and configuration of these continental ice masses, in addition to record the retreat of these ice sheet. Furthermore, deglaciation led to the development of glacial lakes at the margins of the decaying ice masses. The abrupt drainage of these ice-dammed lakes caused massive meltwater discharges that have presumably disrupted the ocean circulation and triggered several climatic fluctuations over the time interval of 15 to 7 ka. However, the precise impact of these meltwater forcings on the climate system is limited by the scarcity of the data on the extent, volume, and chronology of these glacial lakes. These uncertainties are mainly related to the lack of knowledge about the temporal evolution of the ice margin, which largely controlled the evolution of these lakes.

The geomorphological and sedimentary records of the Labrador Sector of the Laurentide Ice Sheet is characterized by landform-terrain assemblages that reflect a complex evolution during the last glacial cycle and subsequent deglaciation. Part of the geomorphological archives also record the development and evolution of large ice-dammed lakes that occupied the main river valleys of the Ungava lowlands. These lakes have drained into the Labrador Sea, a critical area where the North Atlantic deep-water masses that govern the thermohaline circulation are formed. Despite the potential role played by the Ungava lakes in Holocene climatic fluctuations, the evolution and drainage of the Ungava lakes are still poorly documented and constrained. This is in part due to the fact that the regional pattern of deglaciation is inadequately documented for this part of the Labrador Sector, complicating the integration of these meltwater bodies into existing paleogeographic models. Indeed, several questions remain considering the paleogeography of northern Quebec and Labrador, notably regarding

the age and significance of certain landform assemblages, such as the narrow and U-shaped area – commonly named the Horseshoe Unconformity – that separates two large morpho-sedimentary terrains of the Labrador Sector.

The main objective of this thesis is to refine the evolution of one of the most important glacial lakes in Ungava – Lake Naskaupi – and to integrate the development of this lake and adjacent meltwater bodies into the paleogeographic framework of the last deglaciation. To do this, detailed surficial mapping was conducted over a large area of the Ungava lowlands. Numerous elevation measurements of Naskaupi shorelines allowed the characterization of the maximum extension of this lake, as well as its main phases and related drainage episodes. Cosmogenic dating on shorelines constrained the development and drainage of Lake Naskaupi, thereby assessing the role of Ungava glacial lakes in Holocene climate changes. Finally, the context of the last glacial cycle and deglaciation was documented through systematic mapping of landform assemblages, including an exhaustive inventory of striations and associated erosional features, and by cosmogenic dating of glaciomarine deltas and glacial terrains of different nature. Together these data led to the delineation of the main geomorphological assemblages according to their nature, distribution and age. These results also document the ice flow sequence and relative chronology that characterized the evolution of the eastern branch of the Horseshoe Unconformity, which experienced an important ice-divide migration during the late glaciation. This sector of the Laurentide Ice Sheet was also marked by the onset of ice streams.

The main results of this thesis show that:

i) The configuration of Lake Naskaupi was characterized by two basins that evolved independently for a significant part of the deglaciation. The numerous shorelines identified document a complex evolution marked by at least five major stages and significant episodes of drainage. The reconstruction of the main lake stage shows that the maximum meltwater volume of the lake was around 600 km^3. The lake development and evolution have been partly controlled by the presence of cold-based ice conditions during deglaciation.

ii) The ^{10}Be ages obtained on raised shorelines show that the development and drainage of Lake Naskaupi took place in a short time span centered around 8,300 ± 300 a. This suggests that the meltwater discharge from Lake Naskaupi likely contributed to the freshwater forcing that caused the 8.2 ka event, one of the most significant cooling events during the Holocene. These results underline the potential role of the Ungava glacial lakes in Holocene climatic fluctuations. In addition, these data refine the geochronological framework of the last deglaciation by constraining the position of a long flank of the northeastern margin of the Labrador Sector.

iii) The nature and distribution of glacial and deglacial landforms indicate a complex mosaic of subglacial conditions, characterized by a polythermal ice cover that likely relate to the period extending from the last glacial maximum to the end of the last deglaciation. Our investigations show that the converging landform assemblage north of the Horseshoe Unconformity is the result of several distinct glacial events of slightly different ages. Cosmogenic dating of esker-fed glaciomarine deltas yielded ^{10}Be ages of 8,400 ± 300 a, indicating that the swarm of glacial landforms converging towards Ungava Bay formed during the late-glacial interval. This landform assemblage likely resulted from the activity of ice streams between 8 and 10 ka, thereby ruling out models that invokes the presence of a cold-based ice mass centered over Ungava Bay. Overall, the results indicate that what is commonly referred to as the eastern boundary of the Horseshoe Unconformity rather reflects the activity of the Labrador ice-divide during the last glacial cycle. The narrowness of the Horseshoe Unconformity can be explained by a model of capture where the southward propagation of the head of two ice streams converging towards Ungava Bay likely intersected the radially southward ice flow system. The arcuate shape of the Horseshoe boundary and its ice-divide appearance is thus an artefact of the generation/preservation of this landsystem through time. Its position is defined by local topographic specificities, such as the southern limit of the Ungava Bay catchment area, rather than by ice sheet configuration.

Overall, this thesis provides new information on the Ungava glacial lakes and their importance in climatic fluctuations of the last deglaciation. In addition, the combination of extensive mapping and field investigations with cosmogenic dating have also refined the understanding of the architecture and age of the geomorphic and sedimentary assemblages of the Labrador Sector of the Laurentide Ice Sheet, thus contributing to the improvement of paleogeographic frameworks.

INTRODUCTION

0.1 PROBLÉMATIQUE

Le Pléistocène a été marqué par la croissance et la disparition de grands glaciers continentaux ayant joué un rôle important sur le climat de cette période. Les enregistrements paléoclimatiques basés sur la géochimie des microfossiles présents dans les carottes de sédiments océaniques montrent que les cycles glaciaires et interglaciaires sont ponctués de variations climatiques abruptes (Johnsen et al, 1992; Dansgaard et al., 1993; Alley et al, 1997; Ellison et al., 2006) qui auraient été causées par des épisodes d'instabilité des inlandsis (Bond et al., 1992; Broecker, 1994; Hemming et al., 2004) et/ou par le drainage de grands lacs glaciaires (Broecker et al., 1989; Barber et al., 1999; Clark et al., 2001; Clarke et al., 2003; Carlson and Clark, 2012). En effet, ces épisodes d'effondrements et les décharges concomitantes d'icebergs, de même que des injections d'eau de fonte, auraient provoqué des ralentissements marqués de la circulation océanique Nord-Atlantique au cours du dernier cycle glaciaire (Bond et Lotti, 1995; Vidal et al., 1999; Hemming et al., 2004). La reconnaissance de ces fluctuations climatiques et la recherche de mécanismes causaux, impliquant des forçages d'origine glaciaire, a donc ouvert une toute nouvelle perspective en regard de la compréhension détaillée de la dynamique de l'Inlandsis laurentidien (Figure 0.1A), mais également sur l'ampleur et la chronologie des évènements ayant engendré ces excursions climatiques.

Plusieurs études ont récemment mis en évidence des épisodes de ralentissement marqués de la circulation océanique méridionale de l'Atlantique (AMOC) entre 15 et 7 ka, lesquels sont généralement associés à des apports massifs d'eau de fonte en provenance de la calotte laurentidienne (Clark et al., 2002; Ellison et al., 2006; Jennings et al., 2015). De ces fluctuations, l'un des refroidissements les plus marqués de l'Holocène – l'évènement de 8,2 ka d'une durée de 160 ans (Alley et al., 1997; Thomas et al., 2007) – aurait été initié par la vidange abrupte du Lac Agassiz-Ojibway (Barber et al., 1999). Bien que cet évènement représente l'un des forçages climatiques les mieux documentés, des modélisations (Renssen et al., 2002; Clarke et al., 2004) ont montré que les volumes d'eau estimés (environ 160,000 km^3; Leverington et al., 2002) ne seraient pas suffisants pour pleinement expliquer la perturbation océanique observée (Clarke et al., 2003). D'autre part, des travaux récents ont démontré que les phases tardives du Lac Agassiz-Ojibway précédant la vidange finale étaient de moindre élévation, suggérant une surestimation des volumes d'eau associés (Roy et al., 2015; Godbout et al., 2017). Les archives paléoclimatiques suggèrent également que cet évènement est associé à de multiples injections d'eau de fonte distinctes (Ellison et al., 2006; Hilaire-Marcel et al., 2008; Roy et al., 2011) plutôt qu'à un seul et unique épisode (Dyke et Prest, 1987; Thorleifson, 1996; Barber et al., 1999). L'ensemble de ces résultats renforce donc l'hypothèse selon laquelle d'autres sources d'eau de fonte sont nécessaires afin de pleinement expliquer les causes et l'amplitude de l'épisode de 8,2 ka (Clarke et al., 2004).

Au cours de la déglaciation du Secteur Labrador de l'Inlandsis laurentidien, le retrait de la marge glaciaire à contre-pente vers le nord a causé le blocage du drainage naturel des grandes rivières se jetant dans la baie d'Ungava. Cette particularité dans le retrait de la marge, combinée à la production massive d'eau de fonte, a mené à l'accumulation des eaux et conduit à la formation d'importants lacs de barrage glaciaire qui ont occupé les grandes vallées fluviatiles et dépressions attenantes (Figure 0.1B). L'évolution de ces plans d'eau – notamment leur configuration, extension, nombre de phases et durée – est intrinsèquement liée au schéma de retrait et à la configuration de la marge, eux-mêmes dépendant d'une multitude de paramètres dont les patrons/styles de retrait glaciaire, de même que la variation des conditions thermiques à la semelle du glacier.

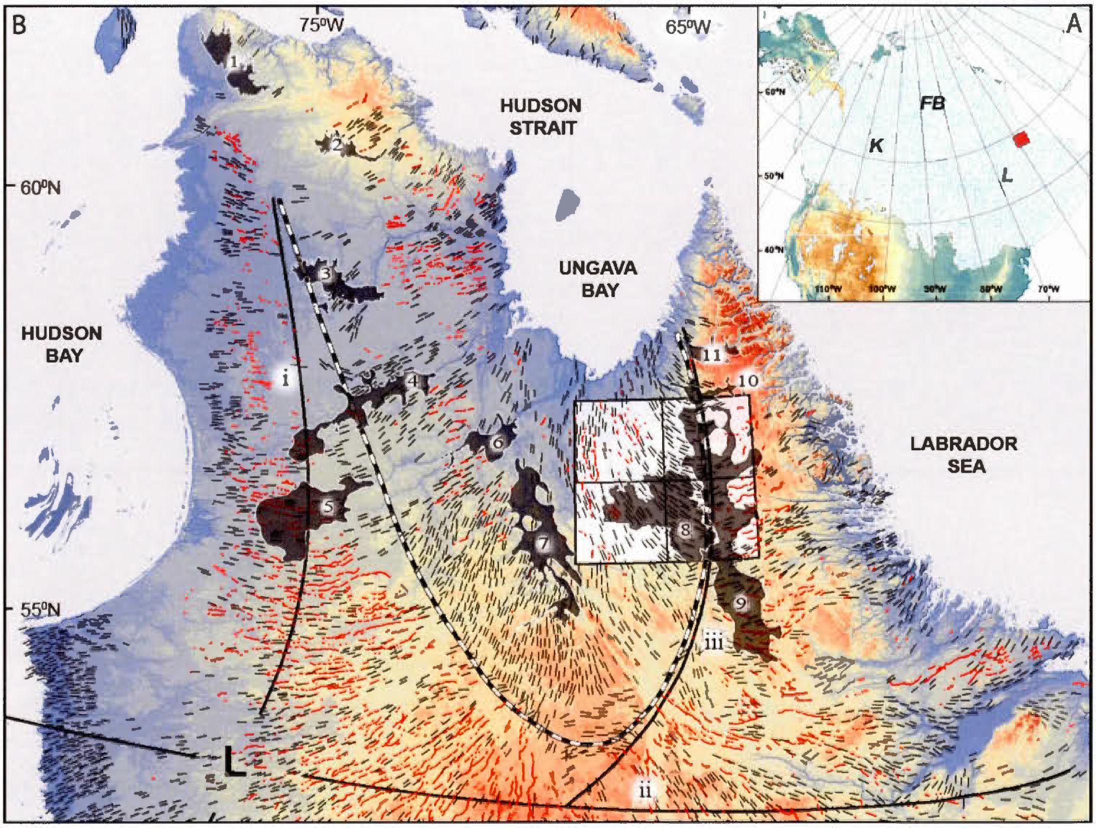

Figure 0.1 A) Représentation de la calotte laurentidienne au dernier maximum glaciaire (Dyke, 2004) et localisation des centres de dispersion : FB (Fox-Baffin), K (Keewatin) et L (Labrador). B) Localisation de la zone d'étude et contexte quaternaire du Nord québécois et du Labrador. Les lignes noires représentent les formes fuselées (Prest, 1968) et les lignes rouges, les eskers (Storrar, 2013). Localisation des lignes de partage glaciaire du Secteur Labrador (Dyke et Prest ,1987) et position présumée de la limite du *Horshoe Unconformity* (Clark et al, 2000): i) Ligne de partage de Payne; ii) Ligne de partage de Caniapiscau; iii) Ligne de partage du Labrador. Localisation des lacs de barrage glaciaire de l'Ungava (modifié de Gray et al., 1993 et Daigneault, 2008) : 1) Lacs Kovik et Frichet-Durouvray-Derville; 2)

Lac Nantais; 3) Lac Payne; 4) Lac Minto; 5) Lac à l'Eau-Claire; 6) Lac aux Mélèzes; 7) Lac Caniapiscau; 8) Lac McLean; 9) Lac Naskaupi; 10) Lac Ford; 11) Lac Koroc.

Mis à part les données préliminaires découlant des travaux réalisés par les pionniers de la géologie glaciaire au Canada (Ives, 1959; Ives, 1960, Matthew, 1961A et 1961B; Barnett, 1963; Barnet, 1967; Barnet et Peterson, 1964) et des travaux plus récents dans le nord de la péninsule de l'Ungava (Daigneault, 2008), peu d'informations existent sur l'évolution détaillée et la chronologie de ces lacs, limitant ainsi l'évaluation du rôle joué par la contribution en eau de fonte de ces plans d'eau dans les excursions climatiques de l'Holocène (Ellison et al., 2006; Thornalley et al., 2011; Jennings et al., 2015). Ceci est en grande partie relié au manque de connaissance sur le patron détaillé du retrait glaciaire et sur les conditions sous-glaciaires qui régissaient le recul des masses de glace résiduelles de ce secteur.

Depuis les premiers travaux ayant mené à la publication de la carte glaciaire du Canada (Hughes, 1964; Prest et al., 1968), la répartition des formes glaciaires et des eskers ont permis d'identifier les secteurs à partir desquels la glace s'est écoulée radialement depuis un centre de dispersion. Les reconstructions ont depuis lors montré une configuration de l'Inlandsis laurentidien centrée autour de l'activité de trois grands centres de dispersions : le centre de Fox-Baffin, le centre du Keewatin et le centre du Labrador (Figure 0.1A). De ces trois centres, le Secteur Labrador fut un des plus dynamiques au cours du dernier cycle glaciaire, avec d'importantes migrations de ces centres de masse et lignes de partage glaciaire (Boulton et Clark, 1990, Veillette et al., 1999). Cette évolution et le caractère dynamique de ce secteur se reflètent dans l'architecture complexe des enregistrements géomorphologiques et sédimentaires qui montrent deux principaux systèmes d'écoulement glaciaire aux directions opposées (Prest et al, 1968). Le principal ensemble géomorphologique est caractérisé par une orientation divergente des formes glaciaires (crag-and-tails, drumlins, moraines de Rogen, formes fuselées) témoignant d'un écoulement orienté globalement vers le sud.

À l'intérieur de cet ensemble, les eskers indiquent un retrait de la marge glaciaire du sud vers le nord jusqu'à proximité de la position tardive présumée de la ligne de partage glaciaire du Secteur Labrador. Au nord de cette position, cet ensemble est abruptement tronqué par un important système convergent vers la baie d'Ungava (Figure 0.1B). Les formes glaciaires (formes fuselées, drumlins, moraines de Rogen) de ce regroupement témoignent d'un écoulement de la glace vers la baie d'Ungava. Les eskers et autres formes de déglaciation témoigneraient d'un patron de retrait de la marge du nord vers le sud. La rencontre de ces deux systèmes est marquée par une étroite zone arquée en forme de fer à cheval, connu sous l'appellation du *Horseshoe Unconformity* (Figure 0.1B). Les reconstructions disponibles pour ce secteur donnent un aperçu global de la géométrie de ces ensembles, de même que pour les patrons de retrait de la marge glaciaire (Dyke et Prest, 1987; Clark et al, 2000; Dyke et al., 2003; Dyke, 2004; Daigneault et Bouchard, 2004; Kleman et al., 2010). Des questions fondamentales demeurent néanmoins quant à la signification glaciodynamique de cette zone et à l'âge des assemblages géomorphologiques la ceinturant, ce qui limite notre compréhension de l'évolution du Secteur Labrador au cours du dernier cycle glaciaire. De plus, la configuration étroite de la zone du *Horseshoe Unconformity*, ainsi que certaines relations de recoupements entre des formes glaciaires, ont mené à des reconstructions paléogéographiques très contrastées (Kleman et al., 1994; Veillette et al., 1999; Clark et al., 2000; Jansson, 2003). Ceci est en partie dû au fait que certaines des reconstructions paléogéographiques disponibles demeurent limitées par l'absence névralgique de contrôle de terrain. Ce déficit de connaissance dans la compréhension de la dynamique glaciaire du Secteur Labrador se traduit notamment par une incapacité à pleinement intégrer la présence des lacs de l'Ungava dans les reconstructions paléogéographiques.

Finalement, une lacune importante dans la compréhension de l'évolution de l'Inlandsis laurentidien, et plus spécifiquement de la partie nord-est du Secteur Labrador, réside dans le manque de contraintes géochronologiques absolues pour certaines régions clefs. En effet, au-delà des territoires envahis par les mers postglaciaires, la rareté du matériel organique complique grandement l'utilisation des méthodes plus traditionnelles de datation telles que celle basée sur le radiocarbone (^{14}C). Le développement et l'application de méthodes novatrices, par exemple la datation par isotopes cosmogéniques ou la datation par luminescence optique, permettent d'entrevoir des avancées substantielles dans la compréhension des évènements ayant marqué l'histoire des régions englacées. La résolution de plusieurs des questions fondamentales portant sur le Secteur Labrador, mais également sur l'importance paléoclimatique des lacs de l'Ungava, passe donc impérativement par l'apport de nouvelles données chronologiques.

0.2 OBJECTIFS

Les pincipaux objectifs de cette thèse se divisent ainsi :

i) reconstruire la paléogéographie et intégrer l'évolution du Lac Naskaupi dans la déglaciation régionale. Évaluer les volumes d'eau piégés lors des phases principales du lac;

ii) développer une approche novatrice afin de dater les constructions littorales dans le but de contraindre l'âge et le drainage du lac Naskaupi. Évaluer à l'aide de ces données géochronologiques inédites le rôle potentiel du drainage du Lac Naskaupi comme forçage climatique durant l'Holocène. Raffiner le patron chronologique du retrait de la marge glaciaire au cours de la déglaciation;

iii) établir un modèle chrono-géomorphologique permettant d'expliquer en partie l'architecture des grands ensembles morpho-sédimentaires caractérisant la partie NE du Secteur Labrador de l'Inlandsis laurentidien. Caractériser la mosaïque de conditions sous-glaciaires régissant le retrait des masses de glace résiduelles afin de comprendre les mécanismes ayant participé au barrage des lacs glaciaires de l'est de l'Ungava (Naskaupi et McLean).

0.3 RÉGION D'ÉTUDE

La région d'étude est à cheval sur les basses terres de la baie d'Ungava et le piémont des monts Torngats (Figure 0.2). Le secteur couvre une superficie de près de 55 000 km^2 correspondant à la limite des feuillets SNRC 1 : 250 000 24G, 24H, 24A et 24B (Figure 0.2). Cette zone a occupé une position géographique privilégiée par rapport au centre de dispersion du Labrador au cours du dernier cycle glaciaire, notamment en raison du fait qu'elle est située à proximité de la ligne de partage glaciaire du Labrador et, d'autre part, qu'elle se trouve à quelques centaines de kilomètres à l'est du lieu de la fonte finale de l'inlandsis à l'Holocène (Allard et al., 1989). Cette région permet aussi l'étude des linéaments glaciaires et eskers associés à l'ensemble convergeant vers la baie d'Ungava, en plus de comprendre les étendues glaciolacustres associées à l'évolution et à la vidange des lacs glaciaires McLean et Naskaupi. La physiographie régionale est constituée des basses terres de la baie d'Ungava qui forment une grande dépression inclinée vers le nord-ouest, ceinturée par deux massifs topographiques : la Fosse du Labrador à l'ouest et la chaîne des Torngats à l'est. (ww.mddelcc.gouv.qc.ca/biodiversite/aires_protegees).

La région d'étude est parcourue par d'importantes rivières s'écoulant vers la baie d'Ungava dont: la rivière à la Baleine, la rivière Qurlutuq, la rivière Tunulic et la rivière George (Figure 0.2). Les rivières à la Baleine et George sont séparées entre elles par une zone d'interfluve marquée par le batholite de De Pas (Figure 0.2). La partie amont de la rivière à la Baleine est légèrement encaissée tandis qu'elle s'écoule, dans sa partie avale, dans une plaine argileuse. La rivière George est très encaissée sur la plus grande partie de son cours jusqu'à la confluence avec la rivière De Pas. En amont de cette zone, la rivière George coule dans une plaine peu accidentée.

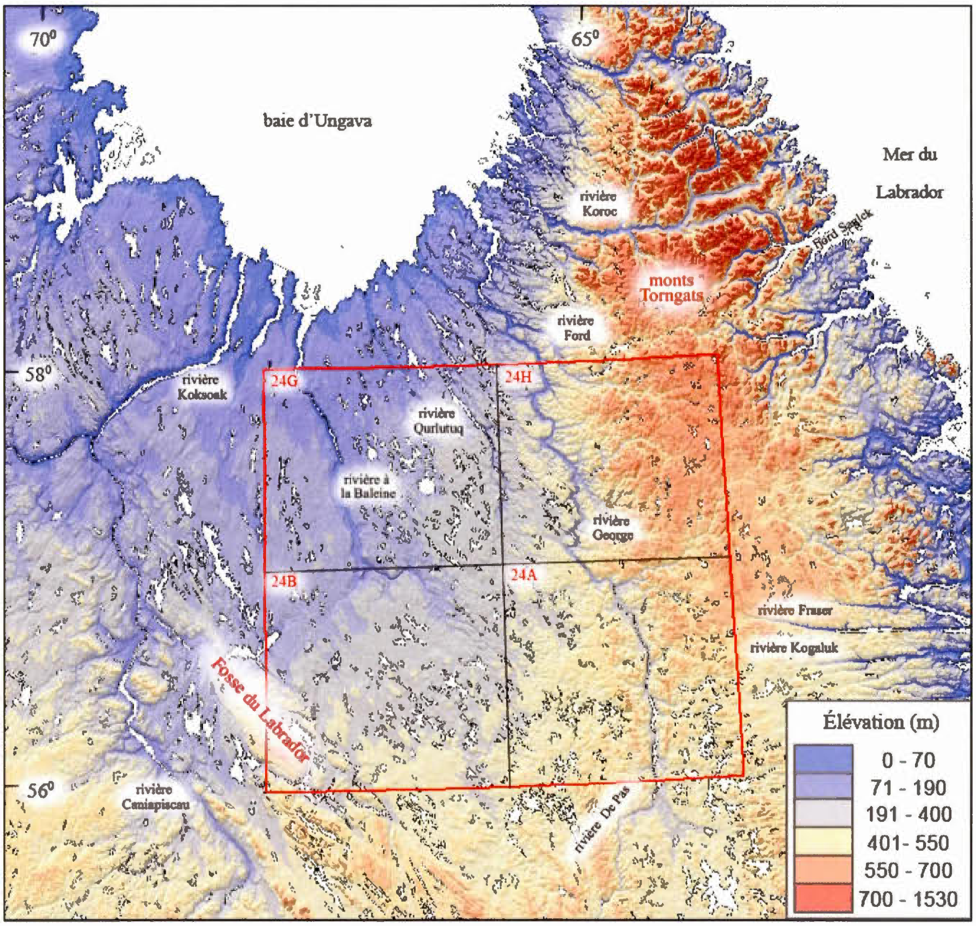

Figure 0.2 Modèle d'élévation (CDEM; résolution de 12 m) numérique montrant la physiographie des basses terres de la baie d'Ungava et les principaux éléments géographiques du secteur à l'étude. Les limites de la zone d'étude sont également représentées.

0.4 MÉTHODOLOGIE

0.4.1 Cartographie des formations superficielles et de la géomorphologie

Les données cartographiques de terrain présentées dans cette thèse ont été obtenues lors des campagnes menées au cours des étés 2012 à 2015 dans le cadre d'un programme d'envergure de cartographie du Ministère de l'Énergie et des Ressources naturelles. Préalablement aux visites sur le terrain, la cartographie systématique des différents ensembles morphologiques et sédimentaires a été réalisée à l'aide de photographies aériennes monochromes (échelle 1 : 40 000 et 1 : 60 000), ainsi qu'à partir d'images satellitaires *Rapideye* de haute résolution (5m). Cette cartographie préliminaire a permis l'identification des secteurs clefs pour la reconstruction de l'évolution du Lac Naskaupi (lignes de rivage, deltas, constructions de drainage, etc.) dont l'élévation et les grandes caractéristiques ont pu être par la suite mesurées et décrites sur le terrain. À l'aide de modèle d'élévation numérique de haute résolution (CDEM; résolution de 12 m), l'analyse ultérieure de ces données a servi en autres choses à reconstruire la configuration des phases majeures du Lac Naskaupi et d'identifier ses principales voies de drainage. De plus, la cartographie des formes glaciaires et de déglaciation a servi à délimiter et circonscrire les grands ensembles morphologiques en fonction de leurs caractéristiques communes (type de forme, orientation, caractéristique sédimentologique, etc.), de leur âge relatif et de leur mode de genèse. Les détails des méthodologies employées sont présentés aux chapitres I, II, III.

0.4.2 Reconstruction de la séquence des écoulements glaciaires

La séquence d'écoulements glaciaires ainsi que la chronologie relative entre les différents mouvements ont été établies par un inventaire exhaustif des marques d'érosion (stries, cannelures, fractures de broutage, etc.) et des relations de recoupement entre les différentes familles d'écoulements glaciaires. Les évidences de mouvements plus anciens ont été répertoriées sur les faces protégées où des modelés glaciaires antérieurs au mouvement récent ont été préservés. Les mesures ont été par la suite comparées avec l'orientation des formes macroscopiques (formes fuselées, *crag-and-tail*, drumlins, etc.), colligées lors de la cartographie et l'analyse des images satellitaire, afin de décrire la séquence d'évènements ayant ponctué l'histoire glaciaire de cette partie du Secteur Labrador.

0.4.3 Géochronologie et analyse combinée d'isotopes cosmogéniques

Plusieurs échantillons ont été soumis à des datations par isotopes cosmogéniques (^{10}Be) afin de contraindre le cadre chronologique du Secteur Labrador de l'Inlandsis laurentidien et de les comparer avec les données géochronologiques existantes, mises à jour pour la région. Vingt blocs formant des lignes de rivage et une surface d'affleurement rocheux ont été échantillonnés afin de contraindre l'évolution et le drainage du Lac Naskaupi. Neuf blocs provenant de deux deltas de contact de glace mis en place dans la Mer d'Iberville ont aussi été échantillonnés afin d'obtenir une limite chronologique inférieure sur les évènements marquants la déglaciation du secteur. Finalement, une étude comparative de zones montrant des conditions sous-glaciaires contrastées a été réalisée à l'aide de l'analyse combinée d'isotopes cosmogéniques (^{26}Al et ^{10}Be), permettant ainsi de documenter l'historique d'exposition, la durée d'enfouissement et/ou l'importance des processus d'érosion auxquels ont pu être soumis ces terrains (Granger and Muzikar, 2001; Nishiizumi et al., 1989, Corbet et al., 2013).

Cette thèse se divise en 5 sections comprenant une introduction générale, trois chapitres rédigés sous format d'article scientifique et un sommaire des contributions comme conclusion. Le premier chapitre décrit le développement, l'évolution et le drainage du Lac Naskaupi au cours de la dernière déglaciation. Le deuxième chapitre aborde l'application de la datation cosmogénique afin d'obtenir des contraintes géochronologiques sur l'existence de ce plan d'eau et sur son drainage. Le troisième chapitre traite de la dynamique glaciaire du Secteur Labrador et de la problématique relative à la signification de la zone du Horseshoe Unconformity. La thèse se termine par une conclusion mettant en relief les contributions et retombées pour les domaines de recherche concernés, en plus d'une ouverture vers d'éventuels axes de recherche pour des travaux futurs.

0.5 BIBLIOGRAPHIE

Allard, M., Fournier, A., Gahé, E., Séguin, M.K. 1989. Le Quaternaire de la côte sud-est de la baie d'Ungava, Québec nordique. Géographie physique et Quaternaire 43: 325–336.

Alley, R.B., Mayewski, P.A., Sowers, T., Stuiver, M., Taylor, K.C., Clark, P.U. 1997. Holocene climatic instability: a prominent, widespread event 8200 yr ago. Geology 25, 483-486.

Barber, D.C., Dyke, A., Hillaire-Marcel, C., Jennings, A.E., Andrews, J.T., Kerwin, M.W., Bilodeau, G., McNeely, R., Southon, J., Morehead, M.D., Gagnon, J.-M., 1999. Forcing of the cold event of 8200 years ago by catastrophic drainage of Laurentide lakes. Nature 400, 344-348.

Barnett, D.M. 1963. Former pro-glacial lake shorelines as indicators of the pattern of deglaciation of the Labrador/Ungava Peninsula. McGill Sub-Arctic Res. Pap. 15, 23-33.

Barnett, D.M. 1967. Glacial Lake MacLean and its relationship with glacial Lake Naskaupi. Geogr. Bull. 9, 96-101.

Barnett, D.M., Peterson, J.A. 1964. The significance of glacial Lake Naskaupi 2 in the deglaciation of Labrador Ungava. Can. Geogr. 8, 173-181.

Bond, G.C., Heinrich, H., Broecker W., Labeyrie, L., McManus, J., Andrews J., Huon, S, Jantschik, R., Clasen, S., Simet, C., Tedesco, K., Klas, M., Bonani, G., Ivy, S. 1992. Evidence for massive discharges of icebergs into the North Atlantic Ocean during the last glacial period, Nature, 360, 245–249.

Bond, G. C., Lotti, R. 1995. Iceberg discharges into the North Atlantic on millennial time scales during the last glaciation. Science 267, 1005–1010.

Boulton, G.S., Clark, C.D. 1990. A highly mobile Laurentide ice sheet revealed by satellite images of glacial lineations. Nature 346, 813-817.

Broecker, W. S., Kennet, J.P., Flower, B.P., Teller, J.T., Trumbore, S., Bonani, G., Wolfli, W. 1989. Routing of meltwater from the Laurentide Ice Sheet during the Younger Dryas cold episode. Nature 341, 318-321.

Broecker, W. S. 1994. Massive iceberg discharges as triggers for global climate change, Nature, 372, 421–424.

Clark, P.U., Marshall, S.J., Clarke, G.K.C., Hostetler, S.W., Licciardi, J.M., and Teller, J.T. 2001. Freshwater forcing of abrupt climate change during the last glaciation: Science 293, 283-287.

Carlson A.E., Clark P.U., 2012. Ice sheet sources of sea level rise and freshwater discharge during the last deglaciation. Reviews of Geophysics 50, 1-72.

Clark, P.U., Pisias, N.G., Stocker, T.F., Weaver, A.J. 2002. The role of the thermohaline circulation in abrupt climate change. Nature 415, 863-869.

Clark, C.D., Knight, J.K., Gray, J.T. 2000. Geomorphological reconstruction of the Labrador sector of the Laurentide Ice Sheet. Quaternary Science Review 19, 1343–1366.

Clarke, G.K.C., Leverington, D.W., Teller, J.T., Dyke, A.S. 2003. Superlakes, Megafloods, and Abrupt Climate Change. Science 301, 922-923.

Clarke, G.K.C., Leverington, D.W., Teller, J.T., Dyke, A.S. 2004. Paleohydraulics of the last outburst flood from glacial Lake Agassiz and the 8200 BP cold event. Quat. Sci. Rev. 23, 389-407.

Corbett L.B., Bierman P.R., Graly J.A., Neumann T.A., Rood D.H. 2013. Constraining landscape history and glacial erosivity using paired cosmogenic nuclides in Upernavik, northwest Greenland. Geological Society of America Bulletin 125, 1539-1553.

Daigneault, R.A., Bouchard, M.A. 2004. Les écoulements et le transport glaciaires dans la partie septentrionale du Nunavik (Québec). Can. J. Earth Sci. 41, 919-938.

Daigneault, R.A. 2008. Géologie du Quaternaire du nord de la péninsule d'Ungava, Québec. Commission Géologique du Canada. Bulletin 533, 126 pages.

Dansgaard, W., Johnsen, S.J., Clausen, H.B., Dahl-Jensen, D., Gundestrup, N.S., Hammer, C.U., Hvidberg, C.S., Steffensen, J.P., Sveinbjörnsdottir, A.E., Jouzel, J., Bond, G. 1993. Evidence for general instability of past climate from a 250-kyr ice-core record. Nature 364, 218-220.

Dyke, A.S., Moore, A., Robertson, L. 2003. Deglaciation of North America. Geological Survey of Canada. Open File 1574, Ottawa.

Dyke, A.S. 2004. An outline of North American Deglaciation with emphasis on central and northern Canada. Dev. Quat. Sci. 2, 373-424.

Dyke, A.S., Prest, V.K. 1987. Late wisconsinan and Holocene retreat of the Laurentide Ice Sheet. Geogr. Physique Quaternaire 41, 237-263.

Ellison, C.R.W., Chapman, M.R., Hall, I.R. 2006. Surface and deep ocean interactions during the cold climate event 8200 years ago. Science 312, 1929-1932.

Godbout, P.M., Roy, M., Veillette, J.J., Schaefer, J.M. 2017. Surface exposure dating of Lake Agassiz-Ojibway shorelines suggests a reassessment of the volume of meltwater discharges during the late deglaciation. Quat. Res. 88, 265-276.

Granger D. E., Muzikar P. F. 2001. Dating sediment burial with in situ-produced cosmogenic nuclides: Theory, techniques, and limitations. Earth and Planetary Science Letters 188, 269-281

Gray, J., Lauriol, B., Bruneau, D., Ricard, J. 1993. Postglacial emergence of Ungava Peninsula, and its relationship to glacial history. Can. J. Earth Sci. 30, 1676-1696.

Hemming, S.R. 2004. Heinrich events: massive late pleistocene detritus layers of the north atlantic and their global climate imprint. Reviews of Geophysics 42, 1-43.

Hillaire-Marcel, C., Helie, J.-F., McKay, J., de Vernal, A. 2008. Elusive isotopic properties of deglacial meltwater spikes into the North Atlantic: example of the final drainage of Lake Agassiz. Can. J. Earth Sci. 45, 1235-1242.

Hughes, O. L. 1964. Surficial geology, Nichicun-Kaniapiscau Maparea. Geological Survey of Canada, Bulletin 106, 20 pp.

Ives, J.D. 1959. The former ice-dammed lakes and the deglaciation of the middle reaches of the George River valley. McGill Sub-Arctic Res. Pap. 6, 9-44.

Ives, J.D. 1960. Former ice-dammed lakes and the deglaciation of the middle reachesof the George River Labrador-Ungava. Geogr. Bull. 14, 44-70.

Jansson, K., Stroeven, A., Kleman, J. 2003. Configuration and timing of Ungava Bay ice streams, Labrador-Ungava, Canada. Boreas 32, 256-262.

Jennings, A., Andrews, J.T., Pearce, C., Wilson, L., Ólafsdóttir, S. 2015: Detrital carbonate peaks on the Labrador shelf, a 13–7 ka template for freshwater forcing from the Hudson Strait outlet of the Laurentide Ice Sheet into the subpolar gyre. Quaternary Science Reviews 107, 62-80.

Johnsen, S.J., Clausen, H.B., Dansgaard, W., Fuhrer, K., Gundestrup, N., Hammer, C.U., Iversen, P., Jouzel, J., Stauffer, B., Steffensen, J.P. 1992. Irregular glacial interstadials recorded in a new Greenland ice core. Nature 359, 311-313.

Kleman, J., Borgstrom, I., Hättestrand, C. 1994. Evidence for a relict glacial landscape in Quebec-Labrador. Palaeogeography, Palaeoclimatology, Palaeoecology 111, 217-228.

Kleman J, Jansson K.N., De Angelis H., Stroeven, A.P., Hättestrand, C., Alm, G., Glasser, N. 2010. North American Ice Sheet build-up during the last glacial cycle. Quaternary Science Reviews 29, 2036-2051.

Leverington, D.W., Mann, J.D., Teller, J.T. 2002. Changes in the bathymetry and volume of glacial Lake Agassiz between 9200 and 7700 14C yr B.P. Quat. Res. 57, 244-252.

Matthew, E.M., 1961A. The Glacial Geomorphology and Deglacierization of the George River basin and Adjacent Areas in Northern Quebec. Doctoral thesis. McGill University, Montreal, p. 211.

Matthew, E.M., 1961B. Deglaciation of the George River basin, Labrador/Ungava. McGill Sub-Arctic Res. Pap. 11, 29-45.

Nishiizumi K., Winterer E., Kohl C., Klein J., Middleton R., Lal D., Arnold J. 1989. Cosmic ray production rates of ^{10}Be and ^{26}Al in quartz from glacially polished rocks. Journal of Geophysical Research 94, 17,907-17,915.

Prest, V.K., Grant, D., Rampton, V. 1968. Glacial Map of Canada. Geological Survey of Canada, Department of Energy, Mines and Resources. Map 1253A.

Renssen, H., Goosse, H., Fichefet, T. 2002. Modeling the effect of freshwater pulses on the early Holocene climate: the influence of high frequency climate variability, Paleoceanography 17, 1020.

Roy, M., Dell'Oste, F., Veillette, J.J., de Vernal, A., Helie, J.F., Parent, M. 2011. Insights on the events surrounding the final drainage of Lake Ojibway based on James Bay stratigraphic sequences. Quat. Sci. Rev. 30, 682-692.

Roy, M., Veillette, J.J., Daubois, V., Menard, M. 2015. Late-stage phases of glacial Lake

Ojibway in the central Abitibi region, eastern Canada. Geomorphology 248, 14-23.

Storrar R.D., Stokes C.R., Evans D.J.A. 2013. A map of Canadian eskers from Landsat satellite imagery. Journal of maps 9, 456-473. DOI: 10.1080/17445647.2013.815591

Thomas, E.R., Wolff, E.W., Mulvaney, R., Steffensen, J.P., Johnsen, S.J., Arrowsmith, C., White, J.W.C., Vaughn, B., Popp, T., 2007. The 8.2 ka event from Greenland ice cores. Quat. Sci. Rev. 26, 70-81.

Thorleifson, L.H., 1996. Review of Lake Agassiz history. In: Teller, J.T., Thorleifson, L.H., Matile, G., Brisbin, W.C. (Eds.), Geological Association of Canada Field Trip Guidebook for GAC/MAC Joint Annual Meeting, pp. 55-84.

Thornalley. D.J., Barker, S., Broecker, W.S., Elderfield, H., McCave, I.N. 2011. The deglacial evolution of North Atlantic deep convection. Science 331, 202-205.

Veillette, J.J., Dyke, A.S., Roy, M. 1999. Ice-flow evolution of the Labrador Sector of the Laurentide Ice Sheet: a review, with new evidence from northern Quebec. Quaternary Science Reviews 18, 993-1019.

Vidal, L.; Schneider, R.R.; Marchal, O.; Bickert, T.; Stocker, T.F.; Wefer, G. 199). Link between the North and South Atlantic during the Heinrich events of the last glacial period. Climate Dynamics. 15, 909–919.

CHAPITRE I

DEVELOPMENT, EVOLUTION AND DRAINAGE OF GLACIAL LAKE NASKAUPI DURING THE DEGLACIATION OF NORTH-CENTRAL QUEBEC AND LABRADOR

Hugo Dubé-Loubert[1,2,3] *et Martin Roy* [2,3]

[1]Bureau de la Connaissance Géoscientifique du Québec, Ministère de l'Énergie et des Ressources Naturelles, 400 boulevard Lamaque, Val-d'Or, Québec J9P 3L4

[2] Département des sciences de la Terre et de l'atmosphère - Université du Québec à Montréal, C.P. 8888, suce. Centre-Ville, Montréal (QC), Canaqa, H3C 3P8

[3] Centre de recherche Géotop - Université du Québec à Montréal, C.P. **8888,** suce. Centre-Ville, Montréal (QC), Canada, H3C 3P8

Publié dans *Journal of Quaternary Science* DOI: 10.1002/jqs.2997

RÉSUMÉ

La déglaciation du Nord québécois et du Labrador a mené au développement d'importants lacs de barrage glaciaire dans les vallées des rivières se drainant vers la baie d'Ungava. L'évolution de ces plans d'eau est très mal décrite en grande partie à cause des incertitudes importantes quant au schéma de retrait de la marge glaciaire de ce secteur. Le Lac Naskaupi a occupé la vallée de la rivière George où une campagne systématique de cartographie de formes associées et de mesures d'élévation des constructions glaciolacustres a révélé une histoire complexe marquée par la succession d'une multitude de phases. Notre reconstruction décrit trois niveaux bien définis soulignant des phases extensives de ce plan d'eau. Les autres niveaux présents sont généralement mal développés et reliés à des épisodes transitoires de courte durée. Durant sa phase principale (N2'), le Lac Naskaupi était formé de deux bassins séparés ayant évolué indépendamment pour un long intervalle de temps. Cette configuration est le résultat de la persistance de conditions de glace à base froide lors du retrait de la marge glaciaire ayant engendré un barrage de glace dans la section centrale de la vallée de la rivière George. L'existence de ce barrage de glace est supportée par la présence d'une construction sédimentaire de grandes dimensions ayant enregistré le drainage abrupt du bassin Naskaupi sud. L'ordre de grandeur des fluctuations d'élévation entre les phases subséquentes suggère l'occurrence d'au moins un autre épisode de drainage majeur avant la vidange finale. La reconstruction de la phase N2' permet le calcul d'un volume d'eau minimum pour le Lac Naskaupi.

ABSTRACT

Deglaciation of north-central Quebec and Labrador led to the development of large ice-dammed lakes in river valleys surrounding Ungava Bay. These lakes are poorly understood due to uncertainties in the regional pattern of ice retreat. Lake Naskaupi occupied the George River valley where systematic mapping of glacial landforms and extensive elevation measurements of shorelines reveal a complex history characterized by multiple lake levels. Our reconstruction documents three well-defined lake levels marking extensive lake stages. Additional lake levels are poorly developed and relate to short-lived, transient lake stages. During its main stage (N2'), Lake Naskaupi consisted of two separate basins that evolved independently for some time. This configuration resulted from the persistence of cold-based ice conditions during the deglaciation that caused the retreating ice margin to remain in the middle section of the river valley. The presence of this ice dam is supported by large-scale outburst flood deposits that record the abrupt drainage of the southern Naskaupi basin. The magnitude of the elevation changes between the remaining lower lake levels suggests the occurrence of at least one other major drawdown before the final lake drainage. Reconstruction of the N2' lake stage provides a minimum meltwater volume estimate for the lake.

1.1 INTRODUCTION

The Labrador ice dome was an active component of the north-eastern sector of the Laurentide Ice Sheet (LIS) during the last glacial cycle, with significant shifts in the position of its ice divide system (Dyke and Prest, 1987; Klassen and Thompson, 1993; Veillette et al., 1999; Dyke, 2004). Deglaciation of the Labrador Sector was equally dynamic, with asymmetrical rates of retreat of its southern (rapid) and northern (slow) ice margins (Clark et al., 2000; Ullman et al., 2016), and release of meltwater that led to the formation of several ice-dammed lakes, such as those that occupied the basins of the main rivers draining into Ungava Bay (Figure 1.1)(Ives, 1960a; Barnett, 1963; Gray et al., 1993). The evolution of these glacial lakes remains poorly understood mainly because their development was closely linked to the pattern of ice retreat, which is still inadequately resolved in this remote region. The glacial history of northern Quebec and Labrador is indeed complex. Streamlined landforms and eskers outline two ice-flow systems consisting in a broad radially divergent (outward spreading) ice-flow that is truncated in the north by an ice flow converging northward into Ungava Bay (Prest et al., 1968). These two opposing ice flow patterns intersect along a sharp and narrow U-shaped boundary that circumscribes the Ungava Bay lowlands (Figure 1.1). This zone of intersection is informally referred to as the Horseshoe Ice Divide, which presumably developed late in the deglaciation (Hughes, 1964; Veillette et al., 1999; Kleman et al., 2010). Uncertainties regarding the evolution of this ice divide throughout the last deglaciation complicate the integration of some of these lakes into current deglaciation frameworks, mainly because the damming required to impede the natural drainage of rivers implies ice margin configurations that are in places incompatible with the documented patterns of ice retreat (Clark et al., 2000). Although previous work reported evidence for at least 10 glacial lakes around Ungava Bay (Ives, 1960a; Barnett, 1963; Gray et al., 1993), little is known about those lakes since most were identified by scattered occurrences of raised shorelines. Despite important gaps in our knowledge of the regional deglaciation, paleogeographic reconstructions provide important insight into the development of these glacial lakes, in particular for those that developed east and southeast of Ungava Bay (Ives, 1960a; Barnett, 1967; Dyke and Prest, 1987; Dyke, 2004). The general orientation and areal distribution of streamlined landforms and eskers in northcentral Quebec and Labrador indicate that the overall pattern of ice retreat was from east to west (Dyke and Prest, 1987). The ice margin initially retreated from the coast of the Labrador Sea and gradually moved westward across the Torngats Mountains, to finally occupy a position somewhere in the Ungava Bay lowlands. Once the ice margin crossed the continental drainage divide between the Labrador Sea and Ungava Bay and blocked the lower reach of rivers, meltwater accumulated between the ice margin to the westnorthwest and the Torngats Mountains to the east, leading to the development of glacial lakes that extended over several tens to >100km in river valleys (Figure 1.1).

The largest of these lakes, Lake Naskaupi, occupied the George River basin, south of Ungava Bay, leaving an extensive record of raised shorelines and associated landforms. Previous work carried out in the 1950s and 1960s focused on the most developed shorelines from two key sectors located in the upper and lower reaches of the river (Ives, 1959, 1960a,b; Matthew, 1961a,b; Barnett, 1963, 1967; Barnett and Peterson, 1964). These discontinuous shorelines were subsequently correlated and associated with a long glacial lake that presumably occupied a large portion of the George River valley (GRV) and its tributaries (Figure 1.1). These long-held reconstructions, however, do not take into account the geometry and pattern of the retreating ice margin. Consequently, the location of the ice margin and outlets that controlled the configuration and surface elevation of Lake Naskaupi remain to be determined. These aspects were later improved upon by development in remote sensing mapping methods that provided insights into the probable extent and evolution of these glacial lakes (Clark et al., 2000; Jansson, 2003; Jansson and Kleman, 2004). However, many features of these reconstructions have yet to be validated by geological data, while geomorphic evidence for postulated drainage events remains to be documented.

Refining the mechanisms that led to the formation of the Ungava glacial lakes is critical to our understanding of the deglaciation of northern Quebec and Labrador and the production of reliable paleogeographic reconstructions. This paper presents a reconstruction of the main stages that marked the history of Lake Naskaupi, drawing together results obtained from the mapping of glacial and deglacial landforms of a large region located west of the Torngat Mountains and south of Ungava Bay, and including extensive elevation measurements of raised shorelines carried out throughout the GRV (Figure 1.1). Our reconstruction also provides an estimate of the meltwater volume associated with the main Naskaupi stage.

1.2 BACKGROUND ON LAKE NASKAUPI

The occurrence of former glacial lakes to the south-west of the Torngat Mountains was first recognized by early 20th century explorers who reported blocky beaches standing several meters above the surface of present-day lakes and rivers (e.g. Prichart, 1911). These shorelines were documented a few decades later through the study of a sequences of raised shorelines present in the Indian House Lake (IHL) area, which forms a bulge a few kilometers wide by _100km long in the upper reach of the George River (Figure 1.2). These shorelines were then associated with a major glacial lake that was named Lake Naskaupi (Ives, 1959, 1960a). Despite a limited number of elevation measurements of shorelines, three lake stages were recognized and named N1, N2 and N3 (N1 being the highest; Ives, 1959, 1960a). Subsequent work by the same research group in the IHL area identified two additional lake levels (N4 and N5) (Barnett and Peterson,1964), for a total of five Naskaupi stages involving lake-level changes ranging from ~40 to 65m (Table 1.1). Parallel investigations in the Whale River valley to the west reported another glacial lake, Lake McLean (Figure 1.1), which was presumably connected to Lake Naskaupi during their early stages (Barnett, 1963; Barnett, 1967). Another key region recording the history of Lake Naskaupi was found _150km north of the IHL area, where topographic rises forming the Pyramid Hills (PH) area expose welldeveloped shorelines (Figure 1.2; Matthew, 1961a,b). Again, five lake levels were mapped, but their absolute elevation could not be properly measured due to the lack of nearby geodesic control points at this time (Matthew, 1961a,b). Nonetheless, the upper three shorelines were then considered equivalent to the upper three lake levels documented earlier in the IHL area.

In the IHL area, the best developed and most extensive shorelines belonged to the N2 lake level, which was then interpreted as the most important lake stage. Characterization of Lake Naskaupi was thus based on N2 shorelines, which initially yielded a postglacial uplift gradient (dipping northward) of 0.30m per km (then measured in feet per mile; i.e. 1.57 ft per mi; Ives, 1960a). This figure was later refined to an apparent north–south tilt of 0.33m per km (1.75 ft per mi; Barnett, 1963). A tilt gradient of 0.38m per km (2 ft per mi) was also determined from N1 shorelines (Ives, 1960a). In the PH area, similar calculations carried out on the upper two shorelines (N1 and N2) yielded a tilt gradient of 0.50 and 0.34m per km, respectively (Matthew, 1961a,b). These results thus showed a noticeable increase in tilt for the N1 lake level, from 0.38m per km (2 ft per mi) in the northern sector of the IHL area (i.e. Haute Falaise or High Bluff in previous work) to 0.50m per km (2.6 ft per mi) in the PH area. These differences were then judged to be somewhat minor given the probable errors inherent to the methodology used. The scarcity of shorelines to the west of the GRV complicated the calculation of the east–west tilt for the N2 stage. Nonetheless, measurements of shorelines near Lake Brisson yielded an apparent value of 0.25m per km towards east (1.32 ft per mi; Barnett, 1963). Based on these values, regional isobases were established and showed a maximum tilt toward N224° (dipping 0.44m per km towards NE (2.31 ft per mi)), consistent with a former ice dispersal center located in the Lake Caniapiscau area, south of Ungava Bay (Dyke and Prest, 1987).

A reconstruction of several Ungava lakes based on digital elevation models (DEMs) and topographic maps identified seven Naskaupi stages (Jansson, 2003). The discrepancies with the previous studies may reflect limitations in mapping resolution and the absence of ground control, as well as the lack of integration of the regional uplift gradients that are critical in establishing reliable shoreline correlations and identifying lake stages. This reconstruction was also based on the retreat of a hypothetical ice mass centered over Ungava Bay; a deglaciation model that remains unsupported by geological data.

In earlier work, the maximum extent of the different lake stages was largely based on the absence of shorelines throughout the river valley. Considering the presence of an ice dam to the west and north of the GRV, the outlet of the N1 lake stage was ascribed to the topographic depression associated with the Kogaluk River, which drains east through the Torngat Mountains and into the Labrador Sea (Figure 1.2) (Ives, 1960a). Several potential outlets were considered for the N2 stage, but none could be determined with certainty. Meltwater overflow was presumably routed to the Labrador Sea through outlet(s) extending east across the Quebec–Labrador drainage divide (Ives, 1960a; Barnett and Peterson, 1964). The extent and outlet(s) of the N3 and remaining lower lake stages were more difficult to evaluate due to the limited occurrence of shorelines, which was interpreted as evidence for stages of shorter duration. Routing of meltwater overflow at that time was thought to have occurred via an outlet to the south formed by the George River/Michikamau col (Figure 1.1), or alternatively to the north, towards Ungava Bay, through lateral drainage along the ice dam or even subglacially (Matthew, 1961a).

The chronological framework for Lake Naskaupi is poorly constrained and has traditionally been based on two radiocarbon ages (8610 ± 925 and 6815 ± 125 14C a BP) obtained on total organic matter (low abundance) sampled from sub-bottom lake sediment cores (Short, 1981). Despite the large uncertainty, these ages form the sole direct chronological control to establish the position of the retreating ice margin and the concomitant lake development in paleogeographic reconstructions (e.g. Dyke and Prest, 1987). Additional considerations on the regional deglaciation may be gained from relative sea-level curves on the Labrador coast that place the full establishment of Lake Naskaupi sometime after 7600 ± 200 14C a BP (Clark and Fitzhugh, 1990).

1.3 METHODS

Our reconstruction of Lake Naskaupi is based on the mapping of raised shorelines and associated geomorphic features and deposits (deltas, spillway channels, wave-cut notches). Additionally, we mapped landforms indicative of ice marginal positions and glaciodynamic conditions to gain insight into the deglaciation of the George River basin. This work was carried out through systematic interpretation of black and white aerial photographs (1: 40 000 and 1: 60 000 scales; Figure 1.3) and 'Rapideye' satellite imagery (5-m resolution) covering an area equivalent to two map sheets at the 1: 250 000 scale (24H and 24A of the National Topographic System of Canada). Preliminary interpretations obtained from the remote mapping were subsequently verified at hundreds of sites in the field using helicopter support over the course of two field seasons.

Elevation measurements of >300 shoreline remnants from 160 sites covering an area of~200km long and 60 km wide along the GRV (Figure 1.3) were obtained through a conventional altimetry method using two Suunto E203 altimeters (accuracy of_1 m). This approach involves simultaneous elevation measurements by two operators and requires the altimeters to be first synchronized (elevation, time, and x, y, z coordinates) at a given geodesic benchmark, where a stationary altimeter records the elevation at fixed intervals (every 2 min). Concurrently, a mobile altimeter measures the elevation of shorelines in the field. All measurements were performed within perimeters of <20 km to stay within the same atmospheric pressure system and minimize uncertainties. Changes in elevation recorded at the benchmark reflect fluctuations in atmospheric pressure, and these can then be used to correct the elevations of shorelines measured during the same time interval. This correction, if needed, is done by simple addition or subtraction of the elevation changes recorded (e.g. Roy et al., 2015).

Naskaupi lake levels were reconstructed by placing the 300 shoreline elevation data into an elevation vs. distancediagram depicting a north–south transect across the study area. For this purpose, the geographical position of each shoreline measured was projected at right angle onto a north–south line running through the middle of the GRV, and thus roughly parallel to the tilt axis defined in earlier studies. We then correlate the most continuous and distinguishable shorelines in three main sectors (Figure 1.3) to assess the extent of the lake levels and gain insights into their relative chronology. Geomorphological evidence of probable lake drawdowns was also documented and a DEM (high-resolution Canadian Digital Elevation Model; resolution of 12 m) was used to reconstruct the areal extent and calculate a meltwater volume estimate for the most important lake stage.

1.4 RESULTS

1.4.1 Geomorphic setting of shorelines

Naskaupi shorelines are found mainly on hillslopes characterizedby a thick cover of glacial deposits (till) and consist of an accumulation of meter-size boulders forming continuous terraces 2–12m wide, which can be followed for hundreds of meters to several kilometers (Figure 1.4A,B). In areas of thin drift cover, the shorelines are smaller in size and extent, or take the form of a sub-horizontal rim of bare bedrock on hillslopes that marks the limit of wave reworking by littoral erosion. A succession of three to four shorelines separated in height by 10–40m were commonly documented

(Figure 1.4C,D). Shorelinesare typically best developed within the GRV and are less prominent in tributary valleys where they are often disturbed by solifluction processes (Figure 1.4E). Shorelines are most abundant on the west-facing slopes (i.e. on the east side of the main and tributary river basins), probably reflecting a greater fetch associated with the prevailing (katabatic) wind direction. The overall lack of shorelines on the western shore of the GRV also suggests that Lake Naskaupi was in contact, at least partially, with the westward retreating ice margin.

1.4.2 Shoreline elevation data

Plotting of the ~300 shorelines in the elevation vs. Distance diagram covering the GRV reveals a scatter in the data that makes the identification of lake levels difficult at first (Figure 5A). Nonetheless, some trends can be distinguished in the IHL area where sub-horizontal alignments of data points outline at least three distinct water planes (Figure 1.5A). The extension of these lake levels into the northern part of thebasin is complicated by the numerous shorelines present in the Wedge Hills (WH) and PH areas. A closer examination of the elevation data indicates that the difficulty in distinguishing lake levels in these two areas is related to the complex shoreline sequences present in tributary valleys (Supporting information, Figure A.1A). The Nutililik, Mitshu and Siimitalik valleys show a chaotic distribution of shorelines that appear to be related to their location to the east of the GRV. Indeed, given the regional east to west pattern of ice retreat, these tributary valleys would have been deglaciated before the main basin formed by the GRV. These tributary valleys therefore probably formed a series of temporary basins that record early and minor glaciolacustrine episodes unrelated to the main lake stages developed later in the core sector of the Naskaupi basin.

This interpretation is supported by the poorly developed character of these shorelines that suggests that the associated lake stages were short-lived. Indeed, these shorelines contain more fine-grained material among the boulders, which reflects incomplete erosion by lakeshore processes. Several minor spillway channels were also documented at variable elevations, thus recording the brief and sudden drainage of these small temporary basins (Figure A.1B). For these reasons, shoreline data from tributary basins are not retained and our reconstruction uses data from the main GRV basin in the IHL, WH and PH areas (Figure 1.5B).

1.4.3 Lake levels in the Indian House Lake area

The distribution of shorelines along the 100-km-long transect formed by the IHL area provides clear evidence for at least three well-defined lake levels above 400m (Figure 1.5B). These slightly inclined water planes depict the influence of postglacial uplift, with the apparent lake levels showing a slight regional dip towards the north. These lake levels are here defined by running a best-fit line through the clusters of shorelines showing a similar elevation trend (Table 1.2). Two additional lake levels might be present above and below, but they are defined by a smaller number of shorelines. We named these five lake stages N0', N1', N2', N3' and N4', in which the bounding stages (N0', N4') represent the less defined lake levels. This labeling follows the nomenclature presented in previous work, whereby the N2' lake level represents the best-defined lake stage.

Although these sub-horizontal lines intercept most of the shorelines present in this sector, a few shorelines are present in between the main lake levels (Figure 1.5B). These intermediate-elevation shorelines may record short-lived, transient stagesthat developed in between the main lake stages. Shorelines lying at elevations higher than the N1' lake level, such as those forming the N0' lake level, are probably associated with the onset of the glaciolacustrine submergence in the IHL basin. These proto-Lake Naskaupi stages probably record the early development of a swarm of smaller meltwater bodies that eventually coalesced when the ice margin retreated west of the

GRV to give rise to the first 'main' stage of Lake Naskaupi, which would correspond to N1'. The scarcity of high-elevation shorelines (above N1') suggests that the duration of these early lake stages was relatively short, with shorelines being formed only in areas where surficial deposit thickness and site location relative to the prevailing wind direction were optimal. The local physiographic setting of the sites where shorelines were measured may also explain some of the variability seen in the elevation data outlining the different lake levels identified.

The uplift gradients calculated from the well-defined N2' and N3' lake levels in the IHL area are 0.16 and 0.17m per km (northward dip), respectively. Tilt values for the other lake levels range from 0.05 to 0.28m per km (Table 1.2). A limited number of shorelines to the west of the valley indicate an east–west tilt rate of 0.06m per km, which shows a eastward dip. The combined maximum tilt gradient for the N2' stage is 0.28m per km with a dip towards 36°.

1.4.4 Lake levels in the Wedge Hills and Pyramid Hills areas

The identification of lake levels in the WH and PH areas is difficult due to the scatter in the shoreline elevation data (Figure 1.5B). In the PH area, the data show a relatively good alignment of shorelines that suggests the occurrence of several lake levels (Figure 1.6), although not as clearly defined as those documented in the IHL area. Based on these correlations, at least five lake levels may be defined, which we named PH1, PH2, PH3, PH4 and PH5 (Figure 1.6). Shorelines of intermediate elevations are also present, but their poor degree of development suggests they are not related to major and widespread lake stages. The uplift gradients for these lake levels vary widely, from 0.14 to 0.69m per km, which are significantly different from those measured in the IHL area (Table 1.2).

In comparison, the WH area shows relatively few shorelines, which are found mostly above 470m (Figure 1.5B). The absence of clear lake levels may be related to the fact that these high-elevation shorelines are located outside (east) the GRV. This part of the mid- to upper segment of the GeorgeRiver basin has also a striking lack of shorelines between 410 and 470m (Figure 1.5B), in contrast to the bounding sectors, notably with the IHL area where a well-defined lake level is present at ~460 m.

The WH area further shows a prominent geomorphological feature consisting of a thick accumulation (30 m) of imbricated meter-size boulders arranged in large-scale alluvial bars extending over 2 km in length (Figure 1.7A–E). This landform is located downstream from a 25- to 30-m-deep meltwater canyon carved into bedrock, while the area surrounding this construction also shows large patches of bare bedrock that indicate significant erosion by meltwater (Figure 1.7F). In addition, large-scale sand and gravel ripples are present downstream from this landform (Figure 1.7G,H). These geomorphological features are reported here for the first time, and together they suggest an abrupt drainage of the glacial lake basin located upstream from this accumulation (Clarke et al., 2009). Such an outburst flood deposit requires the presence of an ice dam in this area, a feature that may explain the lack of continuity in the shoreline sequence within the George River basin (see Discussion).

1.4.5 Lake-level correlations

Together, the difficulty in identifying lake levels in the PH area and the presence of a gap in the shoreline record of the WH area complicate correlations of lake levels throughout the GRV. Because of this limitation, we placed emphasis on N2' shorelines, which together form the best-developed and most extensive lake level that can be followed nearly continuously throughout the IHL area (Figure 1.5B). We then use the geometry associated with the N2' water plane to outline its extent into the northern half of the Naskaupi basin and evaluate its relationship with the shorelines present in the

WH and PH areas. Figure 5C clearly shows that the projection of this IHL N2' lake level does not match any sets of shorelines in the WH area. Furthermore, this approach indicates that N2'-equivalent shorelines should lie at an elevation of 454m in the PH area where only two shorelines were found at this elevation. Of these, one is a poorly developed shoreline located outside the GRV, thereby leaving only one potential N2'-equivalent shoreline. In fact, the best-developed lake level in the PH area (PH3') occurs at a lower elevation. These results thus suggest that the configuration of Lake Naskaupi is more complex than previously proposed. We address this issue in the following discussion.

1.5 DISCUSSION

Previous field-based studies reported five Naskaupi stages (N1 to N5) from two separate sectors of the GRV where the best-developed N2 shorelines were correlated into a single lake occupying the George River basin (Ives, 1959, 1960a; Matthew, 1961a,b; Barnett, 1963, 1967; Barnett and Peterson, 1964). This reconstruction, however, was based on data from a few sites and shoreline correlations were largely articulated around the physical characteristics of shorelines. This approach, as acknowledged by these studies, may not be the most robust correlation tool, as erosional and depositional processes leading to the formation of these shorelines are influenced by a number of factors, including the orientation of the hills with respect to prevailing winds and the thickness of the sediment cover.

In our study, we also identified multiple lake levels in the IHL (N0' to N4') and PH (PH1 to PH5) areas, but the poor degree of development of certain sets of shorelines, as well as their lack of continuity, indicate that some of these lake levels relate to short-lived lake stages. We also documented a set of well-defined and nearly continuous shorelines in the IHL area that forms a clear and unambiguous lake level that probably corresponds to the N2 lake stage of earlier studies, although our results yield a different uplift value. Extension of this N2' water plane to the north also finds very few matchingshorelines, thereby providing little support for the existence of a similar widespread lake level in the PH area. Finding shorelines matching the N2' lake level is also problematic when using the tilt values obtained from previous work (Figure 1.5C).

The differences between the lake-level sequences of the southern and northern sectors of the Naskaupi basin are also reflected in the uplift gradients documented from the bestdeveloped lake levels, with uplift gradients about three to four times lower in the IHL area (N2': 0.16m per km) than inthe PH area (PH3': 0.69m per km) (Table 2). These differences may provide insights into the relative age of shorelines of these two areas. A high uplift gradient suggests that the associated lake level formed relatively early in the deglaciation, whereas a lower gradient implies that some amount of uplift has already occurred before the formation of the shorelines. These results suggest that the shorelines of these two areas may have formed during distinct time intervals, or at least not simultaneously.

These differences in uplift gradients and the difficulty in correlating shorelines within the GRV are probably related to the fact that the IHL and PH areas experienced different deglacial histories, at least for the time interval comprising the N0', N1' and N2' lake stages. The reason for this is because the WH area was still occupied by ice at that time. This segment of the GRV occupies a critical location in the middle of the Naskaupi basin where the shoreline record shows a gap between 410 and 470 m. This is unusual since the physiography and sediment cover of the WH area are similar to the other sectors documented and should thus have allowed the development of shorelines at elevations matching those present in the IHL and PH areas.

The presence of an ice dam in the WH area is also indicated by large-scale alluvial bars and adjoining ripples that record the abrupt meltwater outburst associated with the drainage of the southern Naskaupi (IHL) basin. The geomorphic and sedimentary assemblages in the WH area also suggest that the damming of this sector of the GRV may be related to a zonation of the thermal conditions at the base of the retreating ice margin (Dubé-Loubert et al., 2016a,b). The numerous eskers in the region that show a general (warm-based) ice retreat from east to west are no longer present in the WH area and the northern part of the GRV (Dubé-Loubert et al., 2016a). Here, the surficial geology is characterized by abundant block fields (felsenmeer), extensive areas of frost-shattered bedrock and oxidized glacial deposits. Together, this suggests the persistence of widespread cold-based ice conditions during ice retreat (Figure 1.8). In addition, the numerous lateral meltwater channels in this segment (and west) of the GRV suggest that the ice margin remained frozen at its bed during the deglaciation of this sector (Figure A.2A).

The lack of N2' shorelines in the WH area suggests that the Pinkflood outburst deposits and landforms are related to the drainage of the N2' lake stage of the IHL basin. This interpretation raises questions about the significance of the lower lakes stages (i.e. N3' and N4'), as well as about the overall lake configuration following the break up of this ice dam. In the IHL area, N3' shorelines delineate another relatively well-developed lake level (Figure 1.5B). Extension of this N3' water plane into the PH area intercepts several shorelines forming the PH3 lake level and a well-developed shoreline in the WH area (Figs 1.5B and 1.6), thus underlining a possible connection between the IHL and PH areas during the N3' stage. Similarly, the projection of the IHL N4' lake level into the PH area could also support a connexion between these two basins, but the N4' lake level is poorly defined.

This succession of lake levels documents significant lake-surface drawdowns. These may result from changes in basin configuration triggered by ice retreat, which opened new outlets and caused the lake to expand into newly deglaciated basins. This mechanism may explain lake-level fluctuations of 10–30 m, such as those separating the upper lake levels. However, large-scale drawdowns of 50–100m like those recorded between the N2'–N3' and N3'–N4' lake levels suggest the occurrence of partial lake drainages (Table 1.2), especially considering that potential outlets to the east of the Naskaupi basin do not show elevation differences of this magnitude, while further ice withdrawal (opening of outlets) to the west is incompatible with damming of the lake.

These large drawdowns could be related to drainage under a main ice dam on the lower reach of the George River, in the northern part of the Naskaupi basin. The sector encompassing the presumed location of this ice dam – the area located between the northern limit of the lake and the maximum extent of the postglacial Iberville Sea (maximum elevation at ~100 m; Allard et al., 1989) – is characterized by large areas of bare bedrock surfaces, deep meltwater channels incised into bedrock and giant potholes that suggest erosion by meltwater (Figure A.2).

Whether these erosional features result from the collapse of the ice dam and final lake drainage or from earlier lakedrawdown events cannot be determined. Episodes of subglacial drainages may also have originated from the PH basin while it was separated from the IHL basin. As discussed above, the uplift gradients documented from these lake levels suggest they developed earlier than those of the IHL basin. Further, the drainage of the IHL N2' lake stage requires a lake surface considerably lower in the PH area to allow the meltwater discharge that is recorded by the outburst deposits and landforms of the WH area. If this assumption is correct, it implies a complex history of meltwater submergence for the northern Naskaupi basin, which could explain, in part, the wide variability in the distribution of shorelines in the PH area.

1.5.1 Meltwater volume estimate for Lake Naskaupi stage N2'

Given the complex succession of lake stages, the well-defined and extensive N2' lake level of the IHL area was chosen to estimate the volume of meltwater contained in Lake

Naskaupi. For this purpose, the geometric characteristics (tilt, elevation) of the N2' water plane were used in a DEM to constrain its areal extent. This DEM was subtracted from the tilted N2' water plane to remove elevation variations inherent to the regional uplift gradient, according to methodologies defined in other glacial lake reconstructions (Leverington et al., 2002). Despite the known differences between the IHL and PH basins, the characteristics of the IHL N2' lake level were retained to delineate a corresponding lake surface in the PH area. Although a lake level similar to the IHL N2' lake stage is not present in the PH area, shorelines occur at similar elevation, thus supporting the existence of a lake surface in the northern basin at some point during the deglaciation. We consider this conservative approach provides a realistic lakesurface reference that is consistent with the pattern of lake development outlined in our study.

Figure 1.9 shows the extent of the N2' lake stage in the GRV and its tributaries. The reconstruction indicates that the western shore of the IHL basin was in contact, at least partially, with the west-northwestward retreating ice margin. The position of the ice margin is based on the distribution shorelines, as well as with the location of topographic troughs that require damming to maintain the elevated lake surface. This reconstruction also shows that the southernmost extent of the lake lies outside the study area, just north of Lake Michikamau. This lake limit is based on previous work that reported N2 shorelines near the drainage divide separating the Labrador Sea and Ungava Bay (Ives, 1960a; Peterson, 1965), which is consistent with the extension of the N2' waterplane we document. Several geomorphological indicators show a very good fit with the reconstructed extent of the N2' lake stage (Figure 1.9B), notably the location, areal distribution and elevation of shorelines and deltas, as well as meltwater overflow channels associated with a presumed connection with Lake McLean (Figure 1.10A,B). The reconstruction also agrees well with the separation of Lake Naskaupi in the WH area where the areal distribution of meltwater overflow channels perpendicular to the George River points to the presence of an ice dam (Figure 1.10C). Similarly, the distribution of shorelines and the location of overflow channels north of the PH area concord with the presumed location of the main ice dam (Figure 1.10D). The reconstruction further allows the identification of probable outlets for the N2' lake stage. These are located east of the George River, near the headwaters of the Kogaluk and Fraser rivers, as well as to the south (George River/Michicamau col), where widespread and well-defined meltwater channels occur and support routing of meltwater overflow across the Ungava–Labrador drainage divide into the Labrador Sea. These outlets would also have been operating at thetime of the N0' and N1' lake stages. For the outlets of the N3'–PH3 stage, the presence of channels near Mistinibi Lake suggests that meltwater was probably routed into the Labrador Sea through the continental drainage divide. No topographic lows were identified as potential outlets for the lowelevationand poorly defined N4'–PH4 stage, suggesting that this short-lived meltwater body drained northward into Ungava Bay, probably through a drawdown along the ice dam remnant or subglacially. This stage forms the last important (extensive) Naskaupi paleosurface in the GRV.

Reconstruction of the Naskaupi basin during the N2' lake stage shows an average water depth of ~50m for the IHL basin, for a volume of 495 km^3 (Figure 1.11). In the PH basin, the average water depth is ~95 m, for a volume of 79km^3. The total volume of meltwater for this lake stage is thus 574 km^3 and provides a robust constraint of the meltwater that was contained in Lake Naskaupi at some point during the deglaciation. Because our lake-level reconstruction indicates significant lake-surface drawdowns – with at least one fromthe main IHL basin (i.e. the N2' lake stage), another from a full Naskaupi basin (N3'–PH3 lake stage), and possibly a third one marking the 'final' drawdown (N4'–PH4 lake stage) – this meltwater volume estimate may be considered as a minimum contribution of the meltwater discharges from this lake, which could be greater given the lake history.

1.6 CONCLUSIONS

The geomorphology of the GRV is characterized by prominent sequences of raised shorelines associated with glacial Lake Naskaupi. Numerous elevation measurements of shoreline sequences indicate that the lake evolution was characterized by a complex succession of lake levels. Of these, a few sets of well-defined shorelines delineate three extensive lake stages. Other poorly developed shorelines relate to short-lived lake levels associated with transient stages or early development stages that show complex histories, independent from the main Naskaupi basin.

During its most important stage (N2' lake level), Lake Naskaupi consisted of two basins that evolved independently for a significant part of the deglaciation. This configuration was caused by the presence of an ice dam in the middle reach of the river valley, which is corroborated by large-scale outburst flood deposits that record the abrupt drainage of the southern Naskaupi basin. The drainage of the N2' lake stage was followed by the development of at least one other important lake stage covering the entire river valley. The marked difference in elevation between the lower lake levels (post N2') requires the occurrence of one additional drawdown (partial drainage) event before the final drainage of the lake. Reconstruction of the extent of the N2' lake stage provides the first field-based constraints on the meltwater volume associated with this lake configuration, which yielded an estimate of ~600 km^3. Within the context of the lake history documented, this number represents a minimum contribution for the meltwater discharges from this lake.

These results suggest that the configuration and evolution of Lake Naskaupi was more complex than reported in former reconstructions. This is mostly due to the regional pattern of ice retreat. The general westward ice retreat was in fact irregular and fragmented due to important zonation in the basal thermal regime of the decaying ice margin. Large areas in the middle and northern part of the George River basin show geomorphological indicators of cold-based ice conditions, which were instrumental in the damming of the lake, and played an important role in its configuration and drainage. The local persistence of cold-based ice conditions during the ice retreat is probably related to the fact that the region around Ungava Bay is located nearby the former position of the Labrador Ancestor ice divide where variations in subglacial thermal regime have been documented (e.g. Marquette et al., 2004; Staiger et al., 2005). These results thus refine the deglaciation pattern of this region and provide new elements to existing paleogeographic models dealing with the development of ice-dammed lakes in north-central Quebec and Labrador (e.g. Clark et al., 2000). Concurrently, our study highlights the importance of conducting detailed mapping and field-based investigations in unraveling the history of these glacial lakes. Future work on the evolution (configuration, volume) of glacial lakes around Ungava Bay should focus on developing a geochronological framework that will allow the integration of these lakes and their drainages within the deglaciation of the north-eastern sector of the LIS.

1.7 ACKNOWLEDGEMENTS

Logistical and financial support for this study was provided through a mapping programme of the Ministry of Energy and Natural Resources of the Province of Quebec. Additional funding came from an NSERC Discovery Grant to M.R. Virginie Daubois, Olivier Lamarche and Simon Hebert provided assistance during fieldwork. Comments by Jean Veillette and Patrick Frings on an early draft were greatly appreciated. We thank David Sugden, Martin Margold, Anders Carlson and an anonymous reviewer for their constructive reviews. BCGQ external contribution No. 8449-2016-2017-03.

1.8 REFERENCES

Allard M, Fournier A, Gahé E, Séguin MK. 1989. Le Quaternaire de la côte sud-est de la baie d'Ungava, Québec nordique. *Géographie physique et Quaternaire* **43**: 325–336.

Barnett DM. 1963. Former pro-glacial lake shorelines as indicators of the pattern of deglaciation of the Labrador/Ungava Peninsula. *McGill Sub-Arctic Research Papers* **15**: 23–33.

Barnett DM. 1967. Glacial Lake MacLean and its relationship with Glacial Lake Naskaupi. *Geographical Bulletin* **9**: 96–101.

Barnett DM, Peterson JA. 1964. The significance of Glacial Lake Naskaupi 2 in the deglaciation of Labrador Ungava. *Canadian Geographer* **8**: 173–181.

Clark CD, Fitzhugh WW. 1990. Late deglaciation of the Central Labrador Coast and its implications for the Age of Glacial Lakes Naskaupi and McLean and for Prehistory. *Quaternary Research* **34**: 296-305.

Clark CD, Knight JK, Gray JT. 2000. Geomorphological reconstruction of the Labrador sector of the Laurentide Ice Sheet. *Quaternary Science Review* **19**: 1343–1366.

Clark G, Bush ABG, Bush JWM. 2009. Freshwater Discharge, Sediment Transport, and Modeled Climate Impacts of the Final Drainage of Glacial Lake Agassiz. *Journal of Climate* **22**: 2161-2180.

Dubé-Loubert H, Daubois V, Roy M. 2016a. Géologie des dépôts de surface de la région du lac Henrietta (24H). Ministère de l'Énergie et des Ressources naturelles–Québec, Report RP 2016-01 (includes 1 map): 31 p.

Dubé-Loubert H, Daubois, V, Roy M. 2016b. Géologie des dépôts de surface de la région du lac Brisson (SNRC 24A). Ministère de l'Énergie et des Ressources naturelles–Québec, Report **RP 2016-03** (includes 1 map): 21 p.

Dyke AS. 2004. An outline of North American Deglaciation with emphasis on central and northern Canada. *Developments in Quaternary Sciences* **2**: 373–424.

Dyke AS, Prest VK. 1987. Late Wisconsinan and Holocene retreat of the Laurentide Ice Sheet. Map 1702A, 1:5,000,000. Geological Survey of Canada. *Geographie Physique et Quaternaire* **41**: 237–263.

Gray J, Lauriol B, Bruneau D *et al.* 1993. Postglacial emergence of Ungava Peninsula, and its relationship to glacial history. *Canadian Journal of Earth Sciences* **30**: 1676–1696.

Hughes OL. 1964. Surficial geology, Nichicun-Kaniapiskau map-area, Québec. *Geological Survey of Canada Bulletin* **106**: 20 p.

Ives JD. 1959. The former ice-dammed lakes and the deglaciation of the middle reaches of the George River valley. *McGill Sub-Arctic Research Papers* **6**: 9–44.

Ives JD. 1960a. Former ice-dammed lakes and the deglaciation of the middle reaches of the George River Labrador-Ungava. *Geographical Bulletin* **14**: 44–70.

Ives JD. 1960b. The deglaciation of Labrador/Ungava, an outline. *Cahiers de Geographie du Quebec* **3**: 323–343.

Jansson KN. 2003. Early Holocene glacial lakes and ice marginal retreat pattern in Labrador/Ungava. *Paleogeography, Palaeoclimatology, Palaeoecology* **21**: 473–501.

Jansson KN, Kleman J. 2004. Early Holocene glacial lake meltwater injections into the Labrador Sea and Ungava Bay. *Paleoceanography* **19**: 1-12.

Klassen RA, Thompson FJ. 1993. Glacial history, drift composition, and mineral exploration, central Labrador. *Geological Survey of Canada Bulletin* **435**: 76 p.

Kleman J, Jansson KN, De Angelis H *et al.* 2010. North American Ice Sheet build-up during the last glacial cycle. *Quaternary Science Reviews* **29**: 2036-2051.

Leverington DW, Mann JD, Teller JT. 2002. Changes in the bathymetry and volume of glacial Lake Agassiz between 9200 and 7700 14C yr B.P. *Quaternary Research* **57**: 244–252.

Marquette GC, Gray JT, Gosse JC *et al.* 2004. Felsenmeer persistence under non-erosive ice in the Torngat and Kaumajet mountains, Quebec and Labrador, as determined by soil weathering and cosmogenic nuclide exposure dating. *Canadian Journal of Earth Sciences* **41**: 19-38.

Matthew EM. 1961a. The glacial geomorphology and deglacierization of the George River basin and adjacent areas in northern Quebec. PhD thesis, McGill University, Montreal, Canada.

Matthew EM. 1961b. Deglaciation of the George River basin, Labrador/Ungava. *McGill Sub-Arctic Research Papers* **11**: 29–45.

Peterson JA. 1965. Deglaciation of the Whitegull Lake area, Labrador/Ungava. *Cahiers de Geographie du Quebec* **9**: 183–196.

Prest VK, Grant DR, Rampton VN. 1968. Glacial map of Canada, 1 : 5,000,000. Geological Survey of Canada. Map 1253A.

Prichart HH. 1911. Through trackless Labrador –with a chapter on fishing by Gathorne-Hardy. Sturgis & Walton: New-York.

Roy M, Veillette JJ, Daubois V *et al.* 2015. Late-stage phases of glacial Lake Ojibway in the central Abitibi region, eastern Canada. *Geomorphology* **248**: 14–23.

Short SK. 1981. Radiocarbon date list I: Labrador and northern Quebec, Canada. *Institute of Arctic and Alpine Reasearch* **36**: 1–35.

Ullman DJ, Carlson AE, Hostetler SW *et al.* 2016. Final Laurentide ice-sheet deglaciation and Holocene climate-sea level change. *Quaternary Science Reviews* **152**: 49–59.

Veillette JJ, Dyke AS, Roy M. 1999. Ice-flow evolution of the Labrador Sector of the Laurentide Ice Sheet: a review, with new evidence from northern Quebec. *Quaternary Science Reviews* **18**: 993–1019.

1.9 TABLES

Tableau 1.1 Lake Naskaupi stages from previous works

Elevation of Naskaupi lake stages*		
Stage name	Ives (1959)	Barnett and Peterson (1964)
N1	518 m	533 m
N2	457 m	472 m†
N3	411 m	427 m†
N4		360 m
N5		320 m

Tableau 1.2 Naskaupi Lake levels data documented in this study.

Lake Stages*	Elevation†	Number of shorelines	Uplift gradient (m/km)	Coefficient of correlation
Indian House lake area				
N0'	512	15	0.27	0.93
N1'	503	18	0.28	0.94
N2'	472	36	0.16	0.90
N3'	427	10	0.17	0.94
N4'	323	3	0.05	0.35
Pyramid Hills area				
PH1	495	4	0.45	0.91
PH2	454	4	0.23	0.66
PH3	401	8	0.69	0.80
PH4	348	3	0.14	0.05
PH5	306	3	0.27	0.92

* Elevation at the latitude of the northern IHL area (northing 626 000 m).

†Elevation in meter above sea level (m asl).

1.10 FIGURES

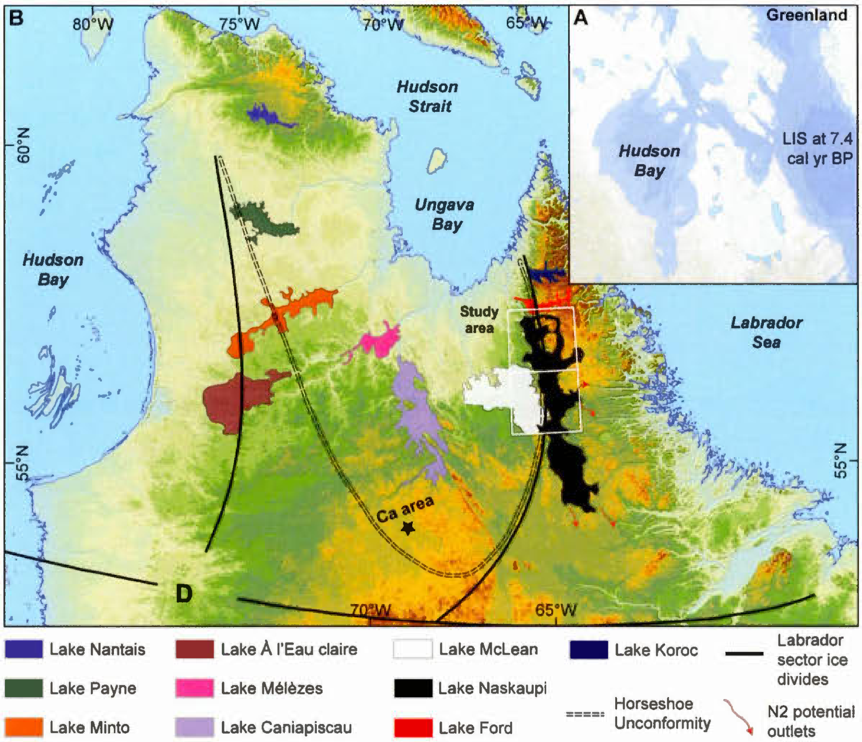

Figure 1.1 (A) The Laurentide ice sheet (LIS) late in the deglaciation (Dyke, 2004). (B) Location of the study area and glacial lakes in the Ungava Bay region (Gray et al., 1993). Also showed: the positions of the ice divides (dark lines) of the Labrador ice dome (D) during the late glacial interval (Dyke and Prest, 1987); the Horseshoe Unconformity (dashed line; Clark et al., 2000); probable outlets (arrows) for the Naskaupi N2 lake stage (Ives, 1960a); and the Lake Caniapiscau area (CA).

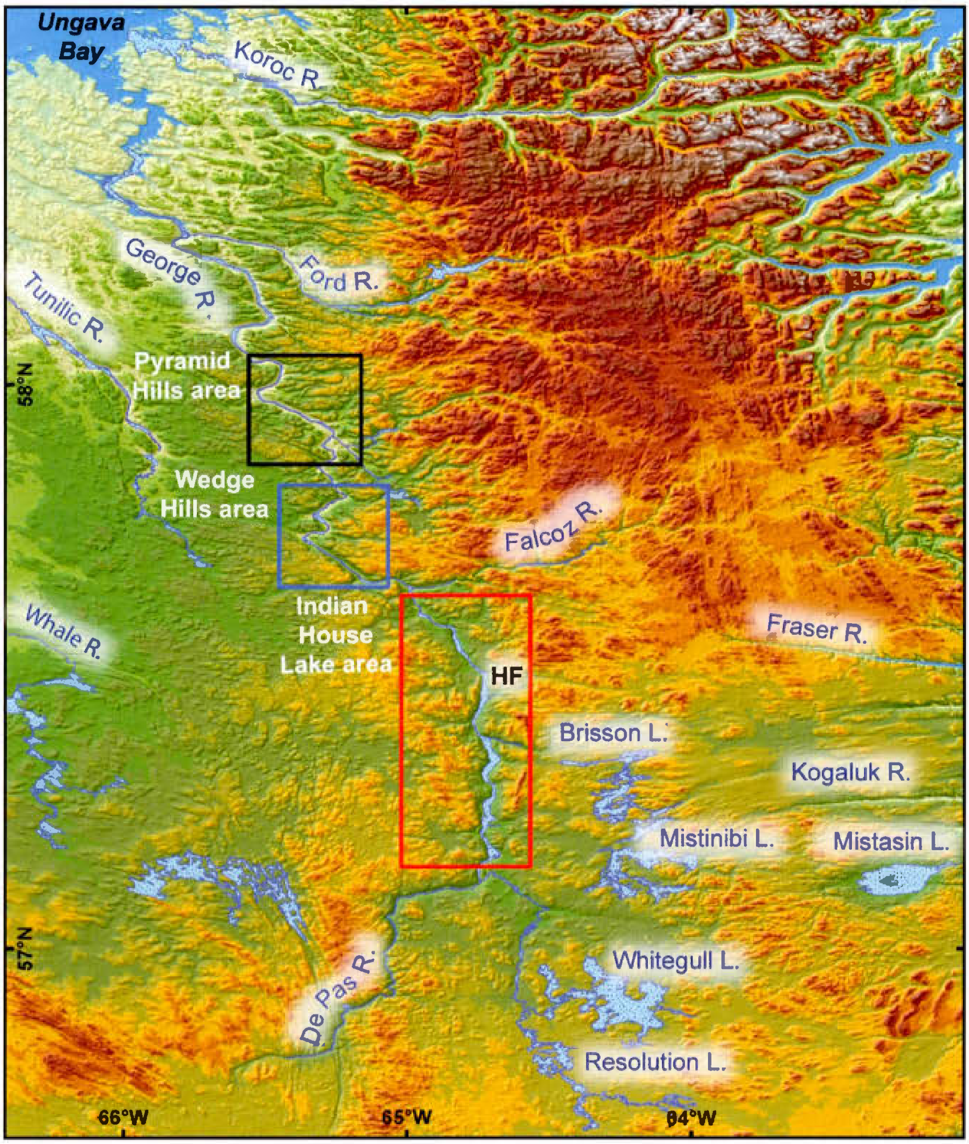

Figure 1.2 Digital elevation model (CDEM; resolution of 12 m) showing the physiography of the George River valley and the three areas (boxes) regrouping the shoreline-elevation data used in the lake-level reconstruction. Also showed are the geographic names used in text. HF: Haute Falaise sector.

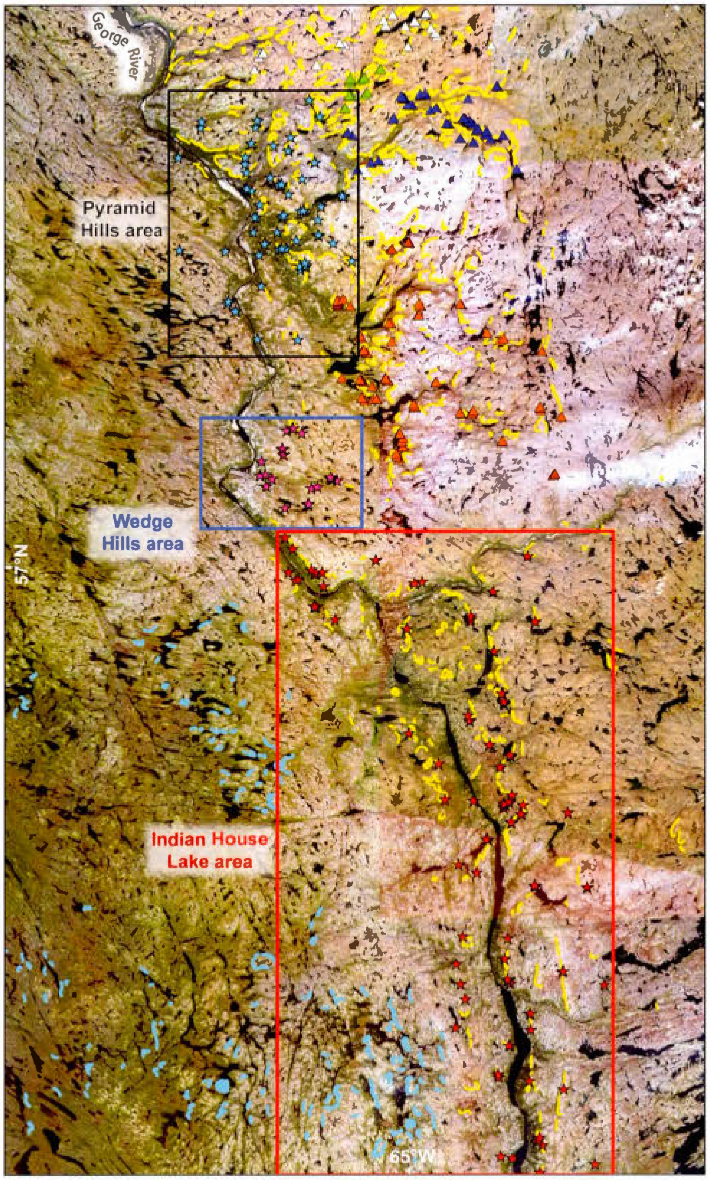

Figure 1.3 Satellite (Rapideye) image showing the distribution of the mapped shorelines (Naskaupi: yellow lines; McLean: light blue lines). Stars show sites of elevation measurements in the Indian House Lake area (red), the Wedge Hills area (pink), and the Pyramid Hills area (blue). Triangles show shorelines measured in the tributary valleys of the Gasnault River (orange), the Siimitalik River (dark blue), the Mitshu River (green), and the Nutillilik River (white).

Figure 1.4 (A) Aerial photograph (1:40,000 scale) showing near-continuous Naskaupi shorelines in the Indian House Lake (IHL) area. (B) Typical Naskaupi shoreline consisting in a well-developed terrace flanked by large boulders (IHL area). (C) Succession of four shorelines (arrows) separated by 10 to 40 m in the Haute-Falaise sector (IHL area). (D) Naskaupi shorelines (arrows) on the emblematic Pyramid Peaks (looking towards the east). Previous work associated these shorelines to the N3, N4 and N5 lake levels (Matthew, 1961a, b). (E) Poorly developed shorelines commonly found in tributary valleys located east of the GRV where shorelines are deformed by solifluction processes.

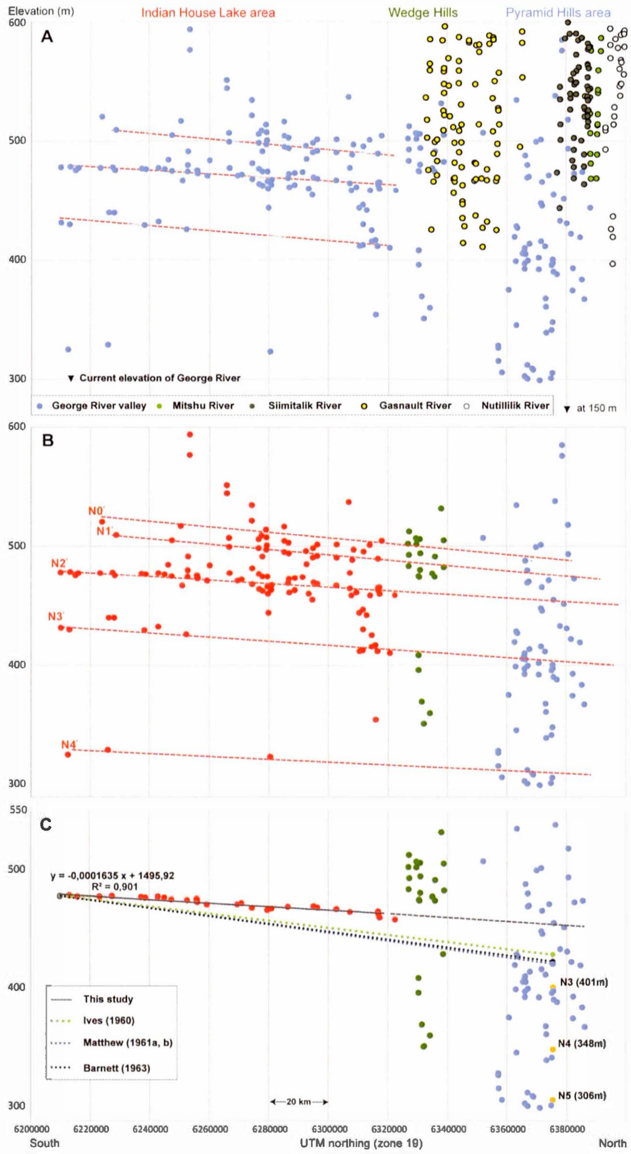

Figure 1.5 (A) Shoreline-elevation data plotted along a north-south transect extending along the GRV. Sub-horizontal alignments of shorelines suggest the presence of at least three lake levels in the Indian House Lake (IHL) area. The continuation of these lake levels in the Wedge Hills and Pyramid Hills (PH) is complicated by the scatter in data. This lack of pattern in the shoreline distribution is due to the shoreline data of the tributary valleys, which cannot be used to reconstruct

lake levels (see text for details). Note the present-day gradient of the river (triangles). (B) Elevation data of shorelines without the tributary basins. Regression lines outline shoreline correlations used to delineate lake levels and to calculate uplift gradients (see Table 2). The N1', N2' and N3' lake levels are well constrained in the IHL area, while the N0' and N4' lake levels are defined by fewer shorelines. (C) Regression lines depicting the regional uplift gradients calculated for N2 (previous studies) and N2' (this study) shorelines. Also showed are the N3, N4, N5 shorelines on Pyramid Peaks (see Figure 4D) and their elevation (this study). Present-day elevation of the George River ranges from 300 m (south) to 150 m (north) in the study area.

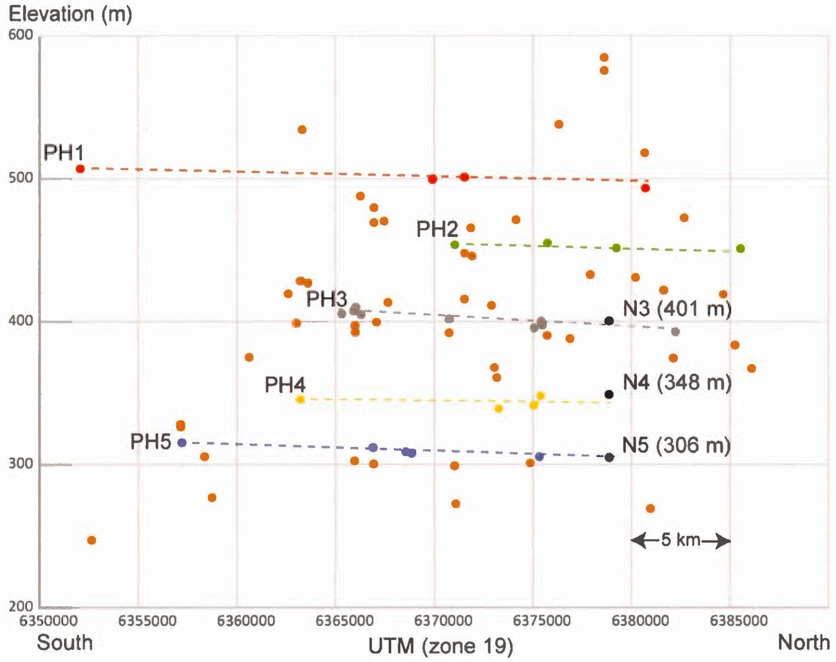

Figure 1.6 Details of the shoreline elevation data from the Pyramid Hills area. The regression lines show correlations of shorelines that may potentially define lake levels. The black dots correspond to the three shorelines described on Pyramid Peaks in earlier studies (see Figure 4D).

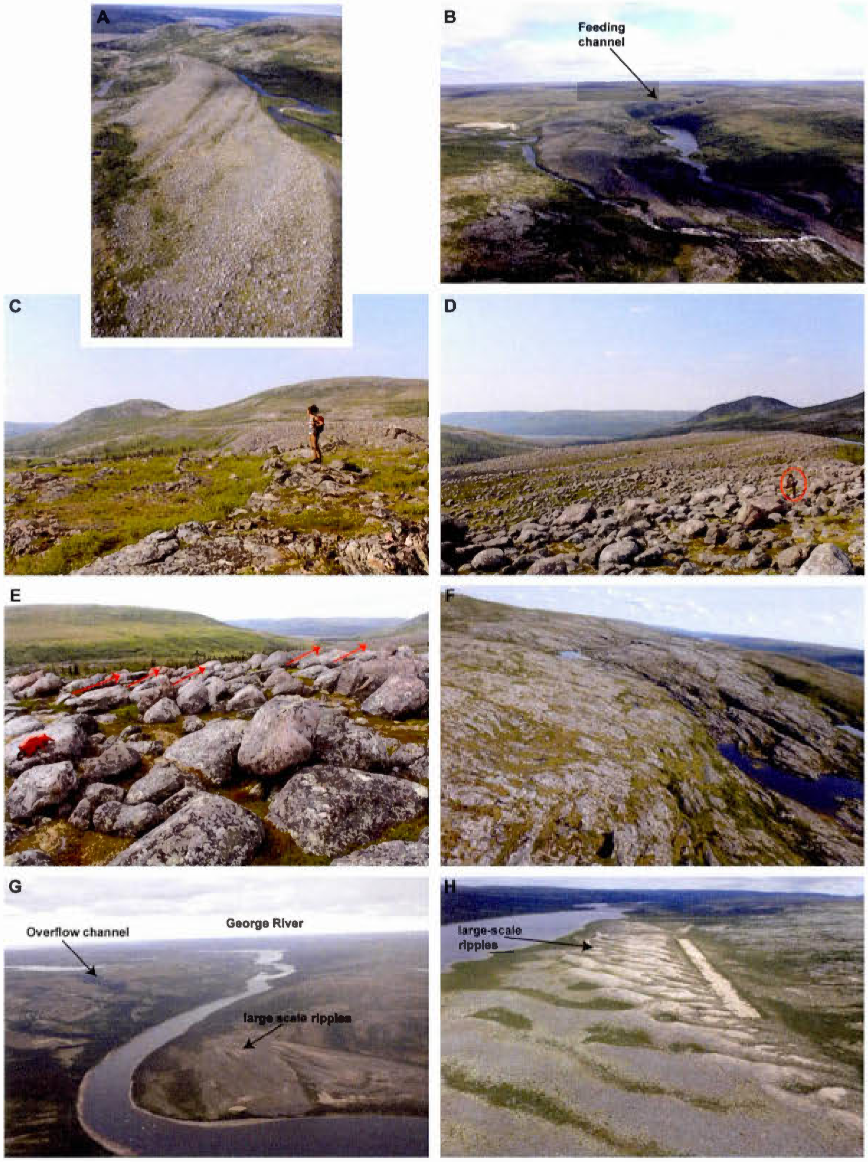

Figure 1.7 Photographs of the meltwater outburst landforms documented in the Wedge Hills area (see Figure 8 for location). (A) Oblique aerial view of the so-called Pinkflood construction consisting in meter-size imbricated boulders arranged in large-scale alluvial bars of ~30 m thick by ~2 km long. View towards the north; George River in background. (B) Meltwater channel incised ~25 m in bedrock located upstream from the alluvial bars. View towards the south. (C-D) Ground view of the

boulders forming the alluvial bars (student for scale). (E) Close-up view of the rounded and multi-metric pink granitic boulders showing an imbrication down-river, toward the north (bag is 60 cm long). (F) Oblique aerial view of bare bedrock surfaces located nearby the Pinkflood construction and indicating massive meltwater erosion. (G) Aerial view looking south into the George River showing overflow channel and large-scale ripples located downstream from the Pinkflood construction. (H) Closer view of the large-scale sand ripples. The airplane landing strip is ~40 m by 700 m. View toward north.

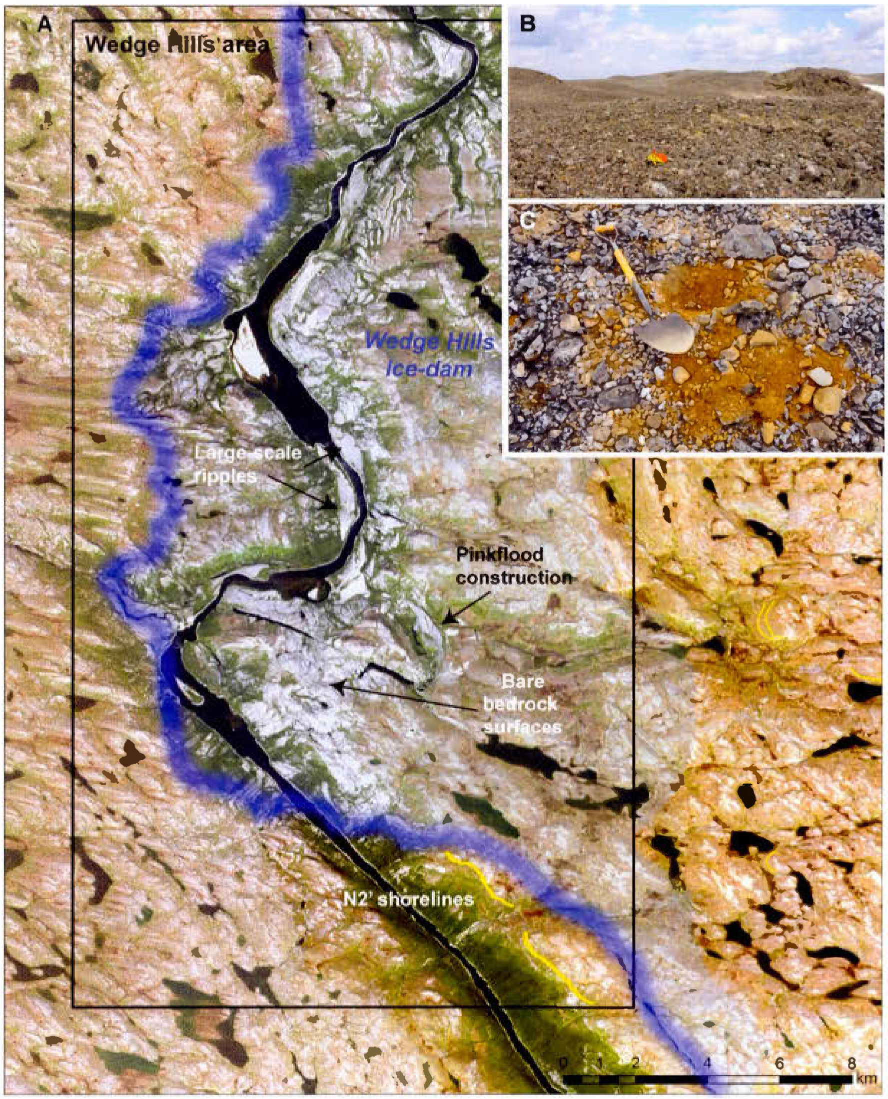

Figure 1.8 (A) Satellite image (Rapideye) showing changes in landforms in the Wedge Hills area. The general area east of the George River is characterized by extensive felsenmeer (B) and thick oxidized deposits (C) that are associated with cold-based ice conditions. The area to the west of the river shows streamlined landforms associated with an earlier deglacial ice flow towards Ungava Bay. The persistence of cold-based ice conditions in the Wedge Hills area caused the damming of this sector and the separation of the Naskaupi basin.

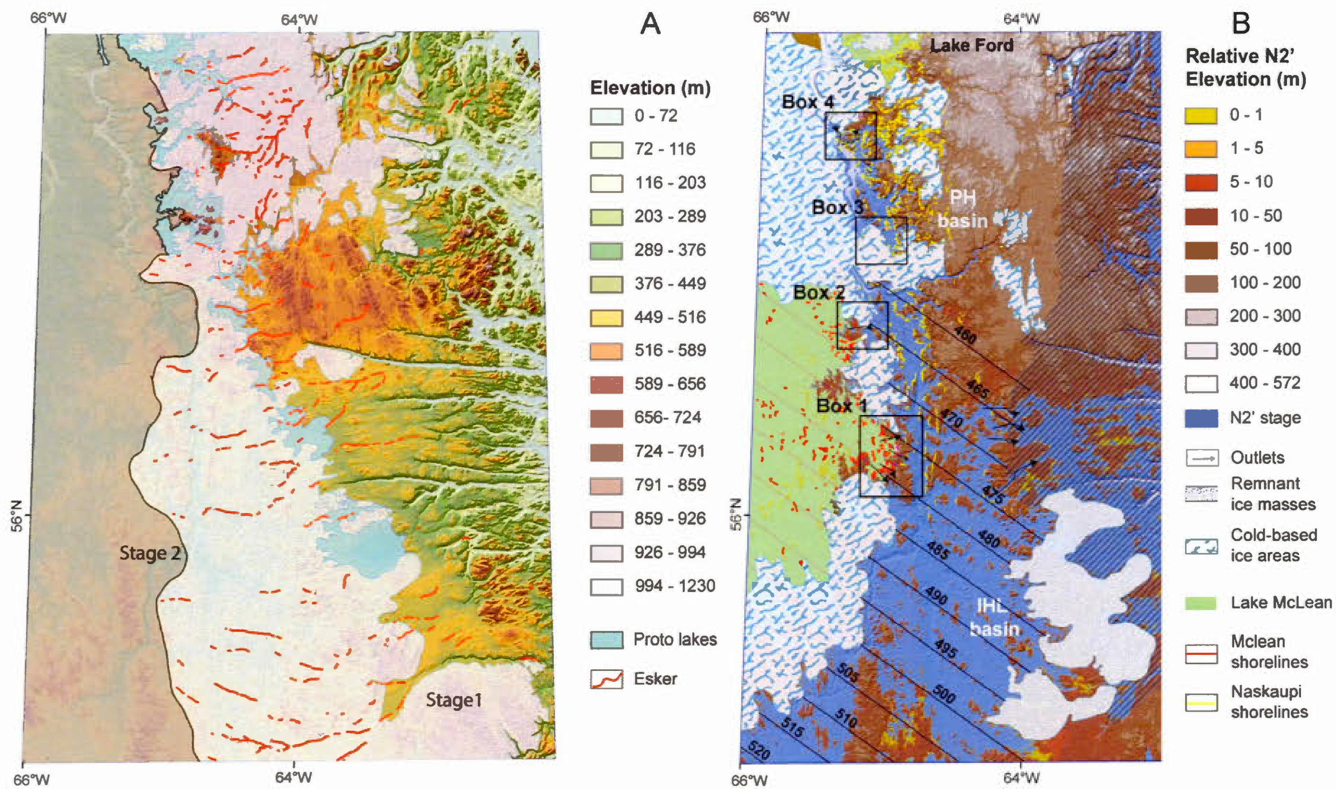

Figure 1.9 Paleogeographic reconstruction showing the development of Lake Naskaupi during the east to west retreat of the ice margin. (A) The ice margin at Stage 1 shows the proto Lake Naskaupi period characterized by the development of small and isolated glaciolacustrine basins that formed as the ice margin freed tributary valleys contiguous to the George River. The deglaciation of this sector is associated with a warm-based ice retreat, as indicated by the numerous eskers (thin red lines) and streamlined landforms. As the ice margin reaches the vicinity of the George River

valley (Stage 2), the sudden disappearance of eskers and numerous lateral meltwater channels indicate a zonation in the subglacial thermal regime, with the occurrence of localized areas of cold-based ice conditions throughout this region. (B) Areal extent of Lake Naskaupi during the N2' lake stage. Oblique black lines in the IHL basin depict the regional isobases (elevation in meters). Boxes 1 to 4 show the areas that are enlarged in Figure 10. Note that the elevations are relative to the N2' waterplane, while the elevations under shaded area to the east are an artefact from the modelling and are not representative.

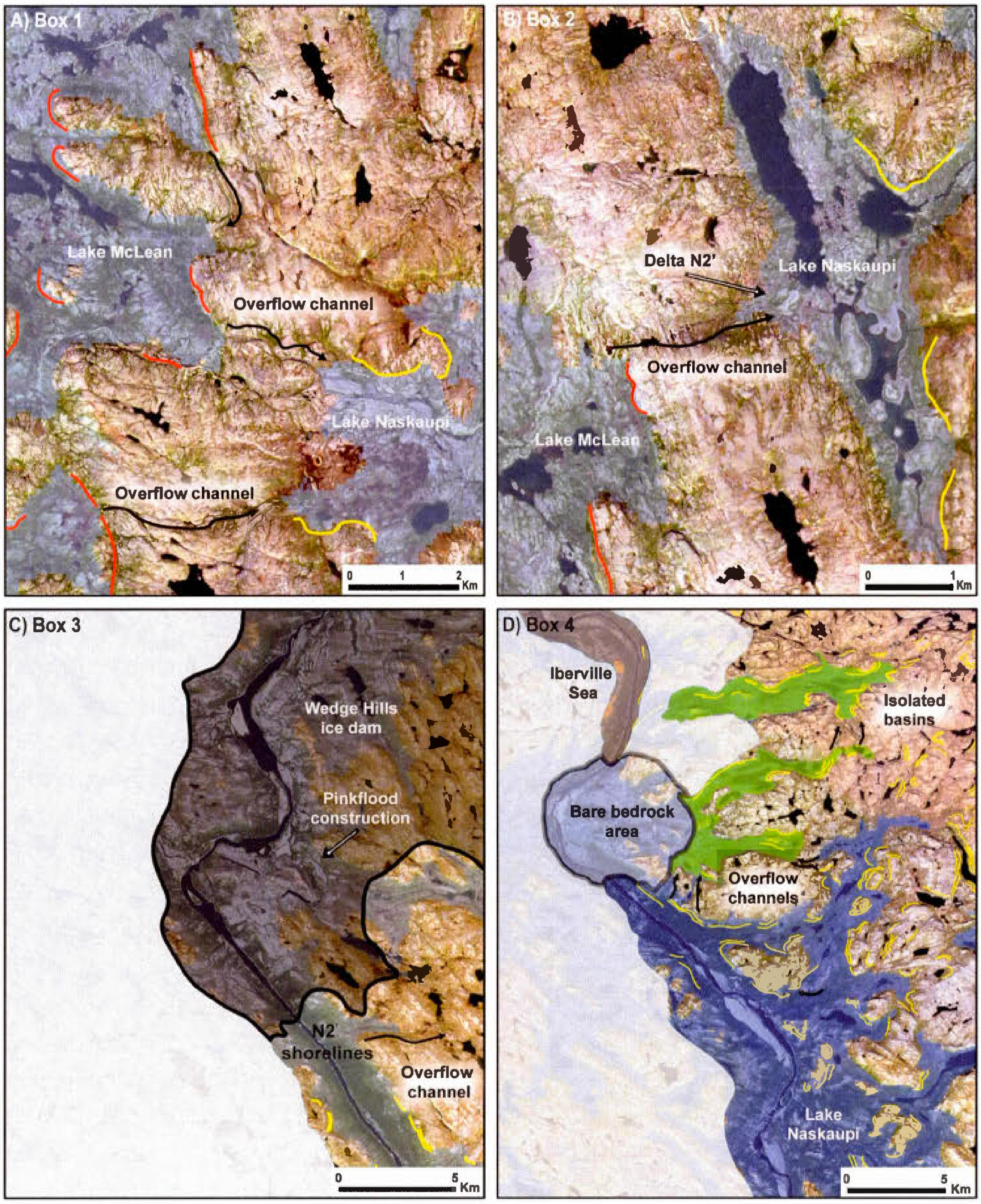

Figure 1.10 Detailed view of the geomorphology of four sectors of the N2' lake stage reconstruction presented Figure 9b. (A) Areal extent of Lake Naskaupi in northwestern part of the IHL basin. The reconstruction shows an excellent fit between

the N2' shorelines (yellow lines) and the location of the meltwater overflow channels coming from Lake McLean (constrained by shorelines in red). (B) Extent of Lake Naskaupi in the northernmost sector of the IHL basin. The location of an overflow channel from Lake McLean feeding a large delta in Lake Naskaupi shows a good agreement with the reconstructed extent of the N2' lake stage. (C) Approximate extent of the cold-based ice dam in the Wedge Hills area (light black shading). The extension of the N2' lake level shows a good fit with the location of shorelines and an overflow channel oriented perpendicular to the George River. (D) Extent of Lake Naskaupi in the northernmost part of the PH basin and the maximum limit of the postglacial Iberville Sea (in brown). These two basins were separated by an ice dam. The large area of bare bedrock (light white area) are interpreted as evidence for massive meltwater erosion during the drainage of the lake (Figure S2). The reconstruction also shows the good agreement between the extent of overflow channels terminating into minor and isolated glaciolacustrine basins (green) occupying tributary basins. An independent lake also occupied the Ford River valley (~70 km to the north), but our investigations showed no connection with Lake Naskaupi.

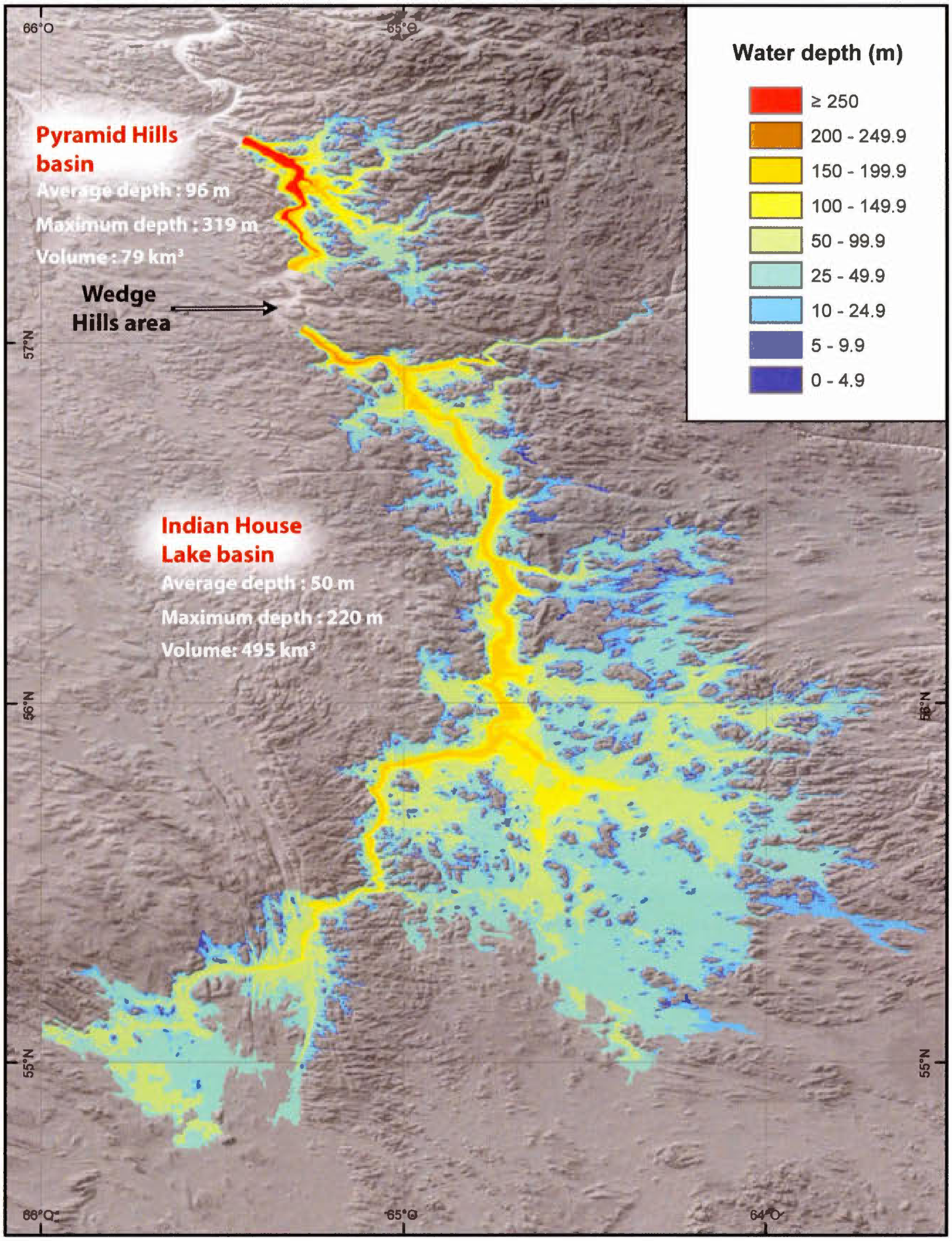

Figure 1.11 Digital elevation model showing the extent and water depth of Lake Naskaupi during the N2' lake stage, which were used to calculate the meltwater volumes contained in the IHL and PH basins.

APPENDICE A

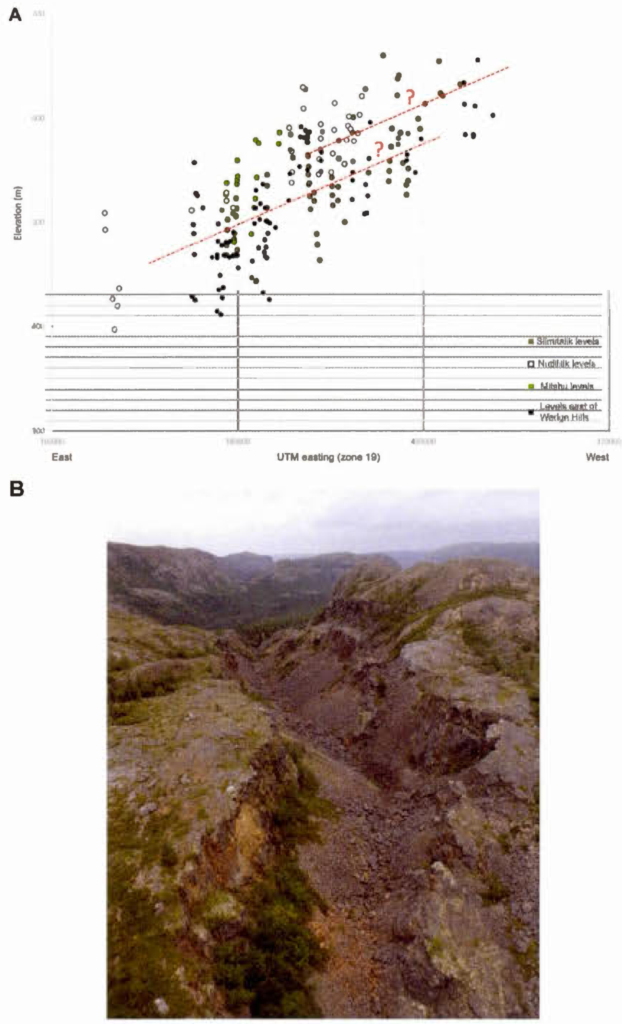

Figure A.1 (A) Elevation data of shorelines measured along east– west transects in tributary valleys located east of the George River valley. These data cannot be used in the lake-level reconstruction due to the lack of consistent pattern (see text for details). (B) Example of spillway channels that record the sudden drainage of these small temporary basins.

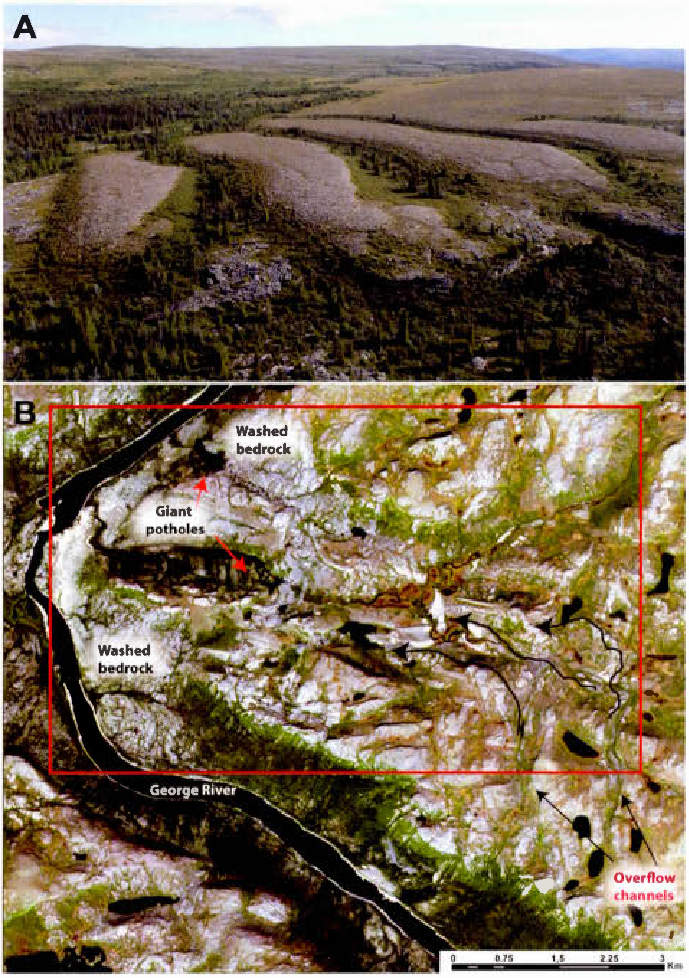

Figure A.2 (A) Typical example of the lateral meltwater channels found west of the GRV and indicating the retreat of an ice margin frozen at its base. Channels were incised into the substrate by meltwater flowing along the ice margin. Channels are ~40m wide by 250m long. (B) Detailed view of the northernmost part of the PH basin. The presence of an ice dam in this sector is suggested by overflow channels perpendicular to the GRV. Abrupt release of meltwater (and erosion) associated with drainage events is indicated by giant potholes and large patches of bare bedrock.

CHAPITRE II

^{10}BE DATING OF FORMER GLACIAL LAKE NASKAUPI (QUEBEC-LABRADOR) AND TIMING OF ITS DISCHARGES DURING THE LAST DEGLACIATION

Hugo Dubé-Loubert[1,2,3], Martin Roy[2,3], Joerg M. Schaefer[4,5] et Peter U. Clark[6]

[1] Bureau de la Connaissance Géoscientifique du Québec, Ministère de l'Énergie et des Ressources Naturelles, 400 boulevard Lamaque, Val-d'Or, Québec J9P 3L4

[2] Département des sciences de la Terre et de l'atmosphère - Université du Québec à Montréal, C.P. 8888, suce. Centre-Ville, Montréal (QC), Canada, H3C 3P8

[3] Centre de recherche Géotop - Université du Québec à Montréal, C.P. **8888,** suce. Centre-Ville, Montréal (QC), Canada, H3C 3P8

[4] Lamont-Doherty Earth Observatory, Geochemistry, 409 Comer Building, 61 Route 9W, P.O. Box 1000, Palisades, NY, 10964, USA

[5] Department of Earth and Environmental Sciences, Columbia University, New York, NY, 10027, USA

[6] College of Earth, Ocean, and Atmospheric Sciences, Oregon State University, Corvallis, OR, 97331, USA

Publié dans *Quaternary Science Reviews* DOI.org/10.1016/j.quascirev.2018.05.008

RÉSUMÉ

Le retrait de la calotte laurentidienne au cours de la dernière déglaciation a mené, dans le secteur nord du Québec, à la formation de plusieurs lacs glaciaires qui se sont drainés à la fin de leur existence via la baie d'Ungava et la Mer du Labrador. Quantifier l'impact potentiel de cet apport en eau de fonte sur les conditions océaniques de surface et le climat demeure toutefois limité par le peu de contraintes chronologiques disponibles en regard de la déglaciation et de l'évolution de ces plans d'eau. Dans cet article, nous présentons 21 nouveaux âges ^{10}Be réalisés sur des lignes de rivage et une construction marquant le drainage du Lac Naskaupi, un des plus importants lacs glaciaires de l'Ungava. Nos résultats indiquent que ce lac aurait débuté à se drainer à partir de sa pleine expansion à 8300 ± 300 a, suggérant qu'il pourrait avoir contribué au forçage climatique holocène initié par le drainage du Lac Agassiz-Ojibway et ayant participé à l'événement de refroidissement de 8,2 ka. Ces nouveaux résultats chronologiques permettent en plus de contraindre la position de la marge glaciaire du Secteur Labrador durant son retrait à travers la région.

ABSTRACT

The last deglaciation of the Laurentide Ice Sheet in northern Quebec and Labrador led to the formation of several glacial lakes that drained into Ungava Bay and the nearby Labrador Sea. Assessing the potential impact of their drainage on ocean surface conditions and climate, however, is limited by the few existing age constraints on ice retreat and associated evolution of these lakes. Here we report 21 ^{10}Be ages from shorelines and an outburst flood landform formed by Lake Naskaupi, one of the largest glacial lakes in this region. The results indicate that the lake drained from its full extent at 8300 ± 300 a, suggesting that it may have contributed to the freshwater forcing initiated by the drainage of Lake Agassiz-Ojibway that caused the 8.2-ka cold event. Additionally, the results provide important constraints on the position of the ice margin of the Labrador Sector during its retreat across this region.

2.1 INTRODUCTION

Retreat of the Laurentide Ice Sheet (LIS) during the last deglaciation caused the formation of glacial lakes around much of its western and southern margins (Dyke, 2004) and routed continental runoff through one of several outlets to the North Atlantic and Arctic oceans (Teller et al., 1990; Licciardi et al., 1999; Wickert, 2016). Episodic drainage of these lakes and routing of freshwater to different outlets may have played an important role in the climate variability during the last deglaciation through their impact on the Atlantic Meridional Overturning Circulation (AMOC) (Barber et al., 1999; Clark et al., 2001; Carlson and Clark, 2012).

Dome of the LIS dammed large rivers flowing into Ungava Bay, forming several large glacial lakes (Figure 2.1) (Ives, 1959, 1960; Barnett, 1963; Gray et al., 1993; Clark et al., 2000; Jansson and Kleman, 2004; Dubé-Loubert and Roy, 2017). These lakes drained when the ice margin retreated sufficiently or became too thin to provide a barrier, allowing them to drain into Ungava Bay. Although smaller than the proglacial lakes that existed at the southern and southwestern LIS margin during the deglaciation (Teller and Leverington, 2004), the Ungava lakes may have contributed to the freshwater forcing that caused climate instabilities of the early Holocene period (Alley et al., 1997). Assessing the importance of their contribution, however, is currently limited by the few existing constraints on their configuration, volume, and chronology. A recent field-based reconstruction of Lake Naskaupi, one of the largest glacial lakes in the Ungava Bay lowlands (Figure 2.1), provides improved constraints on its areal extent, surface-elevation changes, and volume (Dubé-Loubert and Roy, 2017). Here we report ^{10}Be ages on boulders from Lake Naskaupi shorelines as well as on a large outburst flood bar that formed during a rapid drainage event that caused the lake to drop to a lower level. We also estimate the magnitude and duration of this drainage event based on the sedimentology of its associated landforms. These results improve the chronology of the lake evolution and drainage, as well as better constrain the position of the Labrador Ice Dome margin during the deglaciation.

2.2 BACKGOURND ON LAKE NASKAUPI

Lake Naskaupi was originally identified from spectacular sequences of raised shorelines that are exposed along extensive stretches of the George River valley (GRV) (Ives, 1959). Shorelines are typicallywave-cut scarps incised into till that mantles hillslopes of the GRV (Ives, 1959, 1960; Dube-Loubert and Roy, 2017). Shoreline erosion resulted in the formation of 2-12 m-wide terraces that can be followed continuously for tens to hundreds of meters, and up to several km in the southern part of the GRV (Figs. 2.2 and 2.3). The development of the lake required an ice dam located on the lower reach of the George River. Shoreline sequences in the Indian House Lake (IHL) and Pyramid Hills (PH) areas of the GRV (Figs. 2.2 and 2.3) reveal a complex lake-level history marked by at least five lake stages named N1 to N5 (Ives, 1959; Ives, 1960; Matthew, 1961a,b; Barnett, 1963; Barnett, 1967; Barnett and Peterson, 1964). Of these, the shorelines forming the N2 lake level are the best developed and most extensive, and were interpreted as recording the main lake stage (Ives, 1960; Barnett and Peterson, 1964; Barnett, 1967). Despite the large distance separating these two areas (~150 km), correlation of N2 shorelines indicated a single water plane that occupied a large fraction of the George River drainage basin.

Systematic mapping of glacial and deglacial landforms in the GRV recently refined this reconstruction (Dubé-Loubert and Roy, 2017). Based on hundreds of elevation measurements of raised shorelines, four well-defined lake levels were identified (Figure 2.4). Evidence for additional lake levels is present, but the shorelines are poorly developed and less continuous, suggesting short-lived transient stages. A set of well-defined and nearly continuous shorelines corresponding to the N2 lake stage of earlier studies was also identified in the IHL area. However, this major lake level (renamed N2') has no clear equivalent in the PH area to the north (Figure 2.4). At this time, Lake Naskaupi occupied two basins that evolved independently as long as they were separated by an ice dam near the Wedge Hills area (Dube-Loubert and Roy, 2017). A DEM-based reconstruction of a lake extent equivalent to the N2' stage yielded a volume of 575 km3 for the combined southern (IHL) and northern (PH) basins. Large-scale bouldery flood deposits record the abrupt drainage and lowering of the N2' lake level in the southern Naskaupi basin associated with the collapse of the ice dam (Figure 2.5). Lake Naskaupi subsequently extended throughout the entire GRV during the remaining two lower stages (N3' and N4'), which also ended with significant lake-surface drawdowns (Figure 2.4) and concomitant meltwater discharges (Dubé-Loubert and Roy, 2017).

2.2.1 Lake Naskaupi chronology

There are few existing age constraints for Lake Naskaupi. Radiocarbon (^{14}C) ages obtained on bulk organic matter from sediment cores within the George River basin gave ages of 8610 ± 925 ^{14}C a BP (9630 ± 1040 cal a BP) and 6815 ± 125 ^{14}C a BP (7680 ± 110 cal a BP) (Short and Nichols, 1977; Short, 1981; ^{14}C ages are calibrated using CALIB 7.1 (Stuiver et al., 2018), with the large age differences and uncertainties likely reflecting the low abundance of organic material and/or contamination by old organic carbon (Clark and Fitzhugh, 1990). These results were interpreted as minimum ages reflecting the onset of the lake after 9630 cal a BP and its disappearance before 7680 cal a BP (Ives, 1976). Similarly these ages were used in paleogeographic reconstructions to constrain the position of the retreating LIS margin (Dyke, 2004), in which the onset of the development of Lake Naskaupi is placed at around 10,000 cal a BP (9000 ^{14}C a BP), with full development at 9400 cal a BP (8400 ^{14}C a BP).

Deglaciation ages of the Ungava Bay coast to the north and the Labrador coast to the east suggest a younger age for Lake Naskaupi. A minimum age for the final drainage of Lake Naskaupi may be inferred from the timing of the postglacial marine incursion in southeastern Ungava Bay, assumed to be coincident with the collapse of the ice dam, for which 14C dating of marine shells in the George River estuary assigns at 7380 ± 90 a BP (7700 ± 120 cal a BP) (Allard et al., 1989; calibrated with CALIB 7.1 (and a DR of 145± 95 years (Coultard et al., 2010)). The marine incursion, however, is poorly constrained and the ice dam holding the lake may still have existed when the Iberville Sea submerged the Ungava Bay lowlands. Dating of the marine limit on the Labrador coast yielded 14C ages implying that the deglaciation of the central coast east of the GRV occurred between 7600 ± 200 14C a BP (8070 ± 200 cal a BP) and 8500 ± 200 14C a BP (9140 ± 250 cal a BP) (Clark and Fitzhugh, 1990, 1992). Considering that the ice margin had to retreat westward from the coast prior to damming the lake in the GRV, Clark and Fitzhugh (1990) concluded that the earliest the lake could have formed was <8070 cal a BP and that the main stages of Lake Naskaupi developed after 9140 cal a BP.

2.3 ^{10}BE METHODS

We determined ^{10}Be ages on 16 boulders from well-developed shorelines at four sites in the GRV (Figs. 2.2 and 2.4). Two sites are associated with the N2' lake level in the IHL area of the southern Naskaupi basin (Figure 2.3A), and two sites are from the N30 lake level in the PH area (Figure 2.3B) (Dubé-Loubert and Roy, 2017). We also dated four boulders from meltwater outburst landforms in the Wedge Hills area that record the abrupt drainage of the N2' level from the southern Naskaupi basin (Figs. 2.2 and 2.5; site 14HDLPF). The metersize rounded to sub-rounded boulders with a down-river imbrication that form the so-called Pinkflood construction indicate a significant meltwater discharge during this event (Figure 2.5A-E). Finally, we dated a bedrock surface exposed by meltwater erosion of the overlying sediments during the outburst flood event (Figure 2.5F). We used a rock saw to sample approximately 500 g from the upper two cm of the boulder/bedrock surfaces. The boulders and bedrock surface sampled show no evidence of weathering. We chose large boulders (>1m) with bases well anchored in the terrace to avoid any potential post-depositional movements. Boulder surfaces stood at least 1m above the ground to minimize shielding caused by snow cover. All sampling sites were located in open areas, on the crest of hill slopes facing the GRV, ensuring windy conditions that likely prevented any significant snow accumulation. However, assuming our boulders were covered by 0.5m of snow ($\rho = 0.3$ g cm^{-3}) for six months of the year would require a correction of ~3% (Gosse and Phillips, 2001), which is within the age uncertainties from the scaling and production rates calculations. Lake Naskaupi shorelines were formed by reworking of glacial deposits, which were produced by erosional processes (plucking and abrasion) that should have removed inherited cosmogenic signal from previous exposure. Wave erosion removed the finegrained sediment fraction of the deposits, leaving boulder-cored terraces that mark the former lake levels (Figure 2.3C and D). Because the shallow water (<2m) during shoreline formation would only slightly attenuate cosmic rays, we interpret our ages as closely recording the time of shoreline formation rather than shoreline abandonment.

Sample preparation and quartz separation were carried out according to standard laboratory protocols developed at the Lamont- Doherty Earth Observatory Cosmogenic Dating Laboratory (Schaefer et al., 2009). The $^{10}Be/^{9}Be$ ratios were measured at Lawrence Livermore National Laboratory (California, USA). Ages were calculated with version 3 of the online calculator (https://hess.ess. washington.edu) using the Baffin Bay/Arctic 10Be production rate of 3.96 ± 0.15 atoms g^{-1} yr^{-1} (Young et al., 2013) and the nuclide- and time-dependent LSDn scaling scheme (Lifton et al., 2014).

Northeastern Canada has experienced significant post-glacial rebound since the initial deglaciation of the study area, causing ^{10}Be production rates to increase since deglaciation (Cuzzone et al., 2016; Ullman et al., 2016). Additionally, changes in atmospheric depth due to local air pressure evolution in a changing deglacial climate can also have an effect on the ^{10}Be production rates (Stone, 2000; Staiger et al., 2007). We quantify the time-varying effects of uplift and atmospheric pressure on ^{10}Be production rates since exposure of our sites (8.5 ka) following the method established by Cuzzone et al. (2016) and Ullman et al. (2016). We estimated elevation changes at our sites since deglaciation from an isostatic surface loading model with a spatial resolution of 50 km (Mitrovica et al., 1994) that includes the influence of ice loading (using the ICE- 5G reconstruction of ice thickness and its partnering Earth viscosity model, VM2; Peltier, 2004), ocean loading (Mitrovica and Milne, 2003) and variations in Earth rotation (Mitrovica et al., 2005). This method provides an accurate estimate of the vertical land motion, without the intricate effects of global mean sea level (GMSL) rise and the gravitational attraction caused by ice-sheet remnants, which are inherently present in local relative sea level record. The model's ~50-km spatial resolution is fully adequate to capture the spatial variability in the pattern of uplift, mostly because the lithosphere responds as a low-pass filter to the deformation induced by ice-loading. We estimate the time of initial deglaciation as 8.5 ka based on our uncorrected ^{10}Be ages, from which we derive a time-averaged uplift for our sites of 38m. This site-averaged uplift is then subtracted from the measured site elevation, and the corrected elevation is used to calculate the ^{10}Be age (Table 2.1).

The impact of evolving atmospheric pressure due to changing post-glacial climate (Stone, 2000; Staiger et al., 2007) has been estimated for formerly glaciated regions in Fennoscandia (Cuzzone et al., 2016) and south-central Quebec (Ullman et al., 2016) that experienced similar deglacial climate change as our sites. These studies used a coupled atmospheric-ocean general circulation model that indicated an average elevation correction order of 1e10m for these sites, or small enough to exclude from the overall exposure age calculations. Accordingly, we also expect that this atmospheric effect in our study area is negligible, with any corresponding impact on elevation falling within the measurement uncertainties.

We report the glacial lake shoreline or outburst deposit age and its uncertainty by first assessing the geologic uncertainty and average analytic uncertainty of our sample populations (Cuzzone et al., 2016; Barth et al., 2018). The geologic uncertainty is defined as the standard deviation of the boulder ages for each landform. This is compared to the average analytic uncertainty, defined as the average of the AMS measurement uncertainty on each sample from each landform. In the case where the geologic uncertainty is larger than the average analytic uncertainty, the landform age is defined by the arithmetic mean of the sample population and the standard error of the ages (the standard deviation of the ages divided by the square root of the number of samples). Conversely, where the average analytic uncertainty is larger than the geologic uncertainty, we define the landform age as the error-weighted mean of the sample population and the error-weighted uncertainty (one over the sum of one divided by the squared analytic uncertainty for each sample). Although this approach provides the most conservative estimate of landform age and uncertainty, the differences between the twoways of reporting landform age are negligible. In particular, the ages from the two methods differ by < 100 yr, which is well within the landform age uncertainty. We add the production rate uncertainty in quadrature when comparing our ^{10}Be ages to ages based on other dating methods.

2.4 RESULTS : ^{10}BE AGES

^{10}Be ages are presented in Table 1. Analytical uncertainties range between 1.9 and 3.8%. The ^{10}Be concentrations from each landform are generally internally consistent (Table 2.3), with only two boulders (13HDL04-09, 14HSLPF-03) having ages that fall outside the range of the main age cluster in the sample distribution (15,200 ± 300 a and 10,300 ± 200 a; Figure 2.6A), likely reflecting inheritance from previous exposure.

The ^{10}Be ages obtained for eight boulders on two sample sites from N2' shorelines in the IHL area (13HDL06 and 13HDL07) are in ood agreement and yield a mean age of 8200 ± 200 a (Figure 2.6B). The ^{10}Be ages on 7 boulders sampled from two N3' shorelines in the PH area (13HDL01 and 13HDL04) also have good agreement, with a mean age of 8300 ± 200 a (Figure 2.6C). The three boulders and one bedrock sample associated with the outburst drainage event have a mean age of 8500 ± 200 a (Figure 2.6 D).

2.5 PALEOHYDRAULIC CALCULATIONS

Based on the geometry of the canyon through which the meltwater flowed and the sedimentology of the outburst flood bars, we calculated the discharge related to the abrupt lowering of the N2' level in the southern Naskaupi basin using the relation $Q = Av$, where Q is the discharge ($m^3\ s^{-1}$), A is the cross-sectional area of the channel (m^2), and v is the velocity ($m\ s^{-1}$). We determined flood velocity (v) using the equation $v = 0.18\ d^{0.487}$, where d is the b-axis diameter of a clast in mm (Costa, 1983). Our measured b-axes range from 1.5 to 3.5 m, with an average of 2.1m (n = 12; Figure 2.5E), while the average width and depth of the channel is 640 m and 70 m, respectively (Table 2.2). Based on these parameters and a lake volume drop between N2' and N3' of 165 km^3, we calculate an average and maximum paleodischarge of 314,500$m^3\ s^{-1}$ and 429,000$m^3\ s^{-1}$, which lasted 2.2 and 1.6 days, respectively.

2.6 DISCUSSION

The mean ^{10}Be ages of 8200 ± 400 a and 8300 ± 400 a (production rate uncertainties now included) for the N2' and N3' lake levels are statistically indistinguishable from each other. Their similar age is further supported by the mean age of 8500 ± 300 a obtained on the flood deposit associated with the lowering of the N2' level. These results are consistent with ^{14}C dating of marine shells at the mouth of George River (7700 ± 120 cal a BP; Allard et al., 1989), which indicates that a significant fraction of Ungava Bay was likely ice free around this time interval, thereby allowing the final drainage of Lake Naskaupi. Given these coherent geochronological constraints, we conclude that the best estimate for the age of Lake Naskaupi is the mean age of the three landforms (8300 ± 300 a). Considering that the N2 and N3 shorelines dated represent the best-developed lake levels in the Naskaupi basin, which formation implies longer duration stages, as opposed to the poorly-developed shorelines formed during short-lived/transient stages (Dubé-Loubert and Roy, 2017), their similar ages indicate that these lake levels developed during a narrow time interval that falls within the dating error of this mean age. Within this geological context, these results suggest that the lake had a likely duration of only a few centuries. This mean age for Lake Naskaupi is similar to the 8070 cal a BP age estimated in a previous reconstruction (Clark and Fitzhugh, 1990), but significantly younger than inferred by basal ^{14}C ages on sediment cores of 9630 ± 1040 cal a BP (8610 ± 925 14C a BP; Short, 1981) that are currently used to constrain retreat of the Labrador Ice Dome in this region (Dyke and Prest, 1987; Dyke, 2004).

Our paleohydraulic modeling provides constraints on the freshwater discharge from the drainage of Lake Naskaupi. The reconstruction of Naskaupi lake levels indicates that the lake experienced at least three significant drawdowns involving lakesurface lowering of 40-50m (Figure 2.3). Since ice of the Labrador Sector still had to occupy part of Ungava Bay to allow the formation of the lake, the first two drawdowns must have occurred subglacially, while the third one relates to the final drainage of the lake following deglaciation of the upper GRV (Dubé-Loubert and Roy, 2017). Our modeling indicates that the lake drainage from the southern Naskaupi basin had an average discharge of 314,500m^3 s^{-1} (0.3 Sv) over 2 days, about the same order of magnitude as a previous estimate based on a remote sensing (Jansson and Kleman, 2004), although the lake history and drainage route used in this approach differ significantly from the field-based reconstruction we used. Given our constraints on the temporal evolution of Lake Naskaupi, similar discharges likely occurred during the other lake-lowering events until the final lake drainage. The mean ^{10}Be age obtained for two of the main stages of Lake Naskaupi and one of the earliest lake drawdowns (8300 ± 300 a) suggests that the lake may have developed and drained during the 160-yr long 8.2-ka cold event (Thomas et al., 2007). This abrupt cooling is commonly attributed to a perturbation of the AMOC that was triggered by the drainage of the coalescent Lakes Agassiz and Ojibway (Barber et al.,1999), for which numerical modeling yields a freshwater flux estimate of 5 Sv over 0.5 yr, in addition to underline the possible occurrence of multiple filling and flooding events (Clarke et al., 2004) e a mechanism supported by several studies that provide evidence for a two-step drainage (Thorleifson, 1996; Leverington et al., 2002; Ellison et al., 2006; Hillaire-Marcel et al., 2008; Kleiven et al., 2008; Roy et al., 2011; Törnqvist and Hijma, 2012). Recently, however, Roy et al. (2015) and Godbout et al. (2017) found that the configuration of Lake Agassiz-Ojibway prior to its final drainage was likely smaller than previously considered, suggesting smaller floods than those estimated through glaciological modeling (Clarke et al., 2004). Moreover, climate modeling suggests that drainage of Lake Agassiz-Ojibway alone was insufficient to perturb the AMOC (LeGrande and Schmidt, 2008; Clarke et al., 2009; Morrill et al., 2014), and that a combination of lake drainage and rerouted runoff following collapse of ice over Hudson Bay was instead required (Meissner and Clark, 2006; Carlson et al., 2009). These studies thus suggest that the 8.2 ka event is likely to be the result of a complex freshwater-forcing history (Jennings et al., 2015; Lawrence et al., 2016). Within this context, our new results suggest that, although small, drainage of Lake Naskaupi − and possibly other glacial lakes around Ungava Bay, such as Lake McLean (Figure 2.1) −would have contributed to the freshwater forcing of the 8.2-ka event that was initiated by drainage of Lake Agassiz-Ojibway.

The ^{10}Be ages on the Naskaupi shorelines also provide important chronological constraints on the deglaciation pattern of the northeastern flank of the Labrador Sector. Considering that the presence of raised shorelines requires the ice margin to be located in the lower reach of the George River in order to dam the lake, the shorelines dated provide minimum-limiting ages on the nearby ice margin that bounds the western edge of the Naskaupi basin. Our five dated sites form a north-south transect that closely parallels the retreating ice margin across the mainland of north-central Quebec and adjacent Labrador (Figure 2.7). Our results thus add new temporal constraints to studies that document the timing of the east-to-west regional pattern of ice withdrawal in Ungava-Labrador (Clark et al., 2003; Dyke, 2004; Marquette et al., 2004; Staiger et al., 2005) and supports evidence for the rapid demise of the Labrador Dome after Hudson Bay became seasonally ice free at 8.2 ka (Ullman et al., 2016).

2.7 CONCLUSIONS

Changes in volume and extent of the LIS throughout the last deglaciation resulted in the release of vast amounts of meltwater to the ocean. The routing of meltwater was controlled in places by the pattern of ice withdrawal, which impeded drainage pathways and caused the formation of glacial lakes such as Lake Naskaupi. Exposure dating of shorelines and outburst flood landforms marking the main stages of Lake Naskaupi provides the first direct age constraints on the development and drainage of glacial lakes in northern Quebec-Labrador. Our ^{10}Be ages indicate that Lake Naskaupi developed and subsequently drained over a short time interval around 8300 ± 300 a, suggesting that drainage of Lake Naskaupi contributed to the freshwater forcing that caused the 8.2-ka cold event. Although Lake Naskaupi is much smaller than Lake Agassiz-Ojibway, it is one of 10 other glacial lakes in Ungava that developed and likely drained over the same time interval, so that the combined freshwater would have been an important component of the forcing of the 8.2-ka event.

Our new ^{10}Be ages also constrain the timing of retreat of the Labrador Sector ice margin across northeastern Quebec and Labrador, thereby improving paleogeographic reconstructions (Clark et al., 2000; Dyke, 2004) and supporting arguments for century scale demise of the Labrador Dome (Ullman et al., 2016). ^{10}Be dating of the other Ungava glacial lakes should improve our understanding of the history and timing of meltwater discharges of the late deglaciation and their potential role in freshwater forcing of AMOC changes.

2.8 ACKNOWLEDGMENTS

Logistical support for this study was obtained through a mapping program of the Ministry of Energy and Natural Resources of Quebec (MENRQ). Assistance during fieldwork was provided by V. Daubois, S. H_ebert, O. Lamarche and I. Randour. Discussions with J. Ives and J. Veillette were greatly appreciated. P.-M. Godbout assisted in the production of PDF graphs. Uplift data were kindly provided by Glenn Milne (U. of Ottawa). Financial support came from MENRQ (HDL, MR), a NSERC Discovery Grant (MR) and the Climate Center of LDEO (JMS, MR). BCGQ external contribution no. 8449-2017-2018-08. This paper benefited from constructive comments by two anonymous reviewers.

2.9 REFERENCES

Allard M., Fournier A., Gahé E., Séguin M.K., 1989. Le Quaternaire de la côte sud-est de la baie d'Ungava, Québec nordique. Géographie Physique et Quaternaire 43, 325–336.

Alley R.B., Mayewski P.A., Sowers, T., Stuiver M., Taylor K.C., Clark P.U., 1997. Holocene climatic instability: A prominent, widespread event 8200 yr ago. Geology 25, 483-486.

Barber D.C., Dyke A., Hillaire-Marcel C., Jennings A.E., Andrews J.T., Kerwin M.W., Bilodeau G., McNeely R., Southon J., Morehead M.D., Gagnon J-M., 1999. Forcing of the cold event of 8200 years ago by catastrophic drainage of Laurentide lakes. Nature 400, 344–348.

Barnett D.M., 1963. Former pro-glacial lake shorelines as indicators of the pattern of deglaciation of the Labrador/Ungava Peninsula. McGill Sub-Arctic Research Papers 15, 23–33.

Barnett D.M., 1967. Glacial Lake MacLean and its relationship with Glacial Lake Naskaupi. Geographical Bulletin 9, 96–101.

Barnett D.M., Peterson J.A., 1964. The significance of Glacial Lake Naskaupi 2 in the deglaciation of Labrador Ungava. Canadian Geographer 8, 173–181.

Barth A.M., Clark P.U., Clark J., Roe G.H., Marcott S.A., McCabe A.M., Caffee M.W., Cuzzone J.K., Dunlop P., 2018. Persistent millennial-scale glacier fluctuations in Ireland between 24 ka and 10 ka. Geology, doi:10.1130/G39796.1

Carlson A.E., Clark P.U., Haley B., Klinkhammer G.P., 2009. Routing of western Canadian Plains runoff during the 8.2 ka cold event. Geophysical Research Letters 36, doi:10.1029/2009GL038778.

Carlson A.E., Clark P.U., 2012. Ice sheet sources of sea level rise and freshwater discharge during the last deglaciation. Reviews of Geophysics 50, 1-72.

Clark D.C., Knight J.K., Gray J.T., 2000. Geomorphological reconstruction of the Labrador Sector of the Laurentide Ice sheet. Quaternary Science Reviews 19, 1343-1366.

Clark P.U., Fitzhugh, W.W., 1990. Late deglaciation of the Central Labrador Coast and its implications for the Age of Glacial Lakes Naskaupi and McLean and for Prehistory. Quaternary Research 34, 296-305.

Clark P.U., Fitzhugh, W.W., 1992. Postglacial relative sea level history of the Labrador coast and interpretation of the archaeological record. Chapter 9 in L.L. Johnson (ed.), Paleoshorelines and Prehistory: an investigation of method, Boca Raton, 189-213.

Clark P.U., Marshall S., Clarke G.K.C., Hosteler S.W., Licciardi J.M., Teller J.T., 2001. Freshwater forcing of abrupt climate change during the last glaciation. Science 293, 283-287.

Clark P.U., Brook E.J., Raisbeck G.M., Yiou F., Clark J., 2003. Cosmogenic ^{10}Be ages of the Saglek Moraines Torngat Mountains, Labrador. Geology 7, 617-620.

Clarke G.K.C., Leverington D.W., Teller J.T., Dyke A.S., 2004. Paleohydraulics of the last outburst flood from glacial Lake Agassiz and the 8200 BP cold event. Quaternary Science Reviews 23, 389–407.

Clarke G.K.C., Bush A.B.G., Bush J.W.M., 2009. Freshwater Discharge, Sediment Transport, and Modeled Climate Impacts of the Final Drainage of Glacial Lake Agassiz. Journal of Climate 22, 2161-2180.

Coultard R.D., Furze M.F.A., Pieñkowski A.J., Nixon C., England J.H., 2010. New marine ΔR values for Arctic Canada. Quaternary Geochronology 5, 419-434.

Costa, J.E., 1983. Paleohydraulic reconstruction of flash-flood peaks from boulder deposits in the Colorado Front Ranges. Geological Society of America Bulletin 94, 986-1004.

Cuzzone, J.K., Clark, P.U., Carlson, A.E., Ullman, D.J., Rinterknecht, V.R., Milne, G.A., Lunkka, J.P., Wohlfarth, B., Marcott, S.A., Caffee, M., 2016. Final deglaciation of the Scandinavian Ice Sheet and implications for the Holocene global sea-level budget. Earth and Planetary Science Letters 448, 34-41.

Dubé-Loubert H., Roy M., 2017. The development, evolution and drainage of glacial Lake Naskaupi during the deglaciation of north-central Quebec and Labrador. Journal of Quaternary Science 32, 1121-1137.

Dyke A.S., 2004. An outline of North American Deglaciation with emphasis on central and northern Canada. Developments in Quaternary Science 2, 373-424.

Dyke A.S., Prest V.K., 1987. Late Wisconsinan and Holocene retreat of the Laurentide Ice Sheet, Géographie Physique et Quaternaire 41, 237–263.

Ellison C.R.W., Chapman M.R., Hall I.R., 2006. Surface and deep ocean interactions during the cold climate event 8200 years ago. Science 312, 1929-1932.

Godbout P.M., Roy M., Veillette J.J., Schaefer J.M., 2017. Surface exposure dating of Lake Agassiz-Ojibway shorelines suggests a reassessment of the volume of meltwater discharges during the late deglaciation. Quaternary Research 88, 265-276.

Gosse J.C., Phillips, F.M., 2001. Terrestrial in situ cosmogenic nuclides: theory and application. Quaternary Science Reviews 20, 1475-1560.

Gray J., Lauriol B., Bruneau D., Ricard J., 1993. Postglacial emergence of Ungava Peninsula, and its relationship to glacial history. Canadian Journal of Earth Sciences 30, 1676–1696.

Hillaire-Marcel C., Hélie J-F., McKay J., de Vernal A., 2008. Elusive isotopic properties of deglacial meltwater spikes into the North Atlantic: example of the final drainage of Lake Agassiz. Canadian Journal of Earth Sciences 45, 1235–1242.

Ives J.D., 1959. The former ice-dammed lakes and the deglaciation of the middle reaches of the George River valley. McGill Sub-Arctic Research Papers 6, 9–44.

Ives J.D., 1960. Former ice-dammed lakes and the deglaciation of the middle reaches of the George River Labrador-Ungava. Geographical Bulletin 14, 44–70.

Ives J.D., 1976. The Saglek Moraines of Northern Labrador: a commentary. Artic and Alpine Research 8, 403-408.

Jansson K.N., Kleman J., 2004. Early Holocene glacial lake meltwater injections into the Labrador Sea and Ungava Bay. Paleoceanography 19, doi:10.1029/2003PA000943

Jennings A., Andrews J., Pearce C., Wilson L., Ólfasdótttir S., 2015. Detrital carbonates peaks on the Labrador shelf, a 13-7 ka template for freshwater forcing from the Hudson Strait outlet of the Laurentide Ice Sheet into the subpolar gyre. Quaternary Science Reviews 107, 62-80.

Kleiven, H.K., Kissel, C., Laj, C., Ninnemann, U.S., Richter, T.O., Cortijo, E., 2008. Reduced North Atlantic deep water coeval with the glacial Lake Agassiz freshwater outburst. Science 319, 60–64.

Lawrence T., Long A.J., Gehrels W.R., Jackson L.P., Smith D.E., 2016. Relative sea-level data from southwest Scotland constrain meltwater-driven sea-level jumps prior to the 8.2 kyr BP event. Quaternary Science Reviews 151, 292-308.

LeGrande, A.N., Schmidt, G.A., 2008. Ensemble, water isotope-enabled, coupled general circulation modeling insights into the 8.2 ka event. Paleoceanography 23, PA3207, doi:10.1029/2008PA001610. 1.

Leverington D.W., Mann J.D., Teller J.T., 2002. Changes in the bathymetry and volume of glacial Lake Agassiz between 9200 and 7700 14C yr B.P. Quaternary Research 57, 244–252.

Licciardi J.M., Teller J.T., Clark P.U., 1999. Freshwater routing by the Laurentide Ice Sheet during the last deglaciation, mechanism of global climate change at millennial time scales. Geophysical Monograph 112, 177-201.

Lifton N., Sato T., Dunai T.J., 2014. Scaling in situ cosmogenic nuclide production rates using analytical approximations to atmospheric cosmic-ray fluxes. Earth and Planetary Science Letters 386, 149-160.

Marquette G.C., Gray J.T., Gosse J.C., Courchesne F., Stockli L., Marpherson G., Finkel R., 2004. Felsenmeer persistence under non-erosive ice in the Torngat and Kaumajet mountains, Quebec and Labrador, as determined by soil weathering and cosmogenic nuclide exposure dating. Canadian Journal of Earth Sciences 41, 19-38.

Matthew E.M., 1961a. The glacial geomorphology and deglacierization of the George River basin and adjacent areas in northern Quebec. (Doctoral thesis). McGill University, Montreal: 211 pp.

Matthew E.M., 1961b. Deglaciation of the George River basin, Labrador/Ungava. McGill Sub-Arctic Research Papers 11, 29-45.

Meissner K.M., Clark P.U., 2006. The impact of floods versus routing on the thermohaline circulation: Geophysical Research Letters 33, doi:10.1029/2006GL026705.

Mitrovica, J.X., Davis, J.L., Shapiro, I.I., 1994. A spectral formalism for computing 3-dimensional deformations due to surface loads: 1. theory. Journal of Geophysical Research 99, 7057-7073.

Mitrovica, J.X., Milne, G.A., 2003. On post-glacial sea level: I. General theory. Geophysical Journal International 154, 253-267.

Mitrovica, J.X., Wahr, J., Matsuyama, I., Paulson, A., 2005. The rotational stability of an ice-age earth. Geophysical Journal International 161, 491-506.

Morrill C., Ward E.M., Wagner A.J., Otto-Bliesner B.L., Rosenbloom N., 2014. Large sensitivity to freshwater forcing location in 8.2 ka simulations. Paleoceanography 29, 930-945.

Peltier, W.R., 2004. Global glacial isostasy and the surface of the ice-age earth: The ICE-5G (VM2) model and GRACE. Annu. Rev. Earth Planet. Sci. 32, 111-149.

Roy M., Dell'Oste F., Veillette J.J., de Vernal A., Hélie J.F., Parent M., 2011. Insights on the events surrounding the final drainage of Lake Ojibway based on James Bay stratigraphic sequences. Quaternary Science Reviews 30, 682-692.

Roy M., Veillette J.J., Daubois V., Ménard M., 2015. Late-stage phases of glacial Lake Ojibway in the central Abitibi region, eastern Canada. Geomorphology 248, 14-23.

Schaefer J.M., Denton G.H., Kaplan M., Putnam A., Finkel R.C., Barrell D.J., Andersen B.G., Schwartz R., Mackintosh A., Chinn T., Schluchter C., 2009 High-frequency Holocene glacier fluctuations in New Zealand differ from the northern signature. Science 324, 622-625.

Short S.K., 1981. Radiocarbon date list I: Labrador and northern Quebec, Canada. Institute of Arctic and Alpine Research Occasional Paper 36, 1-33.

Short S.K., Nichols H., 1977. Holocene pollen diagrams from subartic Labrador-Ungava: Vegetational history and climatic change. Artic and Alpine Research 9, 265-290.

Staiger J.K.W., Gosse J.C., Johnson J.V., Fastook J., Gray, J.T, Stockli D.F., Stockli L., Finkel R., 2005. Quaternary relief generation by polythermal glacier ice. Earth Surface Processes and Landforms 30, 1145-1159.

Staiger, J., Gosse, J., Toracinta, R., Oglesby, B., Fastook, J., 2007. Atmospheric scaling of cosmogenic nuclide production: climate effect. Journal of Geophysical Research 112, B02205.

Stone J.O., 2000. Air pressure and cosmogenic isotope production. Journal of Geophysical Research: Solid Earth 105, 23753-23759.

Stuiver M., Reimer P.J., Reimer R.W., 2018. CALIB 7.1 [www program] at http://calib.org, accessed 2018-4-3.

Teller J.T., Sun S., Wolfe B., 1990. Catastrophic flooding into Lake Agassiz. Canadian Quaternary Association/American Quaternary Association (CANQUA/AMQUA), Programme and Abstracts, Waterloo, p. 32.

Teller J.T., Leverington D.W., 2004. Glacial Lake Agassiz: A 5000 yr history of change and its relationship to the $\delta^{18}O$ record of Greenland. Geological Society of America Bulletin 116, 729-742.

Thomas E.R., Wolff E.W., Mulvaney R., Steffensen J.P., Johnsen S.J., Arrowsmith C., White J.W.C., Vaughn B., Popp T., 2007. The 8.2 ka event from Greenland ice cores. Quaternary Science Review 26, 70-81.

Thorleifson L.H., 1996. Review of Lake Agassiz history, In Teller, J. T., Thorleifson, L. H., Matile, G., Brisbin, W. C., Geological Association of Canada Field Trip Guidebook for GAC/MAC Joint Annual Meeting, 55-84.

Törnqvist T.E., Hijma M.P., 2012. Links between early Holocene ice-sheet decay, sea-level rise and abrupt climate change. Nature Geoscience 5, 601-606.

Ullman D.J., Carlson A.E., Hostetler S.W., Clark P.U., Cuzzone J., Milne G.A., Winsor K., Caffe M., 2016. Final Laurentide ice-sheet deglaciation and Holocene climate-sea level change. Quaternary Science Reviews 152, 49-59.

Wickert A.D., 2016. Reconstruction of North American drainage basins and river discharge since the Last Glacial Maximum. Earth Surface Dynamics 4, 831–869.

Young N.E., Schaefer J.M., Briner J.P., Goehring B.M., 2013. A ^{10}Be production-rate calibration for the Arctic. Journal of Quaternary Science 28, 515–526.

2.10 TABLES

Tableau 2.1 Samples information and surface exposure ages

Site-sample no.	Lake stage/area	Rock type	Material type / landform*	Latitude (DD)	Longitude (DD)	Altitude (m)	Corrected altitude (m)**	LSNd ± 1 σ (yr)	1 σ (%)
13HDL01-01	N3'/PH	Tonalite	Bldr /Sho	57.50	-65.29	397	435	8100 ± 300	3.7
13HDL01-05	N3'/PH	Tonalite	Bldr /Sho	57.50	-65.29	400	438	8200 ± 200	2.4
13HDL01-08	N3'/PH	Tonalite	Bldr /Sho	57.50	-65.29	397	435	8100 ± 200	2.5
13HDL01-09	N3'/PH	Tonalite	Bldr /Sho	57.50	-65.29	398	436	7800 ± 200	2.6
13HDL04-05	N3'/PH	Tonalite	Bldr /Sho	57.46	-65.2	398	436	8000 ± 300	3.8
13HDL04-06	N3'/PH	Tonalite	Bldr /Sho	57.46	-65.2	397	435	9300 ± 300	3.2
13HDL04-07	N3'/PH	Tonalite	Bldr /Sho	57.46	-65.2	396	434	8600 ± 200	2.3
13HDL04-09	N3'/PH	Tonalite	Bldr /Sho	57.46	-65.2	396	434	15200 ± 300	2.0
13HDL06-01	N2'/IHL	Alkaline granite	Bldr /Sho	56.27	-64.7	478	516	8200 ± 200	2.4
13HDL06-03	N2'/IHL	Alkaline granite	Bldr /Sho	56.27	-64.7	476	514	8800 ± 200	2.3
13HDL06-05	N2'/IHL	Migmatite	Bldr /Sho	56.27	-64.7	477	515	8900 ± 300	3.4
13HDL06-06	N2'/IHL	Migmatite	Bldr /Sho	56.27	-64.7	481	519	7700 ± 200	2.6
13HDL07-03	N2'/IHL	Qtz-rich syenite	Bldr /Sho	56.60	-64.72	463	501	8000 ± 300	3.8
13HDL07-04	N2'/IHL	Granodiorite	Bldr /Sho	56.60	-64.72	462	500	7900 ± 300	3.8
13HDL07-08	N2'/IHL	Alkaline granite	Bldr /Sho	56.60	-64.72	461	499	7700 ± 200	2.6
13HDL07-10	N2'/IHL	Alkaline granite	Bldr /Sho	56.60	-64.72	461	499	8500 ± 200	2.4
14HDLPF-02	PF/WH	Monzogranite	Bldr / OL	57.11	-65.26	376	414	8100 ± 200	2.5
14HDLPF-03	PF/WH	Alkaline granite	Bldr / OL	57.11	-65.26	375	413	10300 ± 200	1.9
14HDLPF-05	PF/WH	Monzogranite	Bldr / OL	57.102	-65.26	377	415	8600 ± 200	2.3
14HDLPF-06	PF/WH	Monzogranite	Bldr / OL	57.10	-65.26	376	414	8800 ± 200	2.3
14HDLPF-R-02	PF/WH	Granite	BO/ OL	57.10	-65.31	415	453	8600 ± 200	2.3

*Bldr: boulder; Sho: shoreline; BO: Bedrock outcrop; OL: outburst landform. **See text for explanation of uplift correction. Shielding by snow is considered negligible (see Methods for details); it would require a correction of <3% on the exposure age calculations in worse-case scenarios.

Tableau 2.2 Modelling results for the Pinkflood meltwater discharge

Parameters	Paleohydraulic estimates
Average B-axis (m)	2.1
Maximum B-axis (m)	3.5
Average velocity ($m.s^{-1}$)	7.00
Maximum velocity ($m.s^{-1}$)	9.60
Depth of the channel (m)	70
Channel width (m)	640
Average discharge ($m^3.s^{-1}$)	314 500
Maximum discharge ($m^3.s^{-1}$)	429 000

Tableau 2.3 Analytical and procedural data

Sample no.	Thickness (cm)	CAMS #	Evapo-corr. carrier (mg)	$[^{10}Be] \pm 1\ \sigma$ (10^4 atoms g^{-1})		
13HDL01-01	1.2	BE40837	0.182	4.77	±	0.20
13HDL01-05	1.6	BE40838	0.183	4.86	±	0.12
13HDL01-08	2.6	BE40839	0.183	4.72	±	0.11
13HDL01-09	1.1	BE40840	0.183	4.64	±	0.10
13HDL04-05	2.5	BE40841	0.183	4.65	±	0.15
13HDL04-06	1.8	BE40842	0.183	5.46	±	0.15
13HDL04-07	2.1	BE40843	0.183	5.04	±	0.13
13HDL04-09	1.8	BE40845	0.183	8.90	±	0.17
13HDL06-01	1.9	BE40846	0.184	5.18	±	0.14
13HDL06-03	0.9	BE37480	0.181	5.58	±	0.15
13HDL06-05	2.1	BE40847	0.182	5.59	±	0.17
13HDL06-06	1.9	BE37481	0.182	4.89	±	0.14
13HDL07-03	2.0	BE37482	0.182	4.98	±	0.17
13HDL07-04	1.6	BE37483	0.182	4.91	±	0.17
13HDL07-08	1.8	BE37485	0.182	4.80	±	0.14
13HDL07-10	2.5	BE37486	0.182	5.26	±	0.13
14HDLPF-2	1.7	BE40966	0.202	4.67	±	0.10
14HDLPF-3	1.5	BE40967	0.202	5.90	±	0.12
14HDLPF-5	1.7	BE40968	0.183	4.95	±	0.14
14HDLPF-6	1.4	BE40969	0.203	5.05	±	0.91
14HDLPF-R-2	2.1	BE40970	0.203	5.11	±	0.10

*Lamont ^{9}Be Carrier 5 concentration was corrected for evaporation, based on continuous monitoring by precise weighing of the carrier. Maximum correction was 1.2%. Rock density is the same for all samples and reach 2.7 g.cm^{-3}. Shielding correction was negligible and have been fixed at 1.00. AMS standard used is the 07KNSTD.

2.11 FIGURES

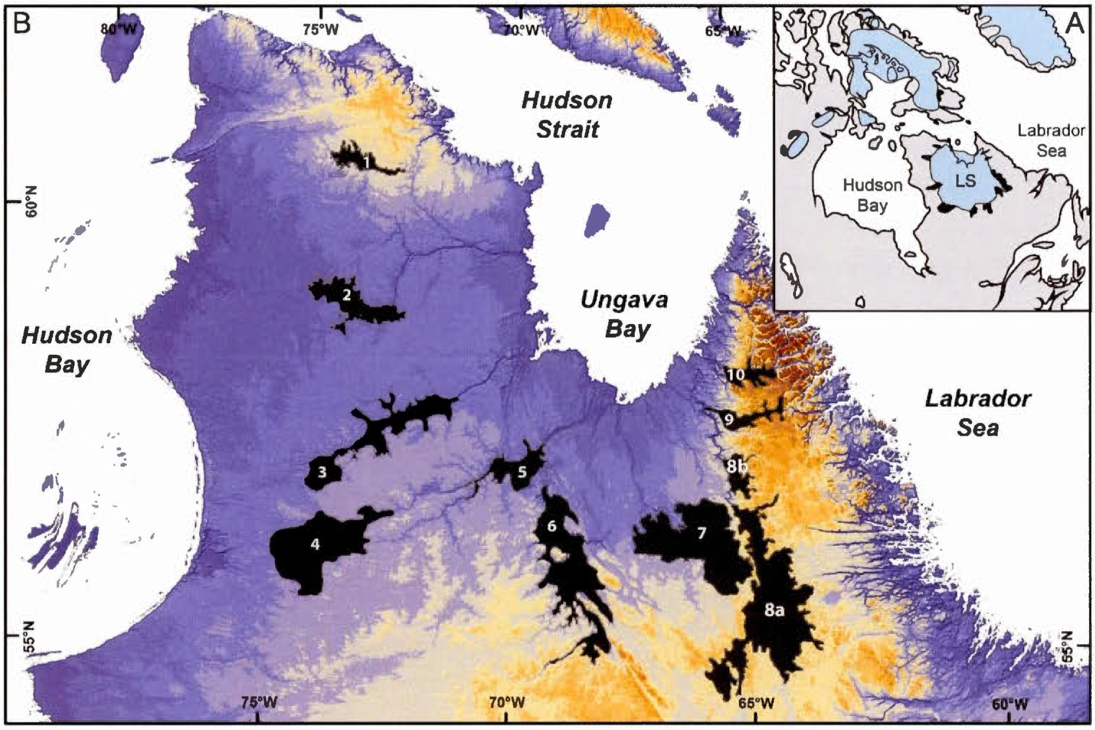

Figure 2.1 (A) Schematic map showing glacial lakes (black) of the Labrador Sector (LS) and other remnants of the Laurentide ice sheet late in the deglaciation (~10 cal a BP; modified from Dyke, 2004). (B) Location of ice-dammed lakes in northern Quebec during the last deglaciation: 1) Lake Nantais; 2) Lake Payne; 3) Lake Minto; 4) Lake à l'Eau-Claire; 5) Lake Mélèzes; 6) Lake Caniapiscau; 7) Lake McLean; 8) Lake Naskaupi (a: Indian House Lake basin; b: Pyramid Hills basin); 9) Lake Ford; 10) Lake Koroc (modified from Dubé-Loubert and Roy, 2017).

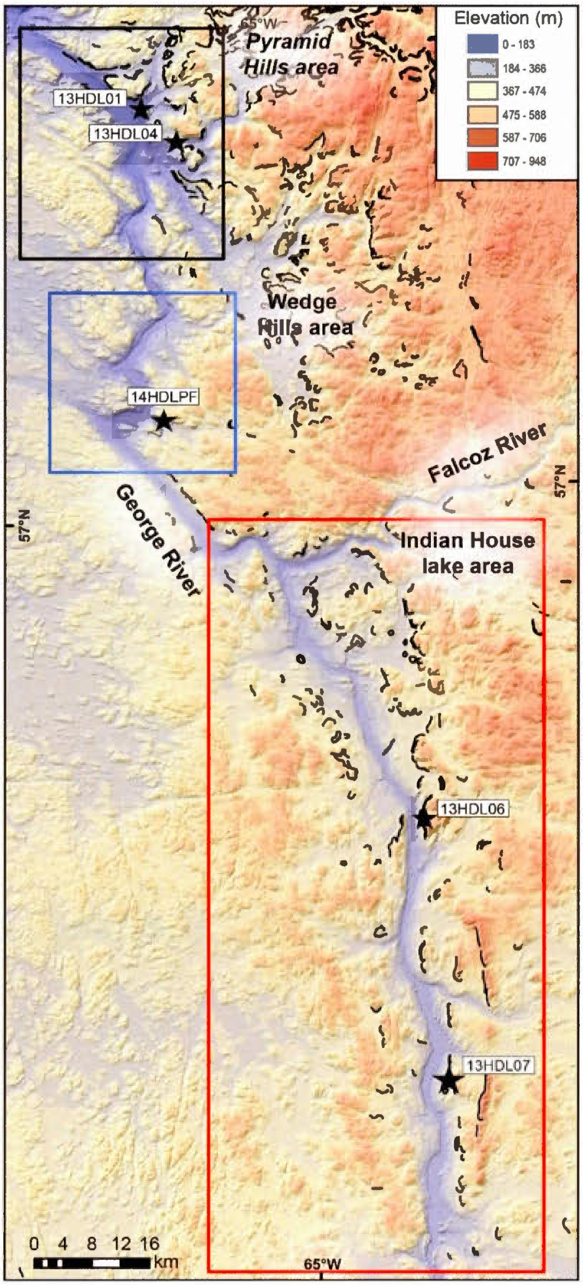

Figure 2.2 Digital elevation model showing the physiography of the George River valley and names of geographic locations and features mentioned in text. Black stars show the location of the dated sites (see Table 1). Thin black lines correspond to Naskaupi shorelines (Dubé-Loubert et al., 2017).

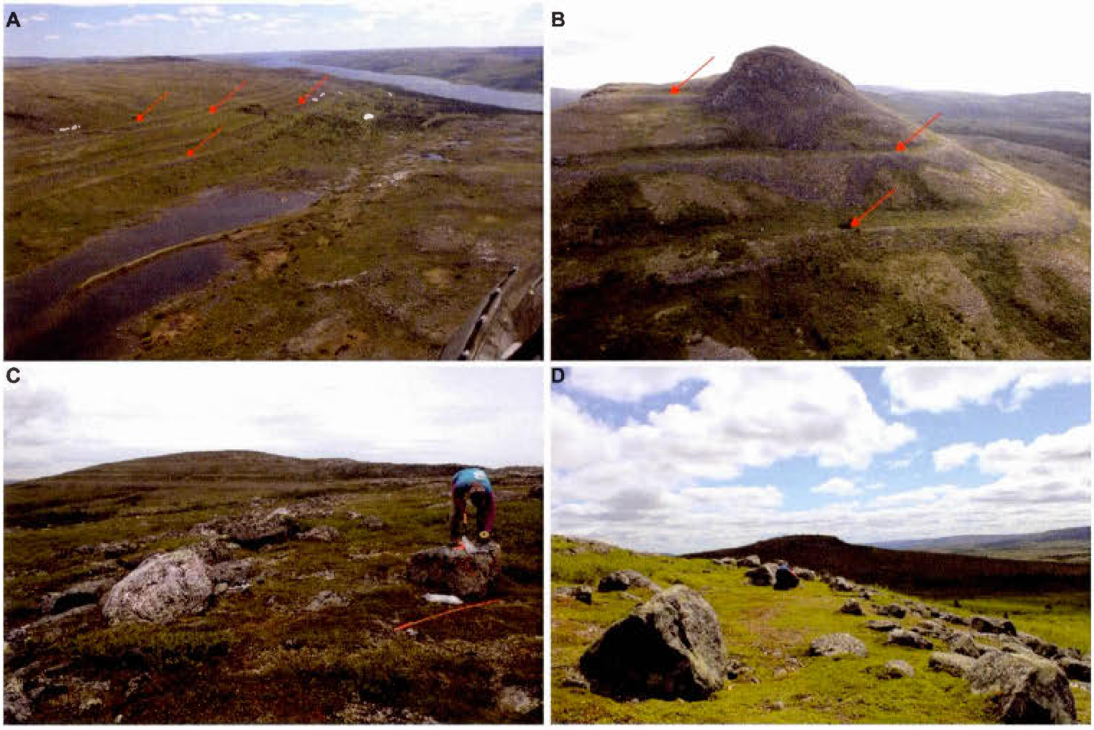

Figure 2.3 Examples of Naskaupi shorelines in the George River valley. A) Oblique aerial view showing four extensive Naskaupi shorelines (red arrows) separated by 10 to 40 m in the Indian House Lake (IHL) area (seen in background). B) Naskaupi shorelines (red arrows) on the emblematic Pyramid Peak in the Pyramid Hills area. C) Ground view of Naskaupi shorelines and example of boulder sampled for ^{10}Be dating (IHL area). D) Typical Naskaupi shoreline consisting of a wave-cut notch flanked by a well-developed boulder-cored terrace (IHL area).

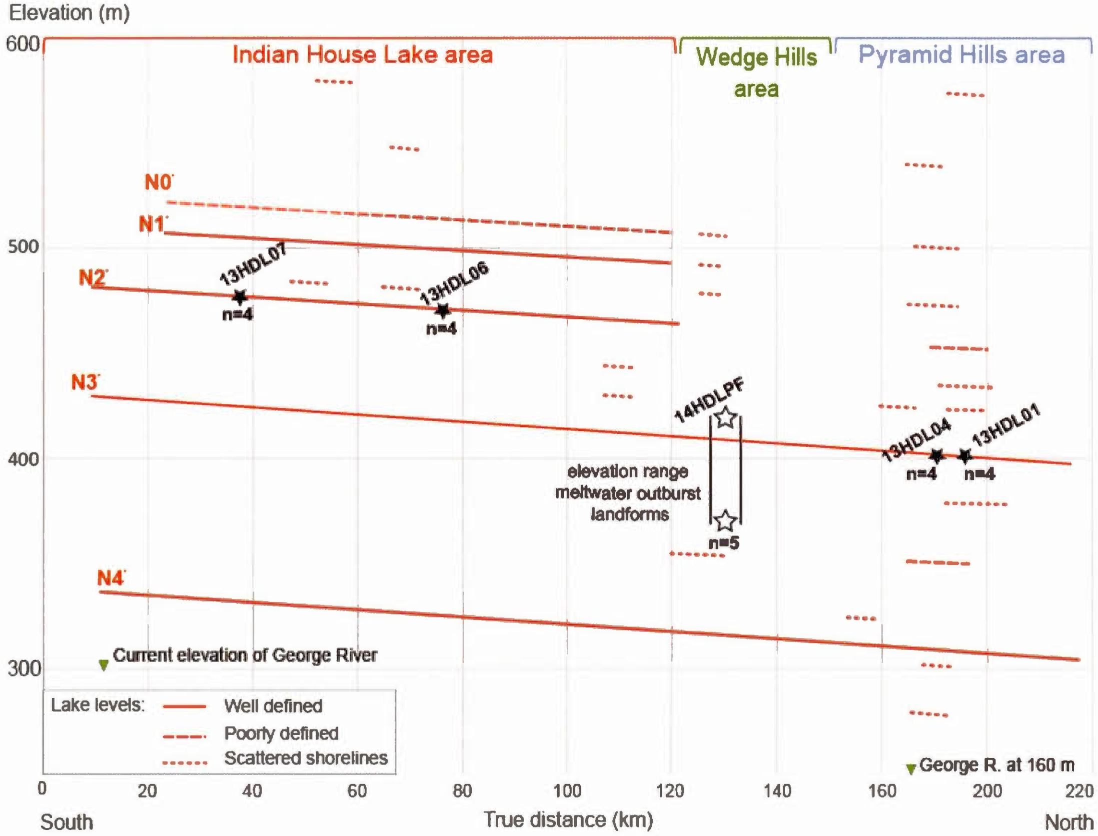

Figure 2.4 North-south transect across the George River valley showing the elevation and extent of lake levels in the three sectors outlined in Figure 2. Lake levels are referred to as N0', N1', N2', N3' and N4' (Dubé-Loubert and Roy, 2017). The inclination of lake levels depicts the regional uplift gradient towards the north. Black stars show the location of shoreline sites sampled and number of samples dated. The white stars and vertical lines show the elevation range of the outburst landforms dated.

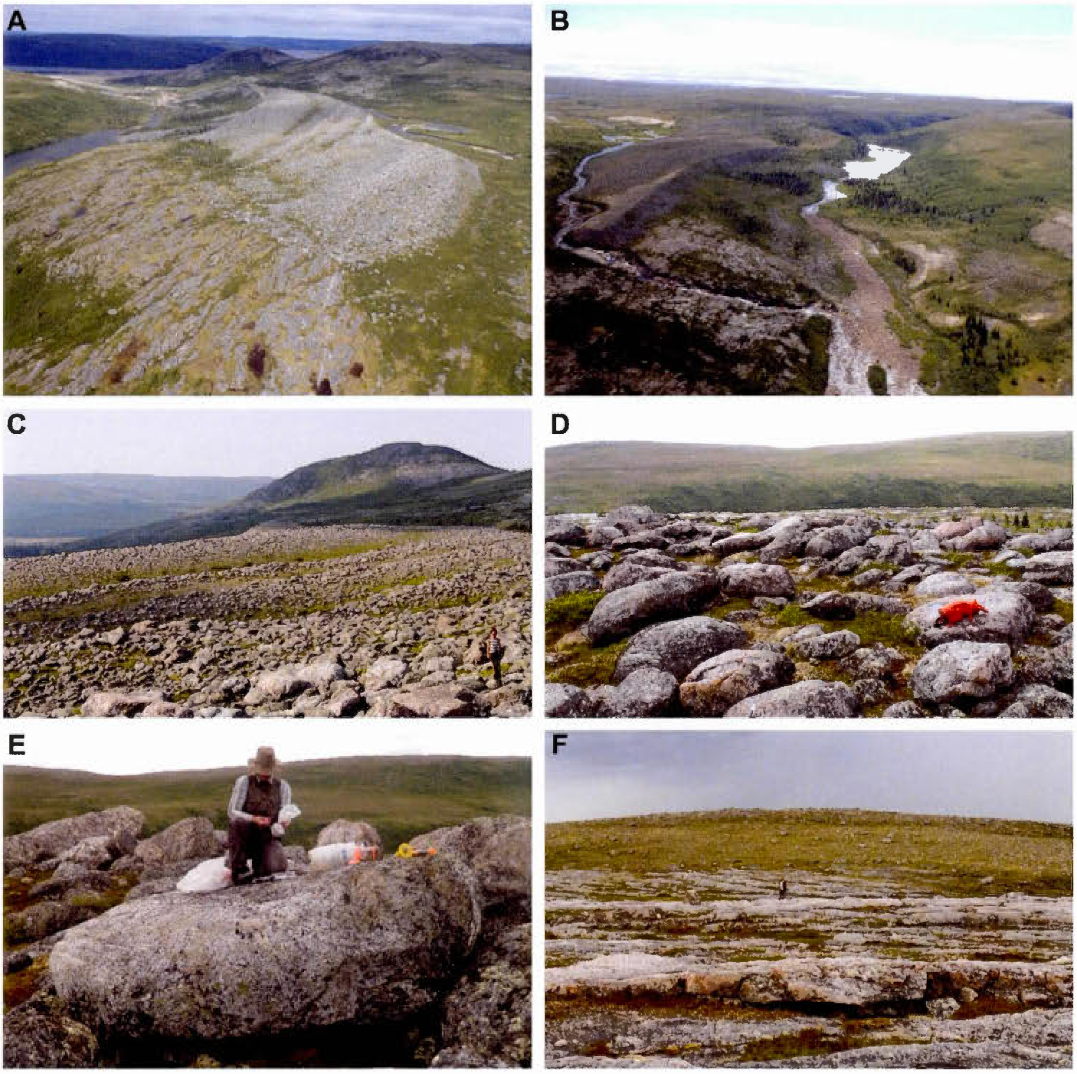

Figure 2.5 Photographs of the so-called Pinkflood outburst flood landform and associated features. A) Oblique aerial view of the accumulation of imbricated boulders arranged in large-scale alluvial bars; landform is about 30 m-thick by 2 km-long (view towards the north). B) Aerial view of the meltwater canyon associated with outburst flood (looking south). C) Ground view of the thick accumulation of pink granitic boulders forming the alluvial bars (looking north; note the person for scale, lower right). D) Detailed view of the rounded to sub-rounded boulders showing an imbrication towards the north (backpack is 50 cm long). E) Example of granitic

boulder sampled for ^{10}Be dating. F) View of the bare bedrock surface formed by channelized meltwater erosion of glacial deposits during the outburst flood. This rock surface was sampled for ^{10}Be dating (view towards the north; note the persons for scale).

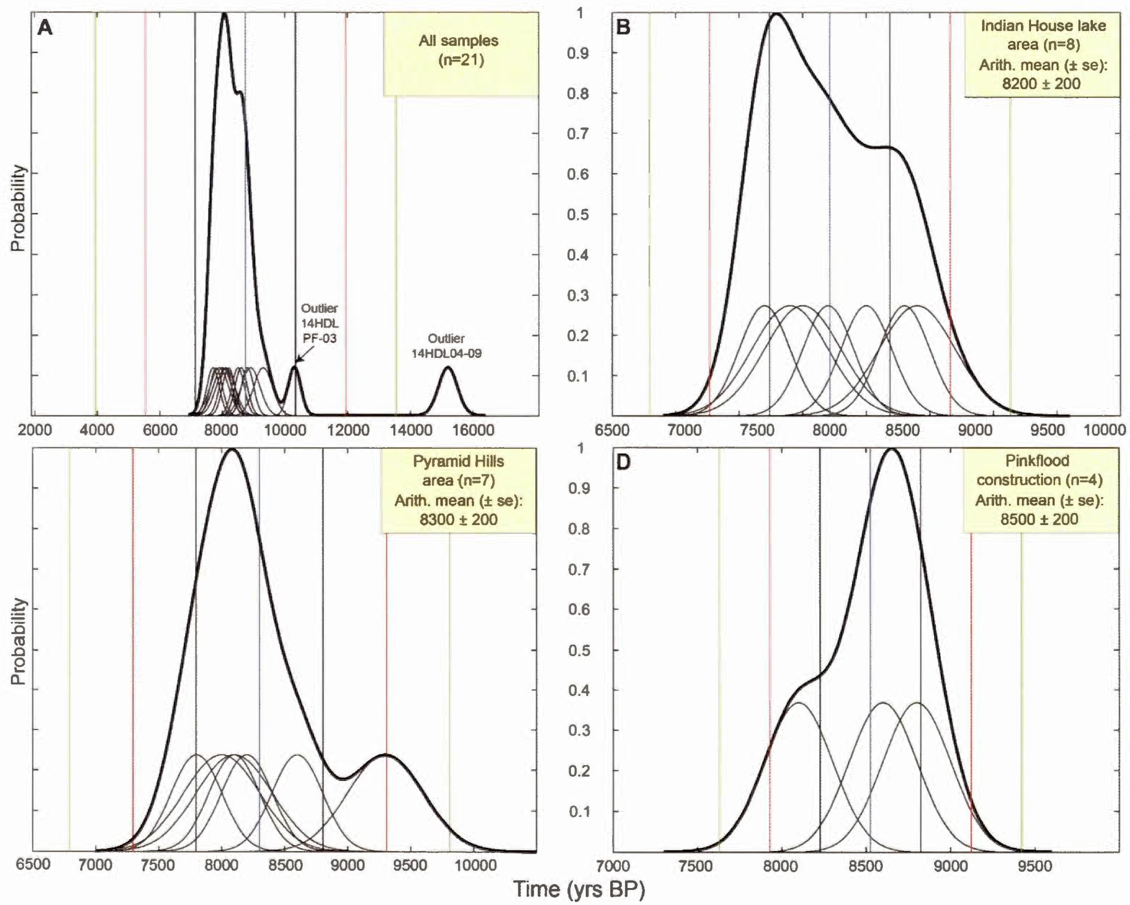

Figure 2.6 Probability distribution function (PDF) plots of ^{10}Be ages for the Naskaupi shorelines and the outburst flood landform dated (see Table 1 for details). Arithmetic mean age and standard error (se) are presented in light yellow

box. Thin black lines represent individual ages and thick black lines show cumulative PDF. Vertical lines: purple line shows the arithmetic mean age; black lines show the 1σ interval; red lines: 2σ interval; green lines: 3σ interval. A) PDF plot for all samples dated in this study. The distribution outlines two outliers (14HDL-PF-09 and 14HDL04-09; see text for details). B) Arithmetic mean age for the boulders sampled from N2' shorelines of the Indian House Lake area. C) Arithmetic mean age for the N3' shoreline samples of the Pyramid Hills area, excluding one outlier. D) Arithmetic mean age for the samples of the Pinkflood outburst flood features, excluding one outlier.

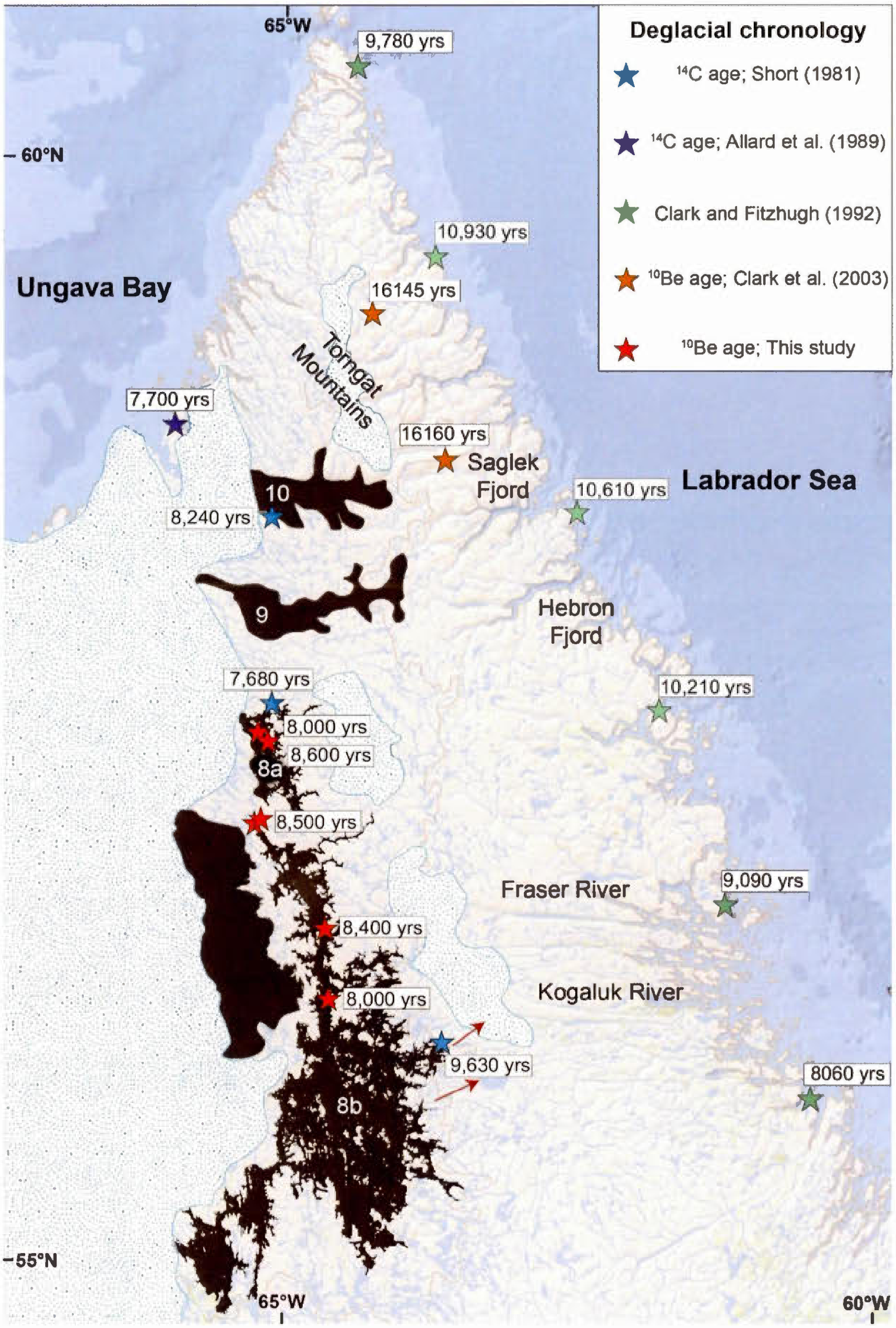

Figure 2.7 Paleogeographic reconstruction showing the areal extent of Lake Naskaupi in the IHL and PH basins (8a and 8b, respectively) during its main stage (equivalent to N2') and the inferred position of the ice margin required to dam this

water plane. The ^{10}Be ages from this study indicate that the ice margin occupied this position west of the George River at around 8,300 ± 300 a. Chronological constraints from other studies are also presented. The older exposure ages from the Torngat Mountains (Clark et al., 2003: recalculated with production rate of Young (2013)) reflect the emergence from the high-relief terrains during the deglaciation, consistent with similar studies in this region (Marquette et al., 2004; Staiger et al., 2005). The discrepancy with ^{14}C ages likely outlines the delay in the establishment of vegetation following the deglaciation or contamination by old organic carbon. Also shown are the areal extent of Lake McLean, Lake Ford and Lake Koroc during the same time interval.

CHAPITRE III

THE EVOLUTION OF THE NORTHEASTERN LABRADOR SECTOR OF THE LAURENTIDE ICE-SHEET DURING THE LAST GLACIAL CYCLE BASED ON FIELD-BASED MAPPING AND SURFACE EXPOSURE DATING OF LANDFORM ASSEMBLAGES

Hugo Dubé-Loubert[1,2,3], Martin Roy[2,3], Joerg M. Schaefer[4,5]

[1] Bureau de la Connaissance Géoscientifique du Québec, Ministère de l'Énergie et des Ressources Naturelles, 400 boulevard Lamaque, Val-d'Or, Québec J9P 3L4

[2] Département des sciences de la Terre et de l'atmosphère - Université du Québec à Montréal, C.P. 8888, suce. Centre-Ville, Montréal (QC), Canada, H3C 3P8

[3] Centre de recherche Géotop - Université du Québec à Montréal, C.P. **8888,** suce. Centre-Ville, Montréal (QC), Canada, H3C 3P8

[4] Lamont-Doherty Earth Observatory, Geochemistry, 409 Comer Building, 61 Route 9W, P.O. Box 1000, Palisades, NY, 10964, USA

[5] Department of Earth and Environmental Sciences, Columbia University, New York, NY, 10027, USA

RÉSUMÉ

Le Secteur Labrador de l'Inlandsis laurentidien regroupe un système complexe de lignes de partage glaciaire séparant des assemblages morphologiques de direction opposée qui se rencontrent le long d'une zone étroite et arquée ceinturant la baie d'Ungava. L'interprétation de cette zone, communément nommée *Horseshoe Unconformity*, a mené à une multitude de reconstructions paléogéographiques contrastées, soulignant les lacunes dans la connaissance de l'histoire glaciaire de ce secteur, notamment en regard du patron de retrait de la marge, de la nature des conditions sous-glaciaires, mais également de la signification (âge) de certains assemblages morphologiques. Nous présentons ici une nouvelle reconstruction de la dynamique et de l'évolution du Secteur Labrador à partir de la cartographie systématique détaillée de marques d'érosion glaciaire et des formes de terrain d'un large secteur du nord-est du Québec et du Labrador. L'application de la datation et d'analyses cosmogéniques (^{10}Be et ^{26}Al) à des deltas glaciomarins, à des surfaces rocheuses prélevées dans des terrains de felsenmeer ainsi qu'à d'autres modelés par les écoulements glaciaires, nous permet de contraindre avec plus de précision le cadre chronologique et le régime thermique sous-glaciaire. Nos résultats indiquent que ce qui est communément décrit comme la limite orientale de la zone du *Horseshoe Unconformity* traduit plutôt l'activité au dernier maximum glaciaire de la ligne de partage du Labrador, séparant des écoulements régionaux opposés de direction ENE et WNW. Notre reconstruction indique également que le secteur à l'ouest et au nord-ouest de cette ligne de partage consiste en une mosaïque d'assemblages morphologiques d'âges légèrement différents, dont le plus jeune est caractérisé par un essaim de formes fuselées allongées et convergentes vers la baie d'Ungava. Nos données chronologiques suggèrent que cet assemblage se serait formé tardivement au cours du dernier cycle glaciaire par l'activité et la propagation vers le sud de la tête de courants de glace. Ces résultats favorisent le modèle de capture mis de l'avant afin d'expliquer l'étroitesse de cette zone de rencontre, pour laquelle nos données montrent des différences

significatives en termes de configuration et de localisation des limites avec les travaux antérieurs. Les données cartographiques excluent l'occurrence de conditions extensives de glace à base froide dans les basses terres de la baie d'Ungava. Ce type de dynamique a seulement été identifiées de façon sporadique sur les hauts plateaux à l'est de la rivière George, où les analyses combinées d'isotopes cosmogéniques (^{10}Be, ^{26}Al) et les résultats géochimiques de la matrice des tills, suggèrent un couvert de glace peu érosif. La nature et la distribution des formes de déglaciation soulignent aussi un changement dans la mode de retrait de la marge glaciaire avec une transition d'un régime de glace à base chaude vers une glace à base froide à proximité du secteur couvert par la ligne de partage glaciaire.

ABSTRACT

The Labrador Sector (LS) of the Laurentide ice sheet regroups a complex system of ice divides that separate landform assemblages of opposite ice flow directions along a narrow U-shaped zone that surrounds Ungava Bay. Interpretation of this so-called Horseshoe Unconformity gave rise to highly contrasting reconstructions, which reflect uncertainties on the glacial history, notably regarding the pattern of ice retreat, the nature of its thermal regime, and the significance (age) of certain landform assemblages. Here we document the dynamics and evolution of the LS through systematic mapping of ice-flow indicators and glacial landforms-terrains in a large area of northeastern Quebec and Labrador. The application of cosmogenic (^{10}Be and ^{26}Al) dating to esker-fed glaciomarine deltas and rock surfaces from felsenmeer and glacially-fluted terrains further constrains the chronological framework and the subglacial thermal regime. Our results indicate that what is commonly portrayed as the eastern branch of the Horseshoe unconformity actually forms an ice divide separating two regional ice flows extending towards the ENE and WNW. This feature belongs to the Labrador Ancestor ice divide and was likely active at the LGM and for some time thereafter. Our reconstruction also indicates that the area west-northwest of the unconformity consists of a mosaic of landform assemblages of different ages, with the youngest assemblage consisting of highly elongated streamlined landforms that indicate a massive convergent NNW ice flow into Ungava Bay, which our geochronological results assign to the late-glacial/deglacial interval. This system may be related to a late-glacial ice drawdown in Ungava Bay and the attendant southward propagation of ice stream corridors. These results lend support for the capture model put forward to explain the Horseshoe boundary, for which our data show significant changes in configuration and location with respect to previous reconstructions. Our mapping and investigations rule out the occurrence in the Ungava Bay lowlands of widespread cold-based ice conditions, which can mainly be found in scattered areas on elevated plateaus located to the east of the George River, where paired cosmogenic isotopes (^{10}Be, ^{26}Al) and till geochemistry provide evidence for a low-erosive ice cover.

The nature and distribution of deglacial landforms also show a change in the deglaciation style across the region, which shifted from warm-based at peripheral areas to a cold-based ice retreat in the core area of the ice divide region.

3.1 INTRODUCTION

The Laurentide Ice Sheet (LIS) played an important role in the climate variability of the last glacial cycle and ensuing deglaciation, primarily through ice-sheet instabilities (collapses) and drainages of ice-dammed lakes causing large discharges of icebergs and meltwater that disturbed the North Atlantic overturning oceanic circulation and associated meridional heat transport (Barber et al., 1999; Clark et al., 2001; Hemming, 2004; Carlson and Clark, 2012; Dubé-Loubert et al., 2018). These climate-forcing events point to significant changes in the LIS configuration, which can be reconstructed through the study of the nature and spatial distribution of glacial landforms and erosive (striation) records, as well as from the attendant patterns of ice retreat and associated ice-margin chronology that together provide a reliable portrait of the general ice-sheet geometry and temporal evolution (Prest, 1968; Dyke and Prest, 1987; Veillette et al., 1999; Clark et al, 2000; Dyke, 2003).

Insights on former ice-sheet dynamics was improved upon the advent of remote sensing analysis of satellite imageries that allowed the recognition of continental-scale features, such as the location of the main ice dispersal centers and associated ice-flow trajectories, including a large number of fast-flowing corridors (ice streams) that likely regulated the ice-sheet mass budget (Boulton and Clark, 1990a,b; Stokes and Clark, 2004; Winsborrow et al., 2004; Margold et al., 2015). This approach, however, remain limited by the scale and resolution of images, while field-based studies have shown the importance of ground observations to validate reconstructions build upon remote mapping methods (Smith and Knigth, 2011; Veillette et al., 2017; McMartin and Henderson). Furthermore, fundamental questions remain regarding the interpretation and age of certain landform assemblages and the nature of the subglacial thermal regime, which introduce uncertainties on the available reconstructions and related ice-sheet dynamics (Kleman, 1994; Veillette et al., 1999; Clark et al, 2000; Kleman et al., 2010). Current issues are in part due to the lack of detailed field-based mapping and the absence of chronological constraints in some key regions.

The Labrador Sector (LS) represents one of the three main components of the LIS and regroups a complex network of ice divides consisting of several branches that surround Ungava Bay (Figure 3.1). The LS was active during the last glaciation, with significant migrations of its ice divides and presumably marked changes in its subglacial thermal regime (Sugden, 1977; Boulton and Clark, 1990a; Kleman, 1994; Kleman and Hättestrand, 1999). This complex evolution is reflected in the geomorphology of northern Quebec and Labrador where the spatial arrangement of the main glacial landforms outline two opposing ice-flow systems spreading from a former center of mass. These two large-scale patterns of ice flows are separated by a long and narrow U-shaped zone that circles up Ungava Bay. The signification of this unique landsystem has long been a subject of debate and gave rise to highly contrasting interpretations (Hughes, 1964; Dyke and Prest, 1987, Kleman, 1994; Veillette et al., 1999; Clark et al., 2000; Jansson, 2004; Kleman, 2010). For instance, some models associate the Ungava Bay glacial lineations and eskers with relict landforms that were preserved under cold-based ice conditions during the last glaciation (Kleman, 1994; Jansson, 2004), while others consider these landforms and the so-called Horseshoe unconformity to be the results of a major drawdown of the Labrador ice dome towards Ungava Bay during the late-glacial interval (Hughes, 1964; Veillette et al., 1999).

Deglaciation of the LS core region was also complex, with asymmetric rates of retreat of its southern (rapid) and northern (slow) ice margins (Ullman et al, 2016) and massive production of meltwater that led to the development of several glacial lakes (Ives, 1960; Gray et al., 1993; Dubé-Loubert et al., 2017). Although current models integrate several geomorphic features of this sector, most fail to fully explain the different terrain assemblages and account for the development of all glacial lakes around Ungava Bay (e.g., Clark et al., 2000). The reason for this is related to uncertainties on the temporal evolution of the ice divides and the configuration of the ice margin throughout the deglaciation. Indeed, many aspects of the glacial history remain inadequately documented, especially regarding the sequence of ice flows that provides information on the migration of ice divides, the configuration and chronology of the ice margin during its retreat, the extent of cold-based ice conditions that regulate ice-sheet dynamics, and the significance of certain landform assemblages (Dyke and Prest, 1987; Kleman, 1994; Veillette et al., 1999; Clark et al., 2000).

Here we document the dynamics and evolution of the LS through systematic mapping of glacial landforms and deposits and measurements of ice-flow indicators in a large area (60 000 km^2) of northeastern Quebec and Labrador (Figure 3.1). The study area lies in a strategic location with respect to the LS configuration. We also present geochemical analyses on glacial deposits (tills) that assess the level of erosion/preservation of glacial terrains, which are combined with measurements of a paired cosmogenic isotopes (^{10}Be, ^{26}Al) from frost-weathered and glacially-scoured rock surfaces that characterize the subglacial thermal regime. Finally, we report ^{10}Be ages from deglacial landforms that bring chronological constraints on geomorphic assemblages and improve the overall chronological framework in the region.

3.2 PREVIOUS WORK AND CHARECTERISTICS OF THE LABRADOR SECTOR

One of the main contributions to our understanding of the LS configuration comes from the Glacial Map of Canada that outlines several sectors with distinct ice flow directions (Prest et al., 1968). Subsequent paleogeographic reconstructions have traditionally portrayed the LS ice divide system as three main branches that were grouped under the name of Labrador Ancestor ice divides (Figure 3.1). One branch is centered over the Ungava Peninsula (the so-called Payne ice divide) and is associated with opposing ice flows towards Hudson Bay and Ungava Bay (Figure 3.1) (Bouchard and Marcotte, 1986). Another branch is located to the south of Ungava Bay (the Caniapiscau ice center) and forms the eastern extension of the Hudson ice divide that separates ice flow towards the north (Ungava Bay) and south (St. Lawrence River basin) (Figure 3.1) (Dyke and Prest, 1987). A third one runs along the Torngats Mountains down to the vicinity of Schefferville (the Labrador ice center) and separate ice flows towards the Labrador Sea and Ungava Bay (Figure 3.1) (Wilson et al., 1958; Prest et al., 1968; Dyke and Prest, 1987).

The glacial landforms (drumlins, crag-and-tails, eskers, Rogen moraines) of the LS also show a complex distribution and spatial arrangement that highlight two major geomorphic systems of opposite direction (Figure1) (Prest et al., 1968). The first system comprises most streamlined landforms of the LS and outlines a divergent ice-flow spreading radially (outward) towards the south, away from a former ice mass that presumably formed the LS dome. Eskers in this system suggest an overall ice retreat roughly towards the north. This major flow pattern is truncated in the north by sets of glacial lineations forming a massive ice flow system converging northward into the Ungava Bay lowlands (Figure 3.1). Eskers within this assemblage are less numerous in comparison with the outward radial ice flow (Veillette et al., 1999) and reflect an ice retreat towards south. The boundary between these two landsystems delineates a narrow U-shaped zone that is commonly referred to as the Horseshoe unconformity (Veillette et al., 1999; Clark et al., 2000). The interpretation of this distinct assemblage of landforms has been a long-standing issue in paleoglaciology and some of the resulting paleogeographic reconstructions have been widely debated.

One model associates the change in ice flows across the Horseshoe unconformity to the development a late-glacial ice divide, which would have undergone a symmetric retreat towars the unconformity where the last ice remnants would have disintegrated (Prest, 1968; Dyke and Prest, 1987; Dyke, 2003). This pattern of ice retreat, however, fails to account for the development of several ice-dammed lakes, notably those that occupied the western and southern river basins draining into Ungava Bay (Clark et al, 2000; Dubé-Loubert and Roy, 2017).

Another model focuses on the marked difference in the spatial arrangement between glacial lineations and a network of meltwater channels in the Ungava Bay lowlands, which was at the core of a reconstruction (Kleman et al., 1994) that departed drastically from the established pattern of deglaciation (Hughes, 1964; Klassen and Thompson, 1993). Northward-trending streamlined landforms in a large region comprising the George and Whale River basins are commonly cross-cut (superimposed) by meltwater channels that are oriented at right angle with the glacial landforms. This deglacial overprint consists in ENE trending channels that were interpreted as proglacial features reflecting the westward retreat of an ice front during the last deglaciation, thus unrelated to the northward ice flow that emplaced the Ungava Bay glacial lineations (Kleman et al., 1994). This glacial landscape was then associated to relict landforms that had been preserved under a cold-based ice dome centered over Ungava Bay. Although the model may account for the damming of several glacial lakes (Clark et al., 2000; Jansson et al., 2004), it is in complete contradiction with the trend of eskers and other deglacial features that indicates a regional pattern of ice retreat towards the south, thus in agreement with the overall trend of streamlined landforms (Veillette et al., 1999; Dyke et al., 2003). Although the presence of a cold-based ice cover in the Ungava Bay region has been used in other reconstructions (Clark et al., 2000; Jansson et al., 2004), the concept assigning the Ungava lowland lineations and eskers to relict features has been mostly abandoned and these landforms are now considered as late-deglacial in age (Kleman et al., 2010). Nonetheless, the extent of cold-based ice conditions in the LS and their role in ice dynamics and the development of glacial lakes remain to be refined.

Surficial geology mapping in the Nichicun-Caniapiscau sector initially led to a model associating the Horseshoe unconformity to the truncation late during the last glaciation of the headward part of the southern radial flow by the ice-flow system converging into Ungava Bay (Hughes, 1964). Subsequent work in central Labrador outlined a complex ice flow sequence in which the convergent ice flow towards Ungava Bay was also assigned as a late event in the relative chronology (Klassen and

Thompson, 1993). Later, extensive detailed mapping of striations and associated cross-cutting relationships in the Caniapiscau area provided further support for this capture model (Veillette et al., 1999), in which the Horseshoe unconformity was associated to the southward propagation of a large ice stream that developed in the Ungava Bay lowlands; an event that was then correlated with the Gold Cove Advance at 9.9-9.4 ^{14}C BP (11.4-10.9 ka; Stravers et al., 1992; Kaufman et al., 1993).

Although these reconstructions (Hughes, 1964; Klasssen and Thompson, 1993; Veillette et al., 1999) considered the landform assemblage in Ungava Bay as the product of a single ice-flow event, subsequent studies have shown that the glacial lineations could be regrouped into several discrete ice streams that likely operated at various times, but during closely-spaced intervals (Clark et al., 2000; Jansson et al., 2003; Winsborrow et al., 2004; Margold et al., 2015). While a total of up to 6 ice streams have been proposed (Clark et al., 2000; Jansson et al., 2003), reconstructions now argue that the complex suite of glacial lineations represents the footprint of two main ice streams, which were regrouped under Ungava fans I and II (Winsborrow et al., 2004; Margold et al., 2015). Based on the available ice retreat chronology (Dyke et al., 2003), the Ungava ice streams (fans I and II) are assigned to the 11.5 to 10.1 cal ka BP interval (Margold et al., 2018).

While this model of capture proposes a viable mechanism to explain the development of the U-shaped unconformity, the evolution of the ice divide system prior to the late-glacial and deglacial interval remains poorly documented. For instance, the large landform assemblages characterizing the LS were initially interpreted as evidence for a long-lived and stable Labrador ice dome (Shilts, 1980), but subsequent mapping from satellite images highlighted the occurrence of additional (older) ice movements that pointed towards more dynamic ice divide system, with important migrations of the different centres of mass (Boulton and Clark, 1990a,b). Accordingly, the sequence of ice flows leading to these apparent reorganizations remain to be documented.

3.3 METHOD

3.3.1 Surficial mapping and till sampling

Mapping of surficial deposits and glacial landforms was carried out in a large area comprising the Whale and George River valleys using satellite images (Rapideye, resolution of 5 m), aerial photographs (1:40,000 scale) and high-resolution Canadian Digital Elevation Model (CDEM; resolution of 12 m). Preliminary interpretations from remote mapping were validated during extensive fieldwork involving helicopter support that covered four summers (2012 to 2015). More than 3,000 sites were visited in order to characterize and document the deposits and landforms. Fieldwork also allowed more than 300 measurements of striations that document former ice flows. A total of 1,200 samples of glacial deposits (till) were collected in order to characterize the sediment composition and document the former subglacial thermal conditions of the different terrains. For this purpose, the major-element geochemistry of the till matrix (<63 μm fraction) was analyzed after a four-acid digestion by Inductively Coupled Plasma Mass Spectrometry (ICP-MS) at Actlabs facility.

3.3.2 Cosmogenic isotopes analyses

Surface exposure dating (SED) was used to gain insights on the age of the landform assemblages and improve the overall chronological framework of the study area. Specifically, ^{10}Be ages were determined on 9 boulders collected from 2 large-scale esker-fed deltas formed in the post-glacial Iberville Sea. We chose large boulders (height >1m) showing no evidence of weathering. Glaciofluvial transport should have caused enough erosion of the boulders to remove inherited cosmogenic signal from previous exposure, if any. We thus interpret our ages as recording the time of delta formation because the shallow water (<2 m) of the depositional settings would only slightly attenuate cosmic rays production.

The cosmogenic isotopes ^{10}Be and ^{26}Al isotopes were measured on four samples collected from bedrock knobs of freshly-eroded glacial lineations (2 sites) and from rock outcrops present in felsenmeer terrains (2 sites) in order to characterize the antiquity of the landform assemblages documented and reinforce our ice-dynamic interpretations based on geomorphological criteria. The combined isotopes provide information on exposure and burial histories, which can potentially be complex in glacial environments (Nishiizumi et al., 1989; Granger and Muzikar, 2001; Briner et al., 2006; Corbet et al., 2013).

At all locations, samples were collected from highly elevated and open sites in order to minimize shielding. The upper two cm of boulders and rock outcrops were sampled with a rock saw to recover ~500 g of material. Sample preparation and quartz separation for ^{10}Be dating were carried out according to standard laboratory protocols developed at the Lamont-Doherty Earth Observatory Cosmogenic Dating Laboratory (Schaefer et al., 2009). The $^{10}Be/^{9}Be$ ratios were measured at Lawrence Livermore National Laboratory (California, USA). Sample preparation for the characterization of cold- and warm-based terrains were done at the GFZ Laboratory (Potsdam, Germany), and $^{26}Al/^{10}Be$ nuclides were measured at the Center for Accelerator Mass Spectrometry at the University of Cologne. Ages were calculated with the online calculator (https://hess.ess.washington.edu) version 3 using the Baffin Bay/Arctic ^{10}Be production rate of 3.96 ± 0.15 atoms g–1 yr–1 (Young et al., 2013) and the nuclide- and time-dependent LSDn scaling scheme (Lifton et al., 2014). For $^{26}Al/^{10}Be$ nuclide analysis, we assume a $^{26}Al/^{10}Be$ production ratio of 6.75 (Balco et al., 2009) and a half-life of 1.36×10^{6} yr (Nishiizumi et al., 2007) and 7.05×10^{5} yr (Nishiizumi, 2004) for ^{10}Be and ^{26}Al, respectively. We report ages and uncertainties of our population following published protocols (Cuzzone et al., 2016; Barth et al., 2018).

Age calculations take into account the post-glacial rebound experienced by the study area since the deglaciation because the on-going isostatic recovery causes a gradual increase of the ^{10}Be production rates throughout this time interval (Cuzzone et al., 2016; Ullman et al., 2016). For this purpose, we quantify the time-varying effects of uplift on ^{10}Be production rates by determining the elevation changes at our sites since their exposure using an isostatic surface-loading model with a spatial resolution of 50 km (Mitrovica et al., 1994). This model includes the influence of ice loading based on the ICE-6G reconstruction of ice thickness and its partnering Earth viscosity model (VM2, Peltier, 2004), ocean loading (Mitrovica and Milne, 2003) and variations in Earth rotation (Mitrovica et al., 2005). The time of initial deglaciation is estimated from the uncorrected ^{10}Be ages obtained at the different sites, for which we derived time-averaged uplift of 38 m for the glaciomarine deltas and the glacially-eroded bedrock knobs, and of 133 m for the felsenmeer sectors. This site-averaged uplift is then subtracted from the measured site elevation, and the corrected elevation is used to calculate the uplift-corrected ^{10}Be ages (Tables 1 and 2).

The changes in atmospheric depth caused by the evolution of local air pressure in a changing post-glacial climate can potentially have an effect on the ^{10}Be production rates (Stone, 2000; Staiger et al., 2007). However, coupled atmospheric-ocean general circulation models have shown that this atmospheric effect is negligible in geological settings similar to our study area (Cuzzone et al., 2016; Ullman et al., 2016). Accordingly, we exclude this correction from the overall exposure age calculations since any corresponding impact on elevation would fall within the measurement uncertainties.

3.4 RESULTS

3.4.1 Landform and sedimentary assemblages

Surficial mapping provides an extensive inventory of landform-sedimentary assemblages that regroups large areas with glacial lineaments and eskers indicative of warm-based ice (erosive) conditions, which coexist with other areas characterized by boulder fields and frost-shattered rock outcrops suggestive of cold-based ice (non-erosive) conditions (Figure 3.2) (Dubé-Loubert et al., 2014). This mosaic of contrasting terrains indicates the occurrence of a significant thermal zonation at the base of the ice-sheet during the last glacial cycle. The mapping of glacio-marine and glaciolacustrine deltas and shorelines in river valleys and other topographic depressions also provides insights on the ice withdrawal pattern during the last deglaciation. The main morphosedimentary zones of the Whale and George River valleys form two distinct assemblages that can be grouped under glacial and deglacial landsystems (Figure 3.2).

3.4.1.1 Glacial landsystems of the George and Whale River Valleys

In the northeastern part of the study area, east of the George River Valley (GRV), the surficial deposits are characterized by large areas of monogenic block fields covering several square kilometers (Zone 1, Figure 3.2). These felsenmeers are primarily found on high topographic plateaus and consist of jointed metre-sized angular boulders and blocks that mantle a thin and oxidized sediment cover (Figure 3.3A). These block fields are pierced in places by intensely frost-shattered and weathered rock outcrops. A few rare outcrops retain evidence of former glacial erosion, with the preservation of small and isolated polished surfaces. In most places, the felsenmeer mantle does not appear to have been modified (reshaped) by recent glacial activity and these terrains likely reflect the persistence of cold-based ice conditions, and possibly former sub-aerial weathering of undefined duration. The intensity of frost-shattering and weathering decreases along the NE-SW regional topographic gradient, with felsenmeer terrains being less developed in the vicinity of the GRV where they are restricted to smaller patches.

The area west of the GRV (Zone 2, Figure 3.2) is marked by the presence of drumlins and crag-and-tails of several hundred meters in length that indicate an ice flow from east to west (Figure 3.3B). These streamlined landforms are composed of greyish silty till showing no evidence of weathering. East-to-northeast oriented crag-and-tails, fluted landforms and roches moutonnées flow are also present in places east of the GRV, in the vicinity of the Falcoz River Valley (Zone 2A, Figure 3.2).

The southeastern part of the study area (Zone 2B, Figure 3.2) is characterized by another swarm of elongated crag-and-tails and drumlinoids composed of relatively fresh till indicating an ice flow towards the east (Figure 3.3C). The pluri-kilometric and low-elevation glacial lineations are confined to a narrow corridor of about 20 km wide and 70 km long part of the Strange Lake ice stream (Batterson, 1989), which has produced a spectacular dispersal train of rare earth elements in the <2 mm fraction of the surface till (Batterson 1989; DiLabio, 1990; Paulen et al., 2017; McClenaghan et al., 2019). These mega-scale glacial lineations (MSGL) gradually disappear to the east, in the vicinity of the Kogaluk River canyon. There, the V-shaped topographic depression does not provide evidence for sustained glacial erosion, thereby indicating that this ice stream likely reached the continental margin and drained directly into the Atlantic Ocean.

The Whale River Valley (WRV) area is also marked by strong variations in the landform and surficial terrain assemblages. The eastern part of this sector that borders the GRV (Zone 3, Figure 3.2) shows extensive areas of hummocky moraine whose irregular mounded surface is punctuated by several kettle pits and metre-sized glacial erratics (Figure 3.3D). The area is mantled by a sandy till blanket commonly pierced by rock outcrops. These characteristics, combined with the lack of glacially-fluted landforms, suggest that those terrains were formed by the melting of a residual ice mass at the end of the deglaciation. On the western end of the WRV (Zone 4, Figure 3.2), the landform assemblage is characterised by two main corridors of elongated drumlins, drumlinoids and crag-and-tails composed of unweathered silty till indicating a fast-flowing ice towards the NNW (Figure 3.3E). These mega-scale lineations alternate with areas of Rogen moraines whose surface is sometimes fluted (Figure 3.3F). These terrains are associated with former ice streams whose upstream portions abut on the hummocky terrains present in Zone 3.

3.4.1.2 Deglacial landsystems of the George and Whale River Valleys

The deglacial landforms documented are primarily represented by eskers and glaciofluvial channels, which show a great variability in terms of composition and spatial distribution and that can be divided in 3 distinct groups. In the eastern part of the study area, eskers are large in size, reaching a few hundred of meters in width and up to 25 m in height while their lengths range from several tens of kms (Zone 1, Figure 3.4; Figure 3.5A). The main ridge is usually steep, sharp-crested and composed of large (> 1m) rounded boulders that are supported by a gravel matrix showing no evidence of weathering. These eskers have a west-to-east orientation and indicate an ice retreat pattern towards the west. These eskers are generally confined to the bottom of the George River tributary valleys but sometimes climb important topographic highs. Over the Strange Lake ice stream terrain, a few eskers are formed by a succession of anastomosing sub-parallel crests and kettle lakes (Figure 3.5B), suggesting a strong fragmentation of the ice margin during its retreat, possibly due to the thinning resulting from the fast flowing ice.

A second group of eskers is found in the western part of the study area, in the WRV (Zone 2, Figure3. 4). They are smaller in size and appear less mature than the eastern set of eskers. They show an average length of ten kilometers, height of 5-6 meters and width of 10 to 20 meters (Figure 3.5C), and are composed of rounded decametric boulders supported by a gravel matrix. Overall, they are mostly discontinuous, forming a succession of flat-top ridges and glaciofluvial outwashs. They are oriented along a NNW-SSE axis, suggesting an ice retreat pattern from north to south. Their spatial distribution extends from the hummocky terrains at the southern end of the study area up to the northernmost part near Ungava Bay, which was invaded by the Iberville Sea (Zone 2, Figure3. 4). These eskers belong to the set of streamlined landforms located north of the Horseshoe unconformity and whose origin and interpretation have been debated in several reconstructions (Kleman, 1994; Veillette et al., 1999; Clark et al, 2000, Jansson et al., 2004).

The geomorphology of the central part of the study area is marked by a lack of eskers. Deglaciation in this region is recorded by numerous side-hill channels that cover the area between the two esker swarms described above (Zone 3, Figure 3.4). These nested ice-marginal channels are of a few hundred meters in length and generally occur in groups of 5 to 6 parallel to each other (Figure 3.5D). The orientation of their long axis is roughly north-south near the George River, and shows a gradual shift to ENE-WSW further to the west. As oppose to eskers that indicate a deglaciation with a warm-based (active) ice margin, these channels are generally associated with the retreat of a cold-based (sluggish) ice margin (Dyke, 1993).

Another set of deglacial landforms relate to the postglacial marine incursion that flooded the isostatically-depressed terrains near Ungava Bay, with raised deltas, beaches and other near-shore deposits, as well as erosive features associated with the reworking of sediments by wave/littoral action. The maximum elevation reached by the Iberville Sea shows significant differences across the region, with marine landforms indicating a marine incursion at elevation up to 160 m in the WRV and 100 m in the GRV, reflecting an asynchronous marine incursion and/or different glacio-isostatic adjustment pattern. Most of the WRV eskers were terminating into Iberville Sea where they built important deltas (Figure 3.5E). These glaciomarine deltas rest directly on fine-grained marine sediments and suggests that the ice margin initially retreated in contact with the Iberville Sea.

3.4.2 Till geochemistry in cold- and warm-based terrains

The major-element chemistry of the till matrix is used to further characterize the extent of cold- and warm-based terrains documented from geomorphic characteristics. For this purpose, we used the Chemical Index of Alteration (CIA) that documents the degree of weathering undergone by a crystalline bedrock (feldspars) source prior to its erosion and transport (Nesbitt and Young, 1982). This CIA index has been used with success in formerly glaciated environments to document the degree of weathering of the material eroded and transported by ice-sheets (Roy et al., 2004; Refsnider and Miller, 2010; Refsnider and Miller, 2013). This approach is suitable in the study area given the composition and homogeneity of bedrock, which consist mainly of Paleoproterozoic migmatic gneiss and granodiorite that are devoid of carbonates (Lafrance et al., 2016). Our premise here is based on the fact that erosion associated with cold-based ice is generally low (or nil) compared to warm-based ice. Consequently, glacial deposits in cold-based regions should have a composition that reflect minimal erosion of rocks or deposits that have experienced long (likely cumulative) periods of subaerial exposure. Conversely, tills in warm-based terrains derive from the erosion of bedrock and deposits that were subject to intense glacial erosion that resulted in the production of fresh/unweathered deposits. Accordingly, the geochemical composition of tills from old/relict terrains should yield high CIA values, while tills in warm-based ice areas should show lower CIA values.

The highest CIA results (70) are confined to the NE part of the study area where felsenmeer and frost-shattered bedrock dominate (Figure 3.6), thereby providing further evidence for limited glacial erosion and transport in this sector, consistent with the geomorphological observations documented from mapping. At the opposite, the lowest CIA results (60) are found in sectors characterized by swarms of streamlined landforms that form ice stream corridors (Figure 3.6). CIA values are less reliable in the southwestern part of the study area because of the presence of distinct bedrock lithologies of the Labrador Trough that comprise carbonate-bearing metasedimentary rocks (Dimroth, 1978). Overall, the large number and density of samples allow a reliable interpolation of the CIA results that delineate several areas characterized by high and low CIA values. The overall pattern of CIA values indicates that high CIA values correspond to areas characterized by felsenmeer and frost-shattered rock outcrops that are suggestive of cold-based areas, while low CIA values are found in well-developed streamlined landforms till plains indicative of an intense glacial activity (Figure 3.6).

3.4.3 Ice-flow sequence and relative chronology

A total of 300 striations and associated erosional features were measured and the different ice-flow directions recorded can be grouped under 4 broad events (Figure 3.7). The oldest movement is towards the NE and was documented from poorly preserved striations and grooves on rare and scattered glacially-polished surfaces present mostly to the east of the GRV (Figure 3.7, pink arrows), in an area characterized by extensive felsenmeer cover and frost-shattered bedrock. Although the geomorphic context suggests that these ice-flow indicators may relate to the old NE movement documented in the Schefferville area (Klassen and Thompson, 1993), differentiating this ice flow from a younger movement of same orientation remains difficult. This ice flow is associated with the few eastward crag-and-tails mapped in the vicinity of the Falcoz River (Zone 2A, Figure 3.2). In the southeast, this movement is cross-cut by the younger ice flow related to the Strange Lake ice stream (Figure 3.7, orange arrows).

A second ice movement towards W to WNW was documented in the area comprised between the George River and the central part of the study area (Figure 3.7, green arrows). In the vicinity of the GRV, this movement intersects the older NE movement, forming a system of opposite ice flows. This ice flow is associated with the set of W- to WNW-trending landforms (crag-and-tails and fluted features) described above. This second movement is in turn cross-cut by a set of younger ice flows converging towards Ungava Bay that form the third regional movement present in the WRV vicinity (Figure 3.7, dark blue arrows). There, widespread striations showing N to NNW ice flows are present, consistent with the orientation of the streamlined landforms that dominate the geomorphology of this sector. These ice flows are associated with the late-glacial Ungava ice streams (Ungava fan I and II; Winsborrow et al., 2004; Margold et al., 2015), which appear to have obliterated older striations, except in a few places where outcrops with sheltered faces show an overlap with the W to WNW movements. The striation measurements show slight inflections in these late ice flows, while the cross-cutting relationships identified are consistent with the scenario of at least 2 surge events.

3.4.4 ^{10}Be SED results

The summary of ^{10}Be ages obtained from 9 boulders belonging to two glaciomarine deltas is presented in Table 1. With the exception of one sample (14HDL-A-06), analytical uncertainties range between 2.52 and 4.2 %. The ^{10}Be concentrations from each deltas are internally consistent (Table 3.1), with only one boulder (14HDL-08) having an age that can be considered as an outlier (13,900 ± 400 a, Table 1). The ^{10}Be ages from delta A (n=5) and B (n=3) yield mean ages of 8,400 ± 300 and 8,400 ± 300 a, respectively.

Results for the ^{10}Be and ^{26}Al analyses of rock surfaces sampled from glacially-eroded bedrock knobs of crag-and-tails (Trans-2 and Trans-3 sites) and from weathered outcrops in felsenmeer terrains (Trans-1 and Trans-4 sites) are presented in Table 3.2. The sites exhibiting "fresh" surfaces showed measured concentrations of 6.0×10^4 and 5.98×10^4 atoms g^{-1} for ^{10}Be and 3.98×10^4 and 3.33×10^4 atoms g^{-1} for ^{26}Al, yielding single-nuclide minimum exposure ages of 9,400 ± 500 and 9,200 ± 400 for ^{10}Be, and 7,900 ± 400 and 6,800 ± 400 for ^{26}Al. The ^{26}Al/^{10}Be ratios from these samples showed values of 6.59 ± 0.45 and 5.74 ± 0.41 respectively, with Trans-3 ratio plotting under the so-called "constant exposure line" of ~6.75 (Figure 3.8).

The weathered rock surfaces outcropping in block fields revealed measured cosmogenic concentrations of ^{10}Be values an order of magnitude higher than those of the two "fresh" samples, with 14.2×10^5 and 12.8×10^5 atoms g^{-1}, while ^{26}Al values are 9.03×10^5 and 7.93×10^5 atoms g^{-1}. The corresponding single-nuclide minimum exposure ages are 18,100 ± 700 a and 18,200 ± 800 ka for ^{10}Be, and 14,800 ± 700 and 14,600 ± 2000 a for ^{26}Al. The ^{26}Al/^{10}Be ratios from Trans-1 and Trans-4 are 6.34 ± 0.38 and 6.21 ± 0.97 respectively, plotting just under the ~6.75 threshold (Figure 3.8).

3.5 DISCUSSION

3.5.1 Glacial morphosedimentary assemblages and their chronological relationships

Mapping and field investigations indicate significant variations in glacial landforms and sediments across the study area that provide evidence for a polythermal ice cover. Extensive areas of boulder fields and highly frost-shattered bedrock indicate the occurrence of widespread cold-based ice conditions to the east and northeast of the GRV (Figure 3.9, purple terrains). This is consistent with the relatively high CIA values documented from a large set of samples that indicate that these terrains were not subject to significant glacial erosion/transport during the last glacial cycle. Indeed, the intensity/level of weathering in some places suggests that part of these terrains likely experienced earlier subaerial (interglacial?) conditions. Assessing the age of these cold-based terrains remains difficult but insights can be gained from measurements of paired cosmogenic isotopes.

A complex exposure history for these terrains is indicated by two rock surfaces sampled in felsenmeer that show ^{26}Al/^{10}Be ratios that fall under the ~6.75 constant exposure line (Table 3.2, Fig 3.8), which indicate at least one period of burial (or exposure interruption, typically by ice) prior to the last exposition (Briner et al., 2006). The concentrations of cosmogenic isotopes measured are somewhat modest, but they remain an order of magnitude higher than those measured from two "fresh" rock surfaces. The results clearly point to an inheritance signal, as indicated by the apparent old ^{10}Be ages of 18,100 ± 700 a and 18,200 ± 800 a ^{10}Be ages (Table 3.2). Cold-based ice conditions have also been reported previously in the region, notably in the Torngat Mountains where ^{10}Be and ^{26}Al exposure dating on high-elevation tors and felsenmeer yielded ages ranging from 73 ± 6 to 157 ± 15 ka, which were interpreted as evidence for a low-erosive ice cover (Marquette et al., 2004). ^{26}Al/^{10}Be ratios (between 4 and 6) also showed that the exposure of the high-elevation terrains has been interrupted during at least one shielding event, namely by ice or till cover (Marquette et al., 2004). The lower ^{26}Al/^{10}Be ratios obtained for the rock surfaces measured in the study areas may reflect minor glacial activity, as indicated by the field investigations that revealed a few and scattered evidence for glacial erosion (striations), which may have partly eroded some of the cosmogenic signal associated with previous exposures. Nonetheless, our results indicate that some of these terrains have an exposure history older than the last glacial cycle.

These cold-based terrains to the east of the GRV coexist with small and areally restricted sectors characterized by occasional glacial lineaments and glacially-sculpted (striated) outcrops that indicate an ice flow towards the northeast (Figure3.9, yellow terrains). This patchwork of cold- and warm-based terrains underlie the existence of a thermal zonation at the base of the ice-sheet, which may be related to the presence of the eastern branch of the Labrador ice divide on the high topographic plateaus of this region. Evidence for a complex polythermal ice-cover in the region has also been documented across an elevation-gradient throughout the Torngat Mountains where high-plateaus are characterised by cold-based (non-erosive) ice conditions and the valley floors by wet-based (erosive) sub-glacial conditions (Staiger et al., 2005).

The occurrence of striations and streamlined landforms in the vicinity and to the west of the GRV indicating a major ice flow towards the WNW outlines a system of opposite ice flows that further delineates the broad location of this ice divide (Fig 3.9, red terrains). Paleogeographic reconstructions assign the activity of this ice divide to (or close to) the LGM (Dyke and Prest, 1987). Cross-cutting relationships between the NE and WNW ice movements also indicate a displacement of the ice divide towards the east, likely in response to the initiation of ice streaming in the Ungava lowlands, which resulted in thinning to the west of the ice mass. A few cross-striation sites show that these LGM ice flows are cut by a younger ice flow related to the Strange Lake ice stream (Figure 3.9, orange terrains). This corridor of fast flowing ice did not drain through the topographic depression formed by the Fraser Canyon, indicating that the ice margin was likely in direct contact with the Labrador Sea when this ice stream was active. Consequently, these results indicate that this system of ice flows relates to a period that followed the LGM, but that likely remained active up to the onset of the deglaciation, as suggested by the configuration of the network of eskers associated with the streamlined landforms (see section 3.5.2).

The large set of streamlined landforms to the west of the WRV that indicates a massive ice flow towards Ungava Bay represents the youngest glacial terrain in the study area (Figure 3.9, blue terrains). The intensity of the glacial activity (erosion) is also indicated by the lowest CIA values documented from the till matrix geochemistry. This ice flow system relates to ice stream corridors, which clearly cross-cut the older westward ice flow system. This relative chronology is consistent with the one reported in other works located south and south-west of the study area (c.f., Klassen and Thompson, 1993; Veillette et al., 1999).

3.5.2 Deglacial morphosedimentary assemblages and ice retreat patterns

Eskers represent the most common deglacial landform in the study area and they can be used as geomorphic markers that document the ice retreat pattern. Indeed, several characteristics of eskers – such as lateral spacing, stream ordering, sinuosity and spatial distribution – have been used to characterize deglacial dynamics in formerly glaciated regions (Brennand, 2000; Boulton et al., 2009; Storrar et al, 2013). However, very few have put forward the dimensional (height, width) and sedimentological characteristics to document changes in the mode and/or relative timing of esker formation.

The development of an esker is directly linked to the hydraulic gradient, which is primarily controlled by ice-sheet topography and surface slope (Shreve, 1972; Syverson et al., 1994; Storrar et al., 2014). Studies have also shown that the dimensions of subglacially-formed tunnels are function of the basal water pressure, which depends on several factors, such as the weight of the overlying ice (ice-surface gradient), the magnitude of the meltwater discharge, the debris concentration at the bed (Shreve, 1985a), and the nature or permeability of the underlying bedrock (Clark and Walder, 1994; Grasby and Chen, 2005). The formation of a continuous ridge is function of the incumbent weight of the ice and its spatial distribution will depend on the areal variations in (lower) basal pressure (Shreve, 1985b.). The configuration and characteristics of esker networks can in turn be used to reconstruct ice-surface profiles and ice thicknesses (Shreve, 1985a).

Based on these considerations, we assign a relative age to the two distinct sets of eskers documented in the study area (Figure 3.10). The large and long eskers that characterize the eastern part of the study area are associated with a time of formation when this sector of the ice-sheet was thick and important in size since the development of this esker system requires a significant hydraulic gradient. Accordingly, the development of these eskers likely relates to a time just after the LGM. In contrast, we associate the small and discontinuous eskers of the northwest sector of the study area (west of the WRV) to a later time, likely corresponding to the late-glacial/deglacial interval when the ice mass was thinner. These small and discontinuous eskers follow the regional topographic gradient (slope) and their formation requires a smaller hydraulic gradient.

The area between the two main sets of deglacial landforms is characterized by a lack of eskers and the presence of numerous side-hill channels (Figure 3.10). This type of channels has been reported in several places in the Arctic (Skidmore and Sharp, 1999; O'Cofaigh et al., 1999) and Antarctica (Atkins and Dickinson, 2007) and is commonly associated to the deglaciation of a subglacially frozen ice margin. These channels form when basal ice temperature is below freezing, preventing the migration of supra/interglacial meltwater to the base, which is then conducted towards the ice front (supra or intraglacially), resulting in the formation of a series of channels parallel (or lateral) to the ice margin (Atkins and Dickinson, 2007). The absence of eskers and other deglacial landforms in this part of the study area, such as outwash plains, is consistent with inferred cold-based ice conditions (Dyke 1993, O'Cofaigh et al., 1999, Atkins and Dickinson 2007). These channels thus indicate that the deglaciation beyond the terrain separating the GRV and WRV occurred under cold-based ice conditions, with meltwater being trapped between the retreating frozen ice margin and the higher slope to the east. These channels are oriented roughly north-south near the GRV and they shift to a ENE-WSW orientation near the WRV, suggesting an initial ice withdrawal towards the west, which was followed by a retreat towards the NNW.

These side-hill channels have been used to develop a different deglaciation model in earlier reconstructions (Kleman et al., 1994; Jansson, 2004). The ENE-trending proglacial channels were then associated to a pattern of ice retreat towards the WSW (Kleman et al., 1994). Because these channels were oriented at angle with streamlined landforms and eskers indicating ice flowing towards the NNW, these channels were considered inconsistent with the glacial landform assemblage they cross-cut. Accordingly, the Ungava Bay streamlined landforms were interpreted as relict features that formed prior to the late-glacial interval and that were preserved under cold-based ice conditions that lasted throughout most of the last glacial cycle (Kleman, 1994). These channels are here associated with the retreat of a frozen ice margin towards W and NNW, which is consistent with the orientation of streamlined landforms and eskers. However, the change documented in the deglacial landform assemblages across the study area indicates a change in the mode of ice retreat during the regional east to west deglaciation, which went from warm-based conditions (eskers) in the east to cold-based ice conditions (side-hill channels) in the center of the study area. The driver(s) acting behind this transition from cold- to warm-based conditions are difficult to identify, but it may reflect a climatically driven change or a response to local glaciological parameters. Nonetheless, this points to a relatively complex spatial arrangement of the thermal basal conditions, which evolved through time and appears to have played an important role in the development and stabilization of the different phases of glacial Lake Naskaupi (Dubé-Loubert and Roy, 2017).

The system of side-hill channels could have formed just before, or perhaps synchronously with the set of small eskers in the Ungava Bay lowlands. If so, these two deglacial landform assemblages suggest polythermal sub-glacial conditions of the retreating ice-margin during the last deglaciation. Indeed, the Ungava Bay eskers imply wet-based ice conditions of the southward retreating ice margin while at the same time, the westward retreating margin at the interfluve between the GRV and the WRV formed side-hill channels. This idea of a polythermal ice-cover during deglaciation is also consistent with the chronological constraints obtained, which suggest that the eskers set were formed at around 8400 ± 300 a, while the eastern ice margin – and the associated side-hill channels – dammed Lake Naskaupi in the George River basin at around 8300 ± 300 a (Dubé-Loubert et al., 2018).

3.5.3 Chronological constraints on landform assemblages

Dating of the two glacio-marine deltas yielded mean ^{10}Be age of 8400 ± 300 a that is consistent with chronological data on the regional deglaciation (Dyke, 2003; Dubé-Loubert et al., 2018). These deltas were fed by eskers that belong to the Ungava Bay landform swarm, thereby indicating that this landsystem developed in late-glacial time, sometimes before the complete deglaciation of this sector, which occurred after the 8100-8700 a interval according to our data. Consequently, these results do not support reconstructions associating these landforms to a relict landscape that was preserved by a cold-based ice mass centered over Ungava Bay (Kleman, 1994; Jansson, 2004). In addition, our mapping did not reveal widespread cold-based ice conditions in the area north of the Horseshoe boundary. Geomorphological features typical of cold-based ice conditions are found on elevated grounds in the northeastern part of the study area where terrain are dominated by block fields and frost-shattered bedrock, and in the center part where side-hills channels were formed during part of the deglaciation.

Additional information on the timing of ice retreat comes from the dating of “fresh” glacially-polished bedrock knobs of crag-and-tails that yielded ^{10}Be ages of 9,400 ± 500 a (Trans-2) and 9,200 ± 400 a (Trans-3) that are roughly consistent with the deglaciation framework of the region (Dubé-Loubert et al., 2018). However, these ages could be considered slightly too old. Indeed, Trans-3 sample shows a $^{26}Al/^{10}Be$ ratio of 5.74 ± 0.41 that indicate a complex burial history, which likely suggests some inheritance of cosmogenic nuclides due to insufficient erosion, common in formerly glaciated environments (Briner and Swanson, 1998; Davis et al., 1999). This may be related to the fact that this landform is located near the former position of the Labrador ice divide, an area typically characterized by low-erosive ice cover.

These new ^{10}Be ages may be used with the available geochronological constraints to gain insights on the rates of ice retreat in the region. If we consider that the glacially-fluted landforms located west of the WRV belong to the same event that produced the Gold Cove surge at 10 ka (Flow IV of Veillette et al, 1999, Figure 3.11A), which culminated with a final position on the southeastern tip of Baffin Island (Stravers et al., 1992; Kaufman et al., 1993), we can use the distance between this location and the ice-contact deltas dated (470 km) to derive a southward rate of ice retreat of 300 m/y. By extrapolating this rate, we can estimate that the northern margin of the LS reached the south of the study area at around 8 ka, which corresponds to the region where streamlined landforms and eskers of the Ungava lowlands begin (Figure 3.10). This rate may be slightly overestimated due to the presence of a calving ice margin (ice shelf) in Ungava Bay, but nonetheless it provides a broad constraint on ice retreat. This suggests that the Ungava Bay landform swarms (and ice streams) located west of the WRV and north of the Horseshoe unconformity have been emplaced sometimes between 10 ka and 8 ka (Figure 3.11A).

Similarly, an estimate for the westward rate of ice retreat may be calculated using available ^{14}C ages that delineate a regional isochrone placing the LS eastern margin on the Labrador Coast at around 10 ka (Clark and Fitzhugh, 1992; Dyke, 2003). Inland, the ^{10}Be ages on the bedrock knobs suggest the onset of ice withdrawal in the vicinity of the GRV at around 9,400 ± 500 a (Trans-2), which is roughly consistent with the mean age of 8300 ± 300 a obtained from the ^{10}Be dating of Lake Naskaupi shorelines that requires the presence of the ice margin in this region (Dubé-Loubert et al., 2018; Figure 3.11B). From these results and the intervening distance between these locations, we can determine an E-W ice retreat rate of 150 m/y.

This difference between the southward and the westward estimates of ice withdrawal rates indicate a rapid ice retreat from north to south and slower withdrawal from east to west. The faster N-S ice retreat could be explained by the marine-based ice margin in the WRV area, a context that usually favours ice calving and rapid ice withdrawal (Figure 3.11B). The slower east-west ice retreat may also explain the asynchronous incursion of Iberville Sea that is indicated by the differences in elevations of marine landforms between the George River (100 m) and Whale River (160 m) estuaries. This pattern of ice retreat points to the progressive isolation of a residual ice mass at the interfluve of the GRV and the WRV between 7 and 8 ka (Figure 3.11C). This residual of the LS likely explains the damming and development of Lake McLean (Barnett 1967), a glacial lake that coexisted with Lake Naskaupi.

3.5.4 The Horseshoe unconformity

The results from surficial mapping, striation measurements and cosmogenic dating outline at least four distinct landform-sediment assemblages representing different glacial events that can be grouped into a relative chronology documenting the evolution of the NE part of the LS. Our reconstruction shows a system of opposing ice flows that is commonly attributed to the eastern branch of the Horseshow ice divide in this region. The landform and terrain assemblage east of this boundary indicates an important regional ice flow towards the east-northeast (Figure 3.9, yellow area), whereas those to the west of this line show another extensive ice flow towards the west-northwest (Figure 3.9, red area). Geomorphological considerations based on the morphology of eskers and the relationships of cross-cutting striations suggest that this system dates back to the LGM and remained active throughout the early part of the deglaciation. Another landform assemblage is present to the southeast of study area and relates to the Strange Lake ice stream (Figure 3.9, orange area). Although this ice-flow system also originates from the same ice divide sector, cross-cutting relationships indicate it has developed after the NE ice flow. The westernmost part of the study area is characterized by another set of glacial lineations and eskers that indicates a massive NNW ice flow towards Ungava Bay, which form another landform and terrain assemblage (Figure 3.9, blue area). These landforms and terrains were produced by the Ungava Bay ice streams under at least two surge events, for which our chronological data assign to the late-glacial/deglacial interval (Figure 3.11A). This ice-flow system clearly crosscuts the west-to-northwestward landform assemblage and does not represent an extension of this ice movement.

The areal extent of the different sets of glacial lineations and their associated relative chronology suggests that the Ungava Bay lowlands ice streams developed through the southward propagation of the fast-flowing ice into a former LS dome, which resulted by the formation of a narrow zone of intersecting ice flows that define the Horseshoe unconformity, thereby landing support to the catchment mechanism documented in earlier studies (Hughes, 1964; Veillette et al., 1999). The initiation of these ice surges in the Ungava Bay lowlands in late-glacial time may also be responsible for the eastward migration of the Labrador ice divide we report. The occurrence of glacial lineaments associated with the southward (outward) ice flow system north of the Horseshoe boundary (Clark et al., 2000) remain features that are difficult to explain.

Our reconstruction indicates that the area north and west of the so-called Horseshoe unconformity consists of a mosaic of terrains that formed through distinct glacial events of slightly different ages, which share an apparent common similarity in the fact that they show a convergence of ice flow towards Ungava Bay. The system of opposing ice flows located in the axis of the GRV thus represents an older feature that is entirely unconnected to the Ungava Bay ice surges, and that likely relates to the so-called Labrador ice divide. Accordingly, the relationship between the two landform assemblages located on either side of the Horseshoe boundary cannot be associated with an ice divide, but rather to the maximum extent (up-ice capture) of a late-glacial system of ice flows. The arcuate shape of the Horseshoe boundary and its appearance as an ice divide position is an artefact of landsystem generation/preservation (Clark et al., 2001) and its position is defined by local topographic configuration such as the southern limit of the Ungava Bay catchment area.

3.6 CONCLUSION

The combination of field-based and remote mapping provides a detailed view of the nature and spatial distribution of landforms and terrains for the northeastern part of the Labrador Sector. The results outline at least four main glacial assemblages related to distinct ice flows that can be grouped into separate events. Extensive striation measurements provide a relative chronology on ice-flow sequence and delineate a narrow zone of opposing ice movements that relate to the former positions of the Labrador ice divide. To the north-east of this divide, terrains consist of felsenmeer and frost-shattered rock surfaces typical of cold-based ice cover, with scattered evidence of glacial activity indicating an old northeastward ice flow. Till geochemical composition and paired cosmogenic isotopes further constrain the former subglacial thermal conditions that prevailed during the last glaciation and subsequent deglaciation. To the west of the presumed divide position, streamlined landforms show a west-northwestward ice flow. Cross-cutting relationship between ice flow striations and geomorphological considerations suggest that this system of opposite ice flows was active likely during the LGM and thereafter. Cross-cutting striations further indicate a eastward migration of this ice divide. This change in configuration appears to be related to the development of another ice flow system further to the west consisting of highly elongated glacial lineations that indicate a massive north-northwestward ice flow into the Ungava Bay lowlands. This landform assemblage relates to the development of at least two prominent ice surges. Surface exposure dating on esker-fed glaciomarine deltas indicate that this geomorphic system formed during the late-glacial interval, thereby ruling out models associating these landforms to relict features preserved under extensive cold-based ice conditions by an ice mass centered over the Ungava Bay during the last glacial cycle.

Our reconstruction suggests that the assemblage of glacial and deglacial landforms north of the so-called Horseshoe unconformity was formed by several distinct glacial events of slightly different ages that share a similar orientation indicating a convergent ice flow towards Ungava Bay. The spatial distribution and extent of the Ungava Bay streamlined landforms suggest that the narrowness of the Horseshoe unconformity relates to the development and subsequent southward propagation of the Ungava Bay ice streams, thus supporting the capture model (Hughes, 1964; Veillette et al., 1999).

Deglacial landforms across the study area can also be divided into three different groups that indicate significant changes in the deglaciation pattern/style through time. To the east of the divide, a large esker network indicates that ice retreat occurred under warm-based conditions. This pattern shifts in the vicinity of the George River where multiple ice-marginal meltwater channels record the retreat of a cold-based ice margin towards west, which appears to have an important role in the damming of glacial lakes Naskaupi and McLean. Finally, to the west, the small eskers that accompany the swarm of streamlined landforms record the southward ice retreat of the margin from the Ungava Bay lowlands towards the uplands late during the deglaciation.

These results indicate that the evolution of the NE part of the LS was highly dynamic during the last glaciation and deglaciation, with important shifts in ice flows and deglaciation patterns, which provide important inputs to paleogeographic reconstructions and strengthen glaciological models of the LIS. This work bring also critical elements in applied sciences like base-metal and diamond exploration in glaciated terrains where knowledge on ice-flow patterns, subglacial conditions and ice-sheet dynamics are highly important.

3.7 ACKNOWLEDGEMENTS

Logistical support for this study was provided through a mapping programm of the Ministry of Energy and Natural Resources of the Province of Quebec. Financial support came from MERNQ (HDL, MR), a NSERC Discovery Grant (MR) and the Climate Center of LDEO (JMS, MR). We thank Hella Wittmann-Oelze at GFZ in Postdam for the cosmogenic analyses. Jack Ives kindly shared insights and historical background on the glacial geology of Ungava-Labrador. Discussions in and outside the field with B. Mclenaghan, R. Paulen, J. Rice and M. Ross were also appreciated. Assistance during fieldwork was assured by V. Daubois, S. Hébert, O. Lamarche and I. Randour. V. Daubois and A-.M. Beauchamp assisted in the production of some figures. BCGQ external contribution no. 8450-2018-2019-04.

3.8 REFERENCES

Atkins C.B., Dickinson W.W. 2007. Landscape modification by meltwater channels at margins of cold-based glaciers, Dry Valleys, Antarctica. Boreas 36, 47-55.

Balco G., Briner J., Finkel R., Rayburn J., Ridge J., Schaefer, J. 2009. Regional beryllium-10 production rate calibration for late-glacial northeastern North America. Quaternary Geochronology 4, 93-107.

Barber D.C., Dyke A., Hillaire-Marcel C., Jennings A.E., Andrews J.T., Kerwin M.W., Bilodeau G., McNeely R., Southon J., Morehead M.D., Gagnon J-M., 1999. Forcing of the cold event of 8200 years ago by catastrophic drainage of Laurentide lakes. Nature 400, 344-348.

Barnett D.M. 1967. Glacial Lake MacLean and its relationship with glacial Lake Naskaupi. Geogr. Bull. 9, 96-101.

Barth A.M., Clark P.U., Clark J., Roe G.H., Marcott S.A., McCabe A.M., Caffee M.W., Cuzzone J.K., Dunlop P. 2018. Persistent millennial-scale glacier fluctuations in Ireland between 24 ka and 10 ka. Geology. https://doi.org/10.1130/G39796.1.

Batterson, M.J. 1989. Glacial dispersal from the Strange Lake alkalic complex, northern Labrador, in R.N.W. DiLabio and W.B. Coker, eds., Drift Prospecting: Geological Survey of Canada, Paper 89–20, 31-40.

Boulton, G.S., Clark, C.D., 1990a. A highly mobile Laurentide ice sheet revealed by satellite images of glacial lineations. Nature 346, 813-817

Boulton, G.S., Clark, C.D., 1990b. The Laurentide ice sheet through the last glacial cycle: the topology of drift lineations as a key to the dynamic behaviour of former ice sheets. Earth Environ. Sci. Trans. R. Soc. Edinb. 81, 327-347.

Boulton, G.S., Hagdorn, M., Maillot, P.B., Zatsepin, S., 2009. Drainage beneath ice sheets: groundwater-channel coupling and the origin of esker systems from former ice sheets. Quaternary Science Reviews 28, 621-638.

Brennand T.A. 2000. Deglacial meltwater drainage and glaciodynamics: inferences from Laurentide eskers, Canada. Geomorphology 32, 263-293.

Briner J.P., Swanson T.W. 1998. Using inherited cosmogenic Cl-36 to constrain glacial erosion rates of the Cordilleran ice sheet: Geology 26, 3-6.

Briner J.P., Miller, G.H., David P.T., Finkel, R.C. 2006. Cosmogenic radionuclides from fjord landscapes support differential erosion by overriding ice sheets. Geological Society of America Bulletin 118, 406–420.

Carlson A.E., Clark P.U., 2012. Ice sheet sources of sea level rise and freshwater discharge during the last deglaciation. Reviews of Geophysics 50, 1-72.

Clark P.U., Fitzhugh, W.W., 1992. Postglacial relative sea level history of the Labrador coast and interpretation of the archaeological record. Chapter 9 in L.L. Johnson (ed.), Paleoshorelines and Prehistory: an investigation of method, Boca Raton, 189-213.

Clark C.D., Knight J.K., Gray J.T. 2000. Geomorphological reconstruction of the Labrador sector of the Laurentide Ice Sheet. Quaternary Science Review 19, 1343-1366.

Clark, P.U., Walder, J.S. 1994. Subglacial drainage, eskers, and deforming beds beneath the Laurentide and Eurasian ice sheets. Geological Society of America Bulletin 106, 304-314.

Clark, P.U., Marshall, S.J., Clarke, G.K.C., Hostetler, S.W., Licciardi, J.M., Teller, J.T. 2001. Freshwater forcing of abrupt climate change during the last glaciation. Science 293, 283-287.

Clark P.U., Brook E.J., Raisbeck G.M., Yiou F., Clark J. 2003. Cosmogenic ^{10}Be ages of the Saglek moraines Torngat mountains, Labrador. Geology 7, 617-620.

Corbett L.B., Bierman P.R., Graly J.A., Neumann T.A., Rood D.H. 2013. Constraining landscape history and glacial erosivity using paired cosmogenic nuclides in Upernavik, northwest Greenland. Geological Society of America Bulletin 125, 1539-1553.

Cuzzone J.K., Clark P.U., Carlson A.E., Ullman D.J., Rinterknecht V.R., Milne G.A., Lunkka J.P., Wohlfarth B., Marcott S.A., Caffee M. 2016. Final deglaciation of the Scandinavian Ice Sheet and implications for the Holocene global sea-level budget. Earth and Planetary Science Letters 448, 34-41.

Davis P.T., Bierman P.R., Marsella K.A., Caffee M.W., Southon J.R. 1999. Cosmogenic analysis of glacial terrains in the eastern Canadian Arctic: A test for inherited nuclides and the effectiveness of glacial erosion. Annals of Glaciology 28, 181-188.

DiLabio R.N.W. 1990. Glacial dispersal trains, in R. Kujansuu and M. Saarnisto, eds., Glacial Indicator Tracing: A.A.-Balkema, Rotterdam, 109-122.

Dimroth, E. 1978. Rapport géologique de la région de la Fossse du Labrador. Ministère des Richesses Naturelles, Report-RG-193 (includes 1 map), 417 p.

Dubé-Loubert H, Roy M. 2014. Glacial landforms of the southern Ungava Bay region (Canada): implications for the late-glacial dynamics and the damming of glacial Lake Naskaupi. Poster Presentation EGU General Assembly (Vienna, Austria).

Dubé-Loubert H, Roy M. 2017. The development, evolution and drainage of glacial Lake Naskaupi during the deglaciation of north-central Quebec and Labrador. Journal of Quaternary Science 32, 1121-1137.

Dubé-Loubert H, Roy M, Schaefer J.M., Clark P.U. 2018. ^{10}Be dating of former glacial Lake Naskaupi (Quebec-Labrador) and timing of its discharges during the last deglaciation. Quaternary Science Reviews 191, 31-40.

Dyke A.S., Prest V.K. 1987. Late Wisconsinan and Holocene retreat of the Laurentide Ice Sheet, Géographie Physique et Quaternaire 41, 237-263.

Dyke A. S. 1993. Landscapes of cold-centred Late Wisconsinan ice caps, Arctic Canada. Progress in Physical Geography, 17, 223-247.

Dyke A.S., Moore A., Robertson L. 2003. Deglaciation of North America. Geological Survey of Canada. Open File 1574, Ottawa.

Granger D. E., Muzikar P. F. 2001. Dating sediment burial with in situ-produced cosmogenic nuclides: Theory, techniques, and limitations. Earth and Planetary Science Letters 188, 269-281

Grasby S. E., Chen Z. 2005. Subglacial recharge into the Western Canada Sedimentary Basin: Impact of Pleistocene glaciation on basin hydrodynamics, Geological Society of America Bulletin 117, 500- 514.

Hemming, S.R. 2004. Heinrich events: massive late Pleistocene detritus layers of the north Atlantic and their global climate imprint. Review of Geophysics 42, 1-43.

Hughes, O. L. 1964. Surficial geology, Nichicun-Kaniapiscau Maparea. Geological Survey of Canada, Bulletin 106, 20 pp.

Ives JD. 1960. Former ice-dammed lakes and the deglaciation of the middle reaches of the George River Labrador-Ungava. Geographical Bulletin 14, 44-70.

Jansson, K., Stroeven, A., Kleman, J., 2003. Configuration and timing of Ungava Bay ice streams, Labrador-Ungava, Canada. Boreas 32, 256-262.

Jansson, K., Kleman, J. 2004. Early Holocene glacial lake meltwater injections into the Labrador Sean and Ungava Bay. Paleoceanography 19, 1-12.

Kaufman, D. S., Miller, G. H., Stravers, J. A., & Andrews, J. T. 1993. Abrupt early Holocene (9.9-9.6 ka) ice-stream advance at the mouth of Hudson Strait, Arctic Canada. Geology 21, 1063-1066.

Klassen R.A., Thompson F.J. 1993. Glacial history, drift composition, and mineral exploration, central Labrador. Geological Survey of Canada, Bulletin 435, 76 pp.

Kleman, J., Borgstrom, I., Hättestrand, C. 1994. Evidence for a relict glacial landscape in Quebec-Labrador. Palaeogeography, Palaeoclimatology, Palaeoecology 111, 217-228.

Kleman, J., Hättestrand, C. 1999. Frozen-bed Fennoscandian and Laurentide ice sheets during the Last Glacial Maximum. Nature, 402, 63-66

Kleman J, Jansson KN, De Angelis H *et al.* 2010. North American Ice Sheet build-up during the last glacial cycle. Quaternary Science Reviews 29, 2036-2051.

Lafrance, I., Bandyayera, D., Charette, B., Bilodeau, C., David, J. 2016. Géologie de la région du Lac Brisson (SNRC 24A). Ministère de l'Énergie et des Ressources naturelles–Québec, Report-RG-2015-05 (includes 1 map): 64 p.

Lifton N., Sato T., Dunai T.J. 2014. Scaling in situ cosmogenic nuclide production rates using analytical approximations to atmospheric cosmic-ray fluxes. Earth and Planetary Science Letters 386, 149-160.

Margold, M., Stokes, C.R., Clark, C.D., Kleman, J. 2015. Ice streams in the Laurentide Ice Sheet: a new mapping inventory. Journal of Maps 11, 380-395.

Margold, M., Stokes, C.R., Clark, C.D. 2018. Reconciling records of ice streaming and ice margin retreat to produce a palaeogeographic reconstruction of the deglaciation of the Laurentide Ice Sheet. Quaternary Science Reviews 189, 1-30.

Marquette G.C., Gray J.T., Gosse J.C., Courchesne F., Stockli L., Marpherson G., Finkel R. 2004. Felsenmeer persistence under non-erosive ice in the Torngat and Kaumajet mountains, Quebec and Labrador, as determined by soil weathering and cosmogenic nuclide exposure dating. Canadian Journal of Earth Sciences 41, 19-38.

McClenaghan, M.B., Paulen, R.C., Kjarsgaard I.M., 2019. Rare Metal indicator minerals in bedrock and till at the Strange Lake peralkaline 4 complex, Quebec and Labrador, Canada. Canadian Journal of Earth Sciences: https://doi.org/10.1139/cjes-2018-0299.

McMartin, I., Henderson, P.J., 2004. Evidence from Keewatin (Central Nunavut) for Paleo-Ice Divide Migration. Géographie Physique et Quaternaire 58, 163-186.

Mitrovica, J.X., Davis J.L., Shapiro I.I., 1994. A spectral formalism for computing 3-dimensional deformations due to surface loads: 1. theory. Journal of Geophysical Research 99, 7057-7073.

Mitrovica, J.X., Milne, G.A., 2003. On post-glacial sea level: I. General theory. Geophysical Journal International 154, 253-267.

Mitrovica, J.X., Wahr, J., Matsuyama, I., Paulson, A., 2005. The rotational stability of an ice-age earth. Geophysical Journal International 161, 491-506.

Nesbitt H.W., Young G.M. 1982. Early Proterozoic climates and plate motions inferred from major element chemistry of lutites. Nature 299, 715-717.

Nishiizumi K., Winterer E., Kohl C., Klein J., Middleton R., Lal D., Arnold J. 1989. Cosmic ray production rates of ^{10}Be and ^{26}Al in quartz from glacially polished rocks. Journal of Geophysical Research 94, 17,907-17,915.

Nishiizumi, K. 2004. Preparation of ^{26}Al AMS standards: Nuclear Instruments & Methods in Physics Research, Section B, Beam Interactions with Materials and Atoms 223–224, p. 388-392.

Nishiizumi K., Imamura M., Caffee M., Southon J., Finkel R., McAninch, J. 2007. Absolute calibration of ^{10}Be AMS standards: Nuclear Instruments & Methods in Physics Research, Section B, Beam Interactions with Materials and Atoms, 258, 403-413.

Ó Cofaigh C., Lemman D.S., Evans D.J.A., Bednarski J. 1999. Glacial landform-sediment assemblages in the Canadian High Arctic and their implications for late Quaternary glaciations. Annals of Glaciology 28, 195-201.

Paulen R.C., Stokes C.R., Fortin R., Rice J.M., Dubé-Loubert H., McClenaghan, M.B. 2017. Dispersal Trains Produced by Ice Streams: An Example from Strange Lake, Labrador, Canada. In "Proceedings of Exploration 17: Sixth Decennial International Conference on Mineral Exploration" edited by V. Tschirhart and M.D. Thomas, 2017, 871-875.

Prest, V.K., Grant, D., Rampton, V. 1968. Glacial Map of Canada. Geological Survey of Canada, Department of Energy, Mines and Resources. Map 1253A.

Refsnider, K.A., Miller, G.H. 2010. Ice-sheet erosion and the stripping of Tertiary regolith from Baffin Island, eastern Canadian Arctic. Quaternary Science Reviews 67, 176-189.

Refsnider, K.A., Miller, G.H. 2013. Reorganization of ice sheet flow patterns in Arctic Canada and the Mid-Pleistocene Transition. Geophysical Research Letters 37, L13502.

Roy, M., Clark, P.U., Raisbeck, G.M., Yiou, F. 2004. Geochemical constraints on the regolith hypothesis for the middle Pleistocene transition. Earth and Planetary Science Letters 227, 281-296.

Schaefer J.M., Denton G.H., Kaplan M., Putnam A., Finkel R.C., Barrell D.J., Andersen B.G., Schwartz R., Mackintosh A., Chinn T., Schluchter C. 2009. High-frequency Holocene glacier fluctuations in New Zealand differ from the northern signature. Science 324, 622-625.

Shilts, W.W., 1980. Flow patterns in the central North American Ice Sheet. Nature 286, 213-218.

Shreve R.L., 1985a. Late Wisconsin ice-surface profile calculated from esker paths and types, Katahdin esker system, Maine. Quaternary Research 23, 27-37.

Shreve R.L. 1985b. Esker characteristics in terms of glacier physics, Katahdin esker system, Maine. Geological Society of America Bulletin 96, 639-646.

Shreve R.L. 1972. Movement of water in glaciers. Journal of Glaciology 11, 205–214.

Skidmore M. L., Sharp M.J. 1999. Drainage system behaviour of a High-Arctic polythermal glacier. Annals of Glaciology 28, 209-215.

Smith, M.J., Knight, J., 2011. Paleoglaciology of the last Irish ice sheet reconstructed from striae evidence. Quaternary Science Review 30, 147-160.

Staiger J., Gosse J., Toracinta R., Oglesby B., Fastook J. 2007. Atmospheric scaling of cosmogenic nuclide production: climate effect. Journal of Geophysical Research 112, B02205.

Stokes, C.R., Clark, C.D., 2004. Evolution of late glacial ice-marginal lakes on the northwestern Canadian Shield and their influence on the location of the Dubawnt Lake palaeo-ice stream. Palaeogeography, Palaeoclimatology. Palaeoecology 215, 155-171.

Stone J.O., 2000. Air pressure and cosmogenic isotope production. Journal of Geophysical Research 105, 23753-23759.

Storrar, R.D., Stokes, C.R., Evans, D.J.A., 2013. A map of large Canadian eskers from Landsat satellite imagery. Journal of Maps 9, 456-473.

Storrar R.D., Stokes C.R., Evans D.J.A. 2014. Morphometry and pattern of a large samples (N20,000) of Canadian eskers and implications for subglacial drainage beneath ice sheets. Quaternary Science Reviews 105, 1-25.

Stravers, J. A., Miller, G. H., & Kaufman, D. S. 1992. Late glacial ice margins and deglacial chronology for southeastern Bafin Island and Hudson Strait, eastern Canadian Arctic. Canadian Journal of Earth Sciences 29, 1000-1017.

Sugden, D. 1977. Reconstruction of the morphology, dynamics, and thermal characteristics of the Laurentide Ice Sheet at its maximum. Arct. Alp. Res, 21-47.

Syverson, K.M., Gaffield, S.J., Mickelson, C.D.M. 1994. Comparison of esker morphology and sedimentology with former ice-surface topography, Burroughs Glacier, Alaska. Geological Society of America Bulletin 106, 1130-1142.

Ullman D.J., Carlson A.E., Hostetler S.W., Clark P.U., Cuzzone J., Milne G.A., Winsor K., Caffe M. 2016. Final Laurentide ice-sheet deglaciation and Holocene climate-sea level change. Quaternary Science Reviews 152, 49-59.

Veillette, J.J., Dyke, A.S., Roy, M., 1999. Ice-flow evolution of the Labrador Sector of the Laurentide Ice Sheet: a review, with new evidence from northern Quebec. Quaternary Science Reviews 18, 993-1019.

Veillette, J.J., Roy, M., Paulen, R.C., Ménard, M., St-Jacques, G., 2017. Uncovering the hidden part of a large ice stream of the Laurentide Ice Sheet, northern Ontario, Canada. Quaternary Science Reviews 155, 136-158.

Winsborrow, M.C.M., Clark, C.D., Stokes, C.R. 2004. Ice streams of the Laurentide Ice Sheet. Géographie Physique et Quaternaire. 58 , 269-280.

Wilson, J.T., Falconer, G., Mathews, W.H., Prest, V.K. 1958. Glacial Map of Canada, Geological Association of Canada, scale 1: 5 000 000.

Young N.E., Schaefer J.M., Briner J.P., Goehring B.M. 2013. A ^{10}Be production-rate calibration for the Arctic. Journal of Quaternary Science 28, 515-526.

3.9 TABLES

Tableau 3.1 Samples informations and surface exposure ages.

Site-sample no.	Rock type	Latitude (DD)	Longitude (DD)	Altitude (m)	Altitude corrected (m)	LSNd ± 1 σ (yr)	1 σ (%)
14HDL-A-06	quartz-rich granite	57.92	-66.75	116.8	78.8	7400± 400	5.4
14HDL-A-07	quartz-rich granite	57.92	-66.75	117.9	79.9	8800 ± 200	2.3
14HDL-A-08	quartz-rich granite	57.92	-66.75	112.0	74.0	9100 ± 300	3.3
14HDL-A-09	Tonalite	57.92	-66.75	121.8	83.8	8800 ± 200	2.3
14HDL-A-10	quartz-rich granite	57.92	-66.75	121.8	83.8	8200 ± 300	3.7
14-HDL-B-01	quartz-rich granite	57.79	-66.59	126.9	88.9	8700 ± 300	3.4
14-HDL-B-04	quartz-rich granite	57.79	-66.59	124.3	86.3	8100 ± 300	3.7
14-HDL-B-06	quartz-rich gneiss	57.79	-66.59	120.9	82.9	8300 ± 300	3.6
14-HDL-B-08	quartz-rich granite	57.79	-66.58	120.4	82.4	13900 ± 400	2.9

Tableau 3.2 Sample location/informations and cosmogenic exposure ages.

Site-sample no.	Type of sample	Latitude (DD)	Longitude (DD)	Altitude (m)	Altitude corrected (m)	$[^{10}Be] \pm 1\ \sigma$ (10^4 atoms g^{-1})	$[^{26}Al] \pm 1\ \sigma$ (10^4 atoms g^{-1})	^{10}Be age (ka)	^{26}Al age (ka)	$[^{26}Al]/[^{10}Be]$
Trans-01	bedrock/felsenmeer	57.90	-64	804.5	672.5	14.25 ± 5.56	90.35 ± 4.08	18,100 ± 700	14,800 ± 700	6.34 ± 0.38
Trans-02	bedrock/crag&tail	57.14	-65.41	504.1	462.1	6.05 ± 2.96	39.83 ± 1.88	9,400 ± 500	7,900 ± 400	6.59 ± 0.45
Trans-03	bedrock/crag&tail	57.25	-65.02	476.8	438.8	5.80 ± 2.49	33.31 ± 1.93	9,200 ± 400	6,800 ± 400	5.74 ± 0.41
Trans-04	bedrock/felsenmeer	57.49	-64.74	688.7	555.7	12.78 ± 5.44	79.35 ± 11.89	18,200 ± 800	14,600 ± 2000	6.21 ± 0.97

Tableau 3.3 Analytical and procedural data

Sample no.	Thickness (cm)	CAMS #	Evapo-corr. carrier added* (mg)	$[^{10}Be] \pm 1\ \sigma$ (10^4 atoms g^{-1})		
14-HDL-A-06	1.7	BE39848	0.183	3.30	±	0.19
14-HDL-A-07	1.42	BE38791	0.183	3.96	±	0.11
14-HDL-A-08	1.24	BE38792	0.183	4.05	±	0.11
14-HDL-A-09	3.28	BE38793	0.183	3.90	±	0.10
14-HDL-A-10	1.51	BE38794	0.183	3.68	±	0.15
14-HDL-B-01	2.3	BE38795	0.183	3,92	±	0.11
14-HDL-B-04	1.73	BE38796	0.183	3,66	±	0.15
14-HDL-B-06	2.36	BE38797	0.183	3,71	±	0.12
14-HDL-B-08	1.33	BE38798	0.183	6,22	±	0.19

*Lamont ^{9}Be Carrier 5 concentration was corrected for evaporation, based on continuous monitoring by precise weighing of the carrier. Maximum correction was 1.2%. Rock density is the same for all samples and reach 2.7 $g.cm^{-3}$. Shielding correction was negligible and have been fixed at 1.00. AMS standard used is the 07KNSTD.

3.10 FIGURES

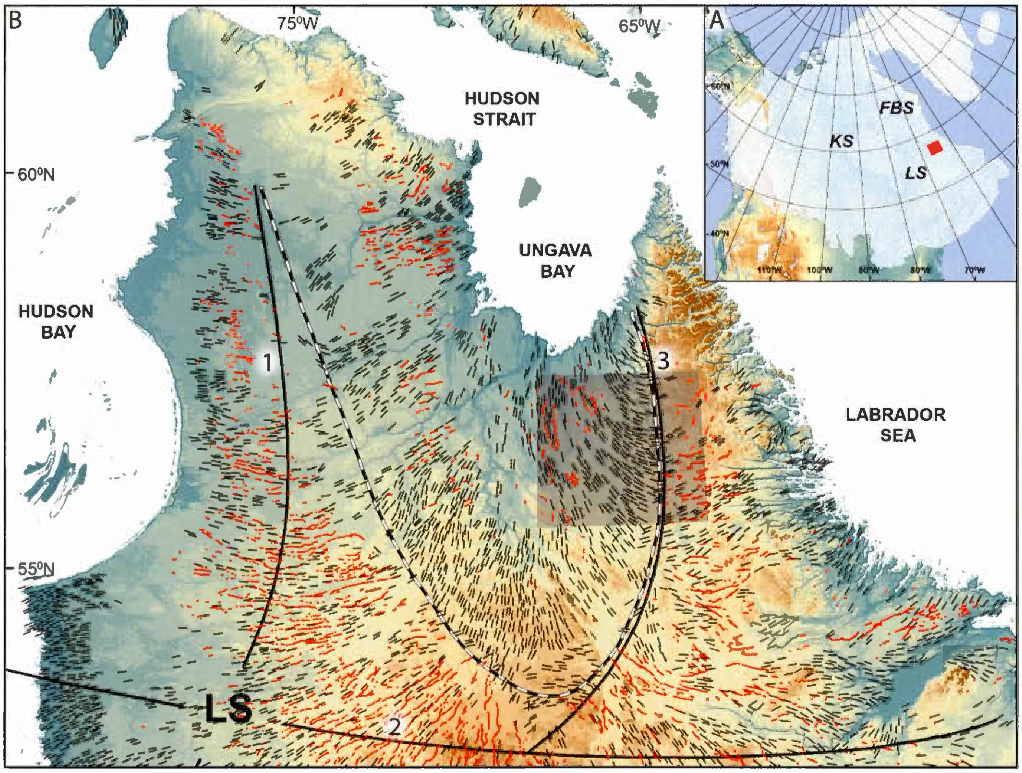

Figure 3.1 (A) Schematic map showing LIS configuration during the last glacial maximum (LGM) (Dyke and Prest, 1987): i) FBS: Fox-Baffin sector; ii) KS: Keewatin sector; iii) LS: Labrador sector. (B) The main glacial and deglacial features of the LS showing the radially (divergent) ice-flow spreading southward and the massive Ungava converging landform assemblage (Prest, 1968). The LS consists in three ice-divides grouped under the name Labrador Ancestor ice-divide: 1) Payne center, located over Ungava peninsula; 2) Caniapiscau center, located in the Caniapiscau region, and 3) Labrador center, located in the axis of the George River valley. The LGM presumed ice-divide position of LS ice dome is marked by "LS" (Dyke and Prest, 1987) and the Horseshoe unconformity position (white and black dashed line) is from Clark et al (2000).

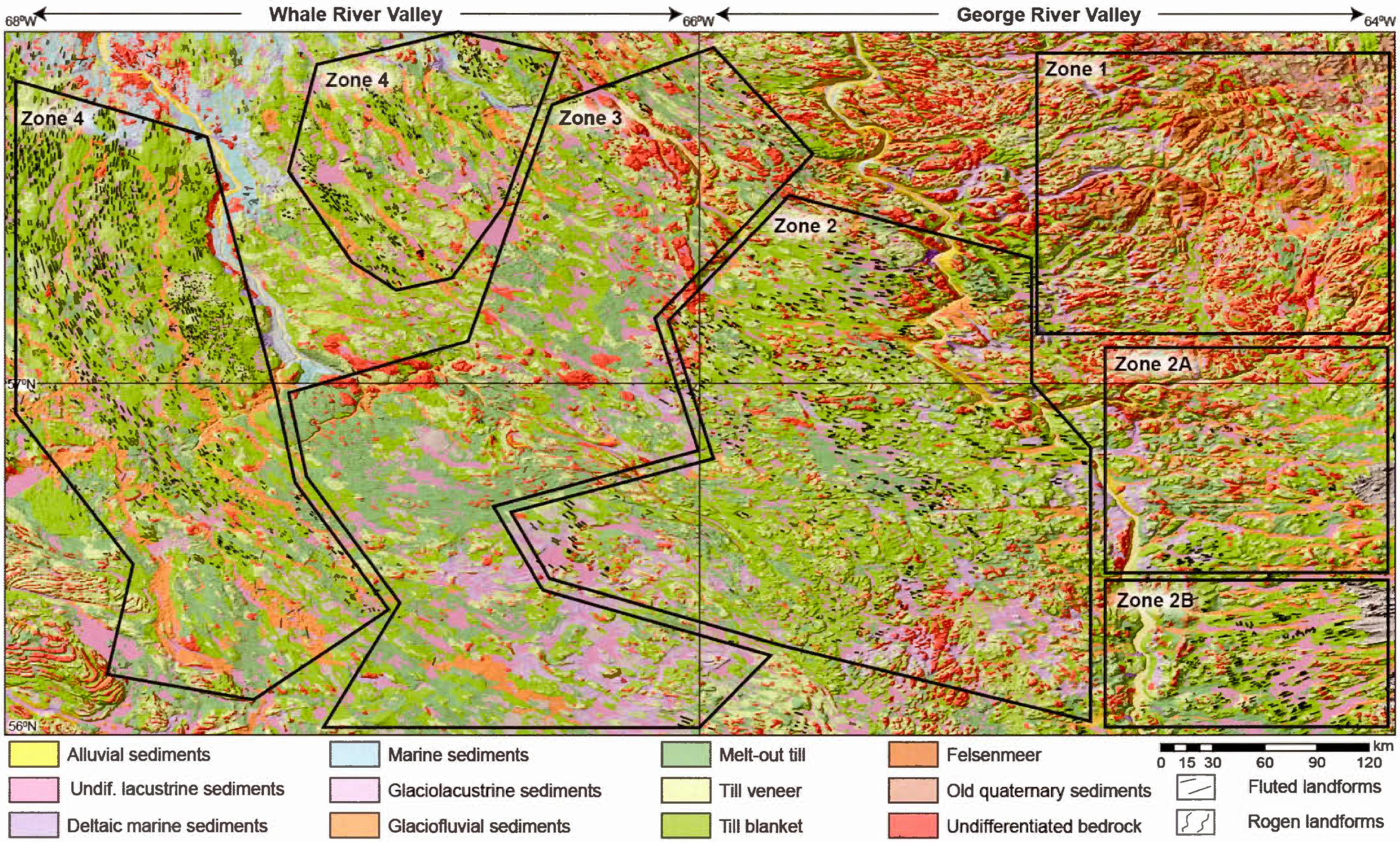

Figure 3.2 Detailed surficial mapping of the study area (see Figure 3.1 for location). The black lines delineate zones showing strong sedimentological and geomorphological contrasts through the WRV and GRV.

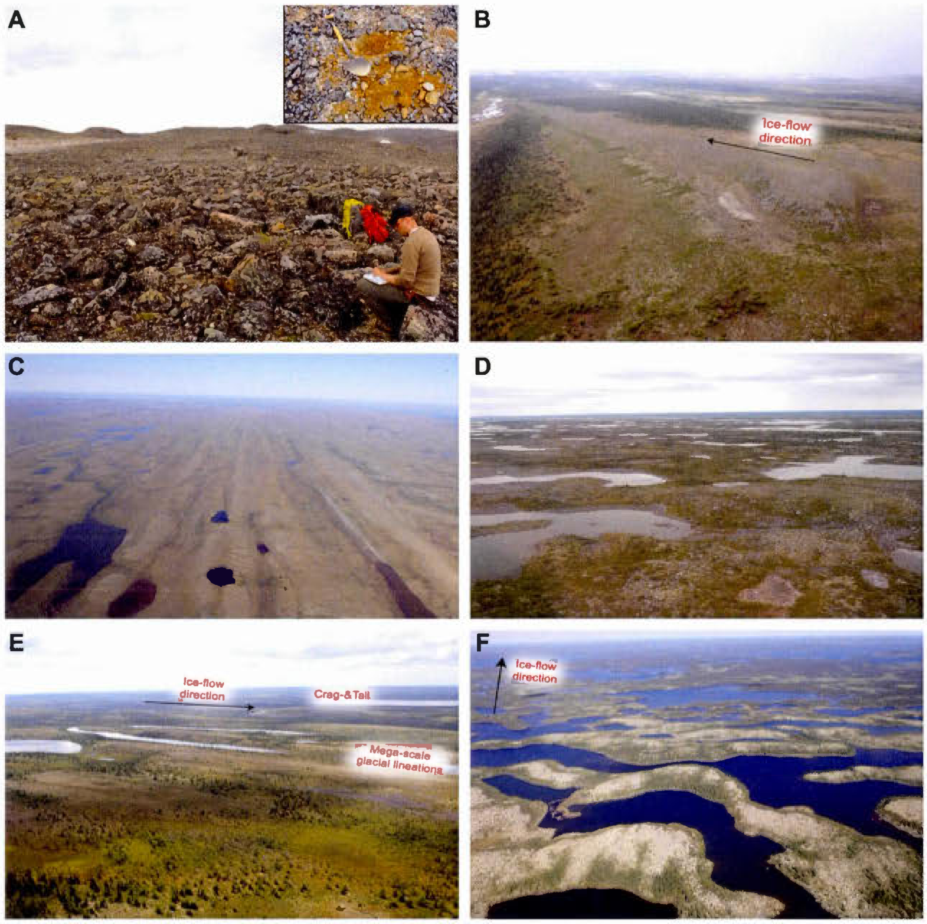

Figure 3.3 A) The general area northeast of the George River is characterized by extensive felsenmeer with interstitial oxidized matrix (zoom) related to preservation of weathered landscape under cold-based ice conditions. B) Crag-and-tails on the western side of GRV formed by a westward ice flow. C) Example of MSGL from the Strange Lake ice stream. D) Large areas of irregular mounded surface punctuated by of hummocky moraines, large glacial erratics and kettle pits that suggest the presence of a stagnant residual ice mass at the interfluve of the GRV and the WRV at the end of the deglaciation. E) Example of MSGL and crag-and-tails forming the ice stream corridors of the western end of the WRV formed by NNW to NW ice flow. E) Example of fluted Rogen moraines superimposed by glacial lineations of ice stream corridors in the WRV.

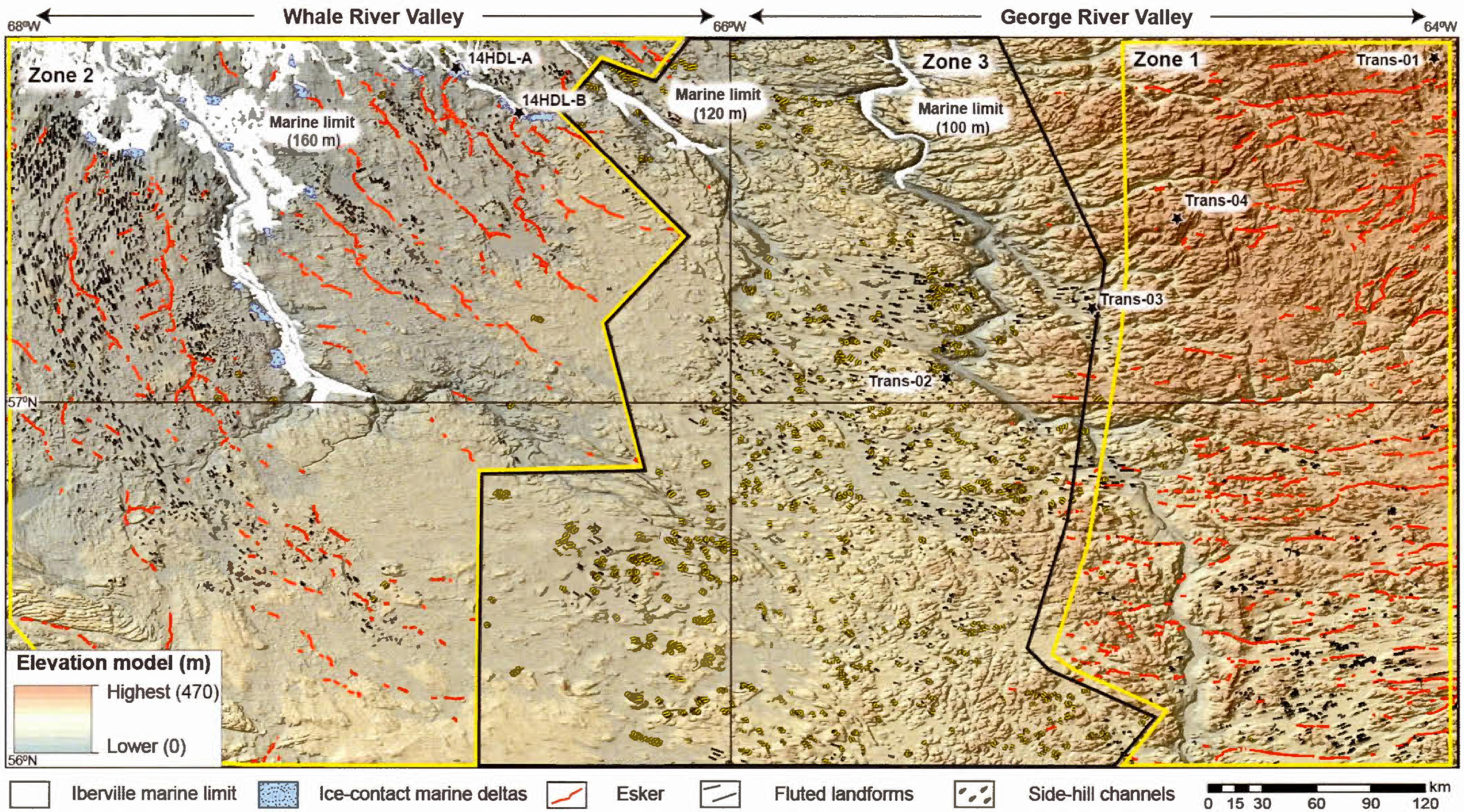

Figure 3.4 Deglacial landform assemblages mapped in the GRV and WRV areas. The yellow boxes delimit the GRV and WRV eskers swarms and the black one, the sector marked by the absence of esker and the presence of side-hill channels. Black stars show the location of the cosmogenic samples analysed (see Tables 1 and 2).

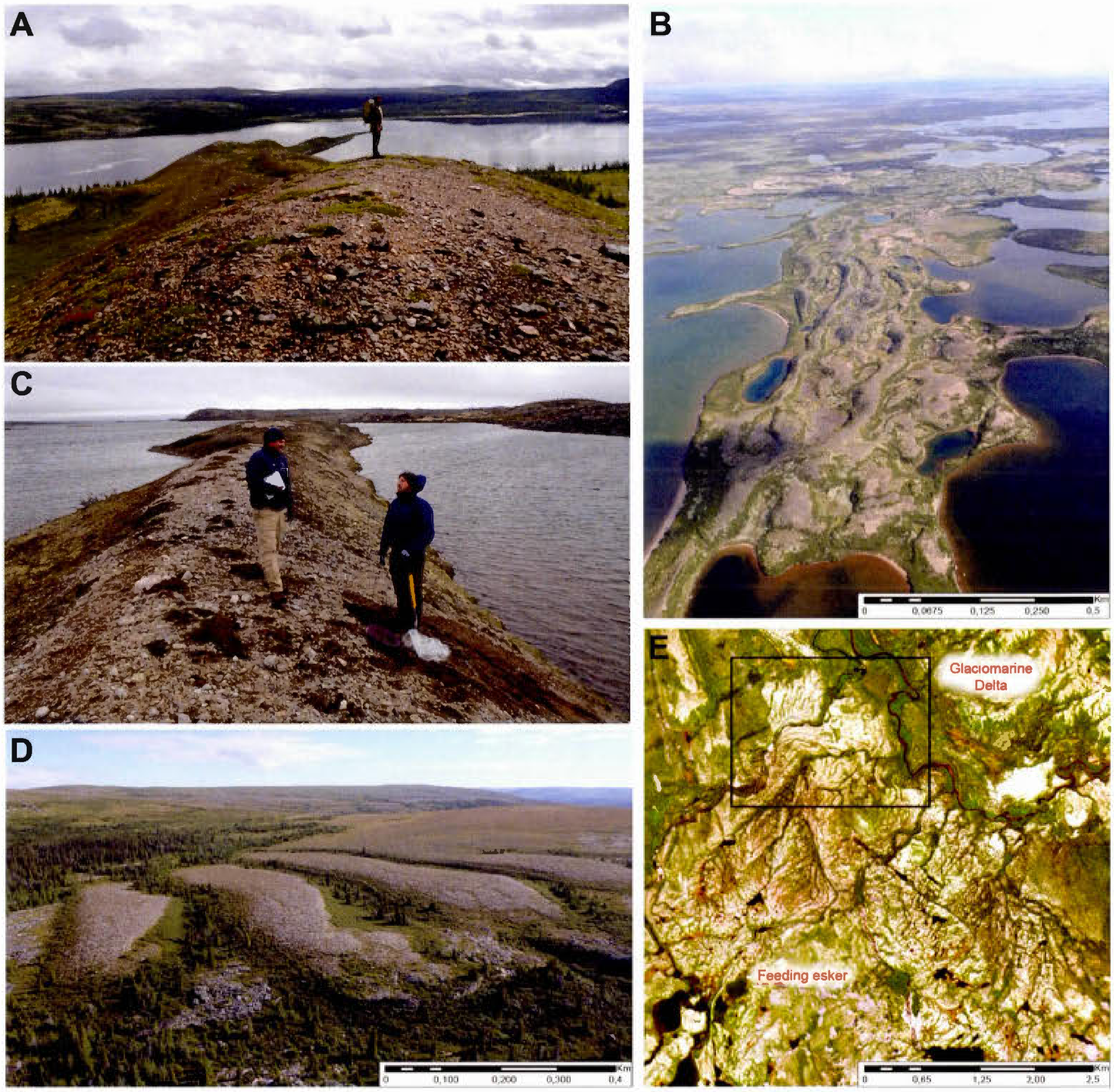

Figure 3.5 A) Example of the GRV esker assemblage orientated roughly west-east. These eskers reflect an ice withdrawal towards the west. View towards the east. B) Eskers in the Strange Lake ice stream terrain are formed of anastomosing crests highlighting the strong fragmentation of the ice margin. View towards the east. C) Example of the WRV esker swarm orientated roughly north-south. These eskers reflect an ice retreat pattern from north to south. View towards north. D) Example of the side-hill channels west of the GRV. These channels also mark the disappearance

of the GRV eskers. View towards north. E) Satellite (Rapideye) image showing a glaciomarine deltas formed into the Iberville Sea in the WRV area.

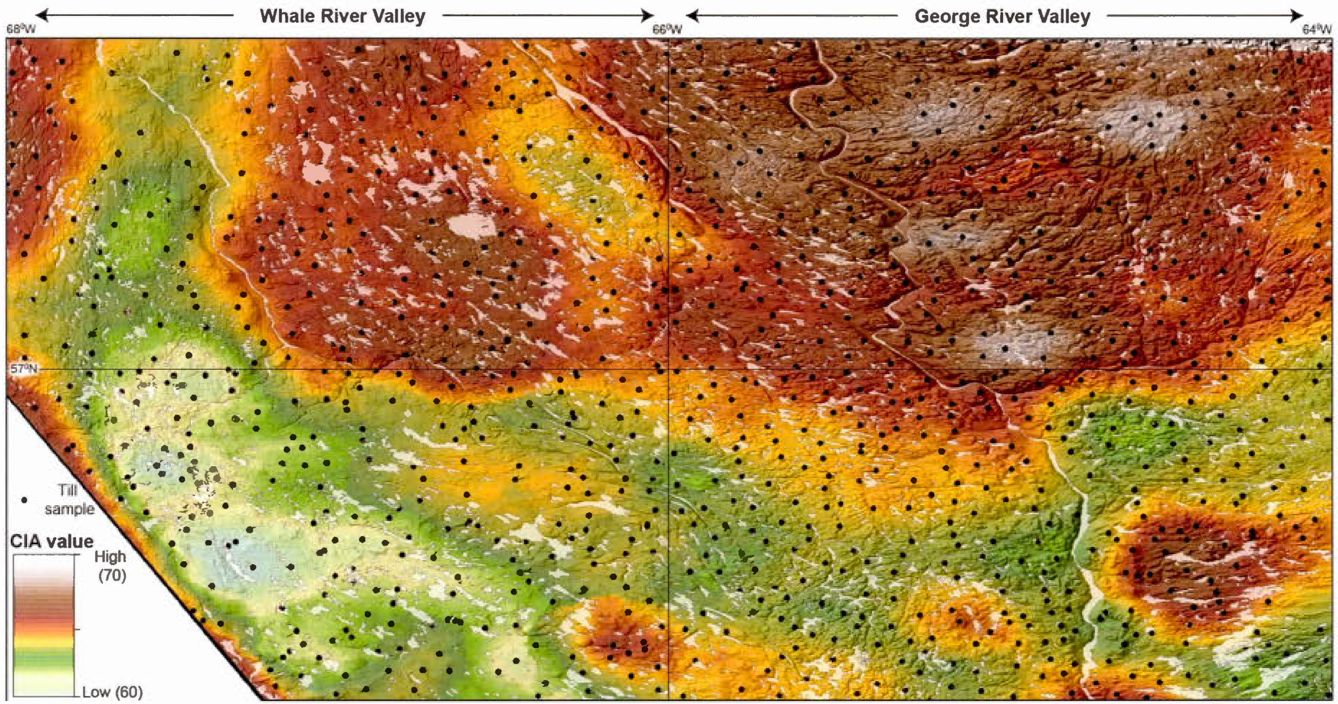

Figure 3.6 Interpolation of CIA results determined from till geochemistry. The black dots show the till samples. The CIA results range from 60 to 70 for sectors characterized by respectively warm- and cold-based ice conditions. Values for the Chemical Index of Alteration are calculated using the following equation where oxides are expressed in molar proportions and CaO* is the amount of CaO from non-carbonates minerals: $CIA = (Al_2O_3 / (Al_2O_3 + CaO^* + NaO + K_2O)) * 100$.

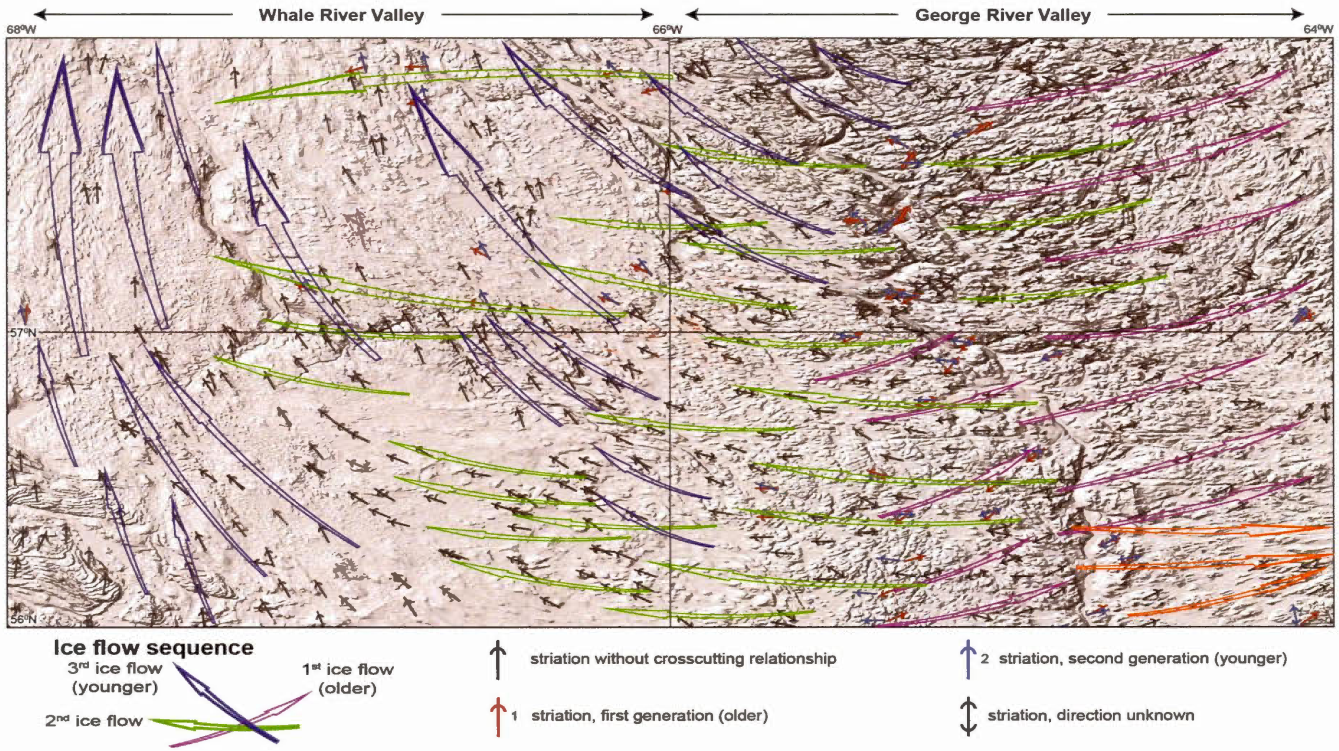

Figure 3.7 Ice-flow sequence and relative chronology based on the orientation and spatial distribution of striations and other erosional marks, glacial landforms and associated cross-cutting relationships. Orange arrows are related to the Strange Lake ice stream.

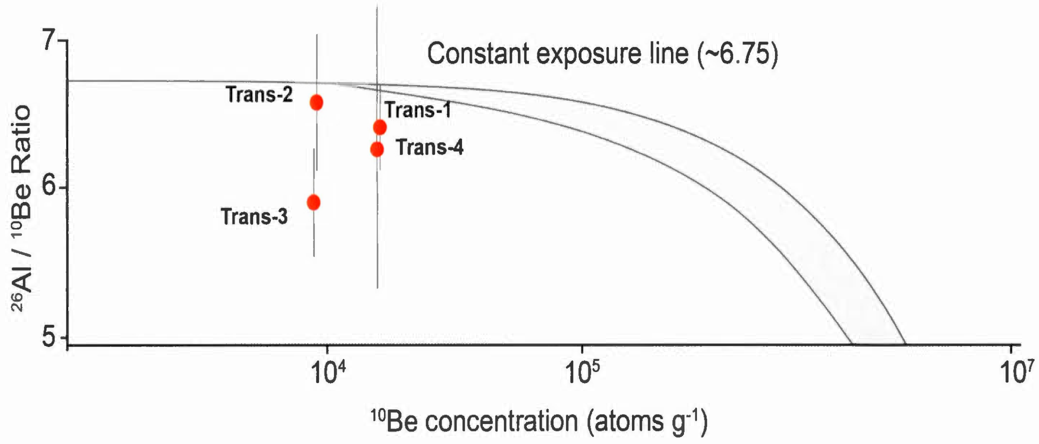

Figure 3.8 $^{26}Al/^{10}Be$ ratios plotted against ^{10}Be concentrations for 2 bedrock knobs of freshly-eroded glacial lineations (Trans-2 and 3) and for 2 bedrock outcrops present in felsenmeer terrains (Trans-1 and 4).

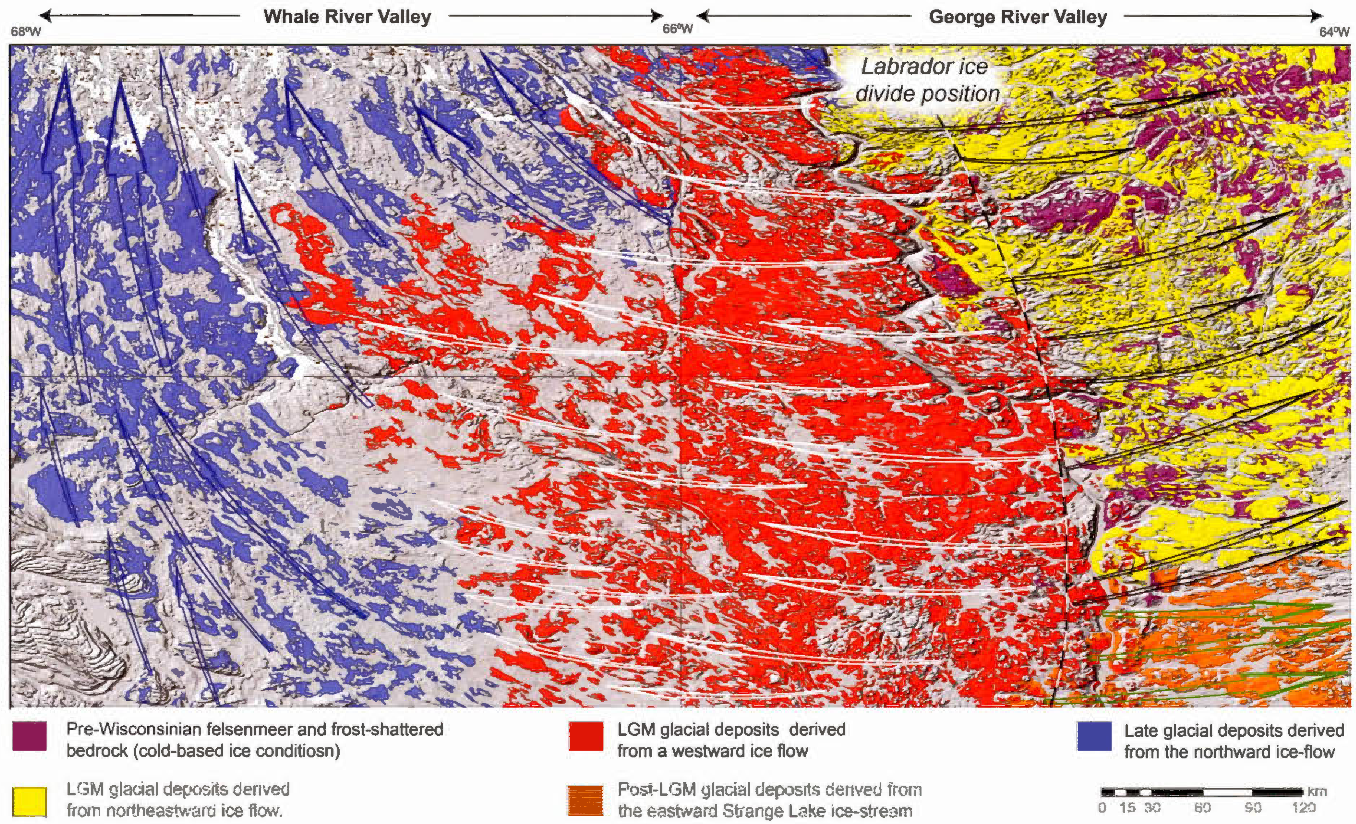

Figure 3.9 Glacial landform-sedimentary assemblages and their chronological assignment based on the ice-flow sequence relative chronology (colored arrows), detailed surficial mapping, and surface exposure dating (SED) results. The black and white dashed line mark the eastern Labrador Ancestor ice-divide position.

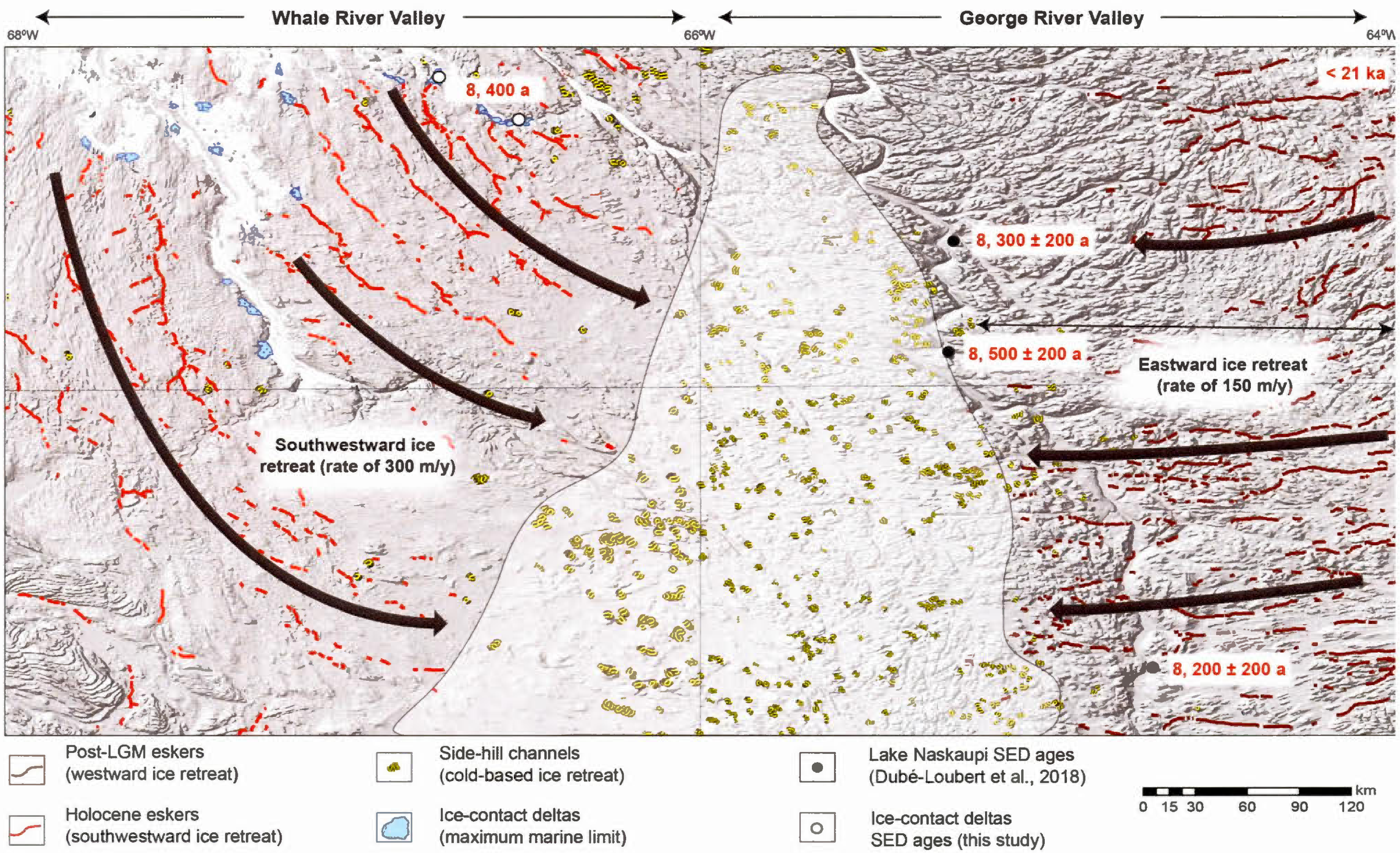

Figure 3.10 Deglacial landform assemblages and their chronological assignment based on the dimension and sedimentological characteristics of eskers, SED results, and ice-retreat directions (black arrows) and rate estimates.

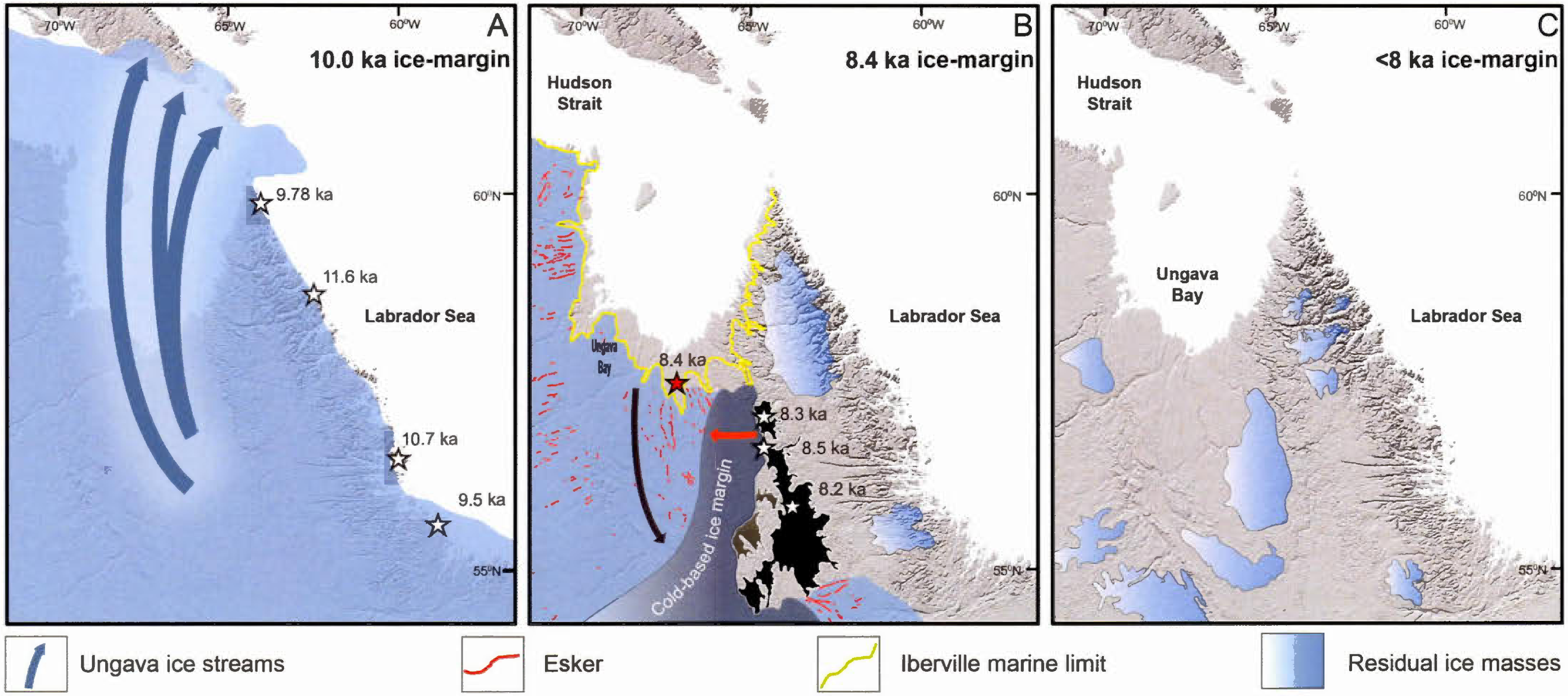

Figure 3.11 Paleogeographic reconstruction of the northeastern part of the Labrador Sector showing the ice-margin retreat during the last deglaciation. A) Inferred ice-margin position at 10.0 ka modified from Dyke, 2003. White stars represent chronological constraints along the Labrador coast from Clark and Fitzhugh (1992). Large ice streams that developed in the Ungava lowlands have been correlated with the Gold Cove Advance that culminated at around 10 ka (Stravers et al., 1992; Kaufman et al., 1993). B) Ice-margin position at 8.4 ka. Red star represent chronological constraints from this study (esker-fed deltas) and marked the ice-margin position in contact with the Iberville Sea at 8.4 ka. Eskers of

this sector suggest an ice-margin retreat towards southwest as marked by the black arrow. White stars represent ^{10}Be ages from Dubé-Loubert et al., (2018) and indicate that the ice margin occupied a position west of the George River at around 8,300 ± 300 a. From that position, the eastern ice-margin retreated under cold-based ice conditions roughly toward west as marked by the red arrow. The black and green polygones represent respectively the Lake Naskaupi and the Lake Mclean. C) The final stages of deglaciation have isolated several residual ice masses between 7 and 8 ka. whose presumed position is illustrated on this figure. These zones are generally marked by extensive areas of hummocky moraine whose irregular mounded surface is punctuated by several kettle pits and metre-sized glacial erratics.

CONCLUSION

L'objectif principal de cette thèse est de documenter l'évolution spatio-temporelle du Lac Naskaupi et de cadrer son développement dans la dynamique glaciaire des phases tardives de la dernière glaciation et déglaciation du Secteur Labrador de l'Inlandsis laurentidien.

Le premier article (chapitre I) porte sur l'évolution et de la vidange du Lac Naskaupi. Les principales contributions de cet article sont de départager la succession complexe des différentes phases du Lac Naskaupi, de définir la configuration du lac durant sa phase principale et de caractériser précisément le taux de gauchissement associé à ce plan d'eau. De plus, le mode de drainage a été établi à partir d'une construction sédimentaire importante (le *Pinkflood*) qui enregistre la vidange du bassin sud durant la phase N2' et la coalescence des bassins au cours des phases subséquentes. La reconstruction des niveaux lacustres fournit des évidences d'abaissement marqués qui témoignent fort probablement d'autres épisodes de drainage. Finalement, l'estimation du volume d'eau contenu durant la phase principale (~600 km^3) apporte une contrainte minimale sur la contribution en eau de fonte en provenance de ce plan d'eau considérant les évidences d'autres épisodes de drainage au cours de son évolution.

Le deuxième chapitre amène de nouvelles données chronologiques sur l'existence et le *timing* de la vidange du Lac Naskaupi. La forte cohérence des résultats obtenus sur les phases majeures, et sur une construction de drainage, suggèrent que le lac s'est développé, a atteint sa pleine expansion et a initié son drainage dans un court intervalle de temps. L'âge moyen de 8,300 ± 300 a obtenu à partir de 21 âges ^{10}Be peut donc être associé à l'initiation de son drainage. Ces âges ^{10}Be suggérent que la vidange et la décharge massive d'eau de fonte en provenance du Lac Naskaupi (et potentiellement des autres de lacs glaciaires de l'Ungava) aurait pu contribuer à l'épisode de refroidissement marqué de 8,2 ka. Malgré leur dimension modeste en comparaison avec le Lac Agassiz-Ojibway dont le drainage est généralement identifié comme principale cause de l'événement de 8,2 ka, la proximité des lacs de l'Ungava avec les zones critiques de formation des masses d'eau froides de la Mer du Labrador font de leurs contributions en eau de fonte un élément non-négligeable. Ces âges, combinés à l'estimation des volumes impliqués, s'avèrent être de bons analogues dans la compréhension des processus actuels tels que la fonte des glaces du Groënland et autres glaciers de l'Arctique. Les âges obtenus fournissent également d'importantes contraintes chronologiques sur le schéma de déglaciation de la partie NE du Secteur Labrador et sur la position de la marge endiguant les différentes phases du lac.

Finalement, le chapitre III met en relation différentes données cartographiques, géochronologiques et analyses compositionnelles afin, entre autres choses, de délimiter les ensembles morpho-sédimentaires formant la partie NE du Secteur Labrador en fonction de leur âge de formation et de leur composition. Les nouvelles données géochronologiques, obtenus sur des deltas glacio-marins (âges ^{10}Be, ~8,400 a) formés dans la Mer d'Iberville indiquent que les formes au nord de la limite du *Horseshoe Unconformity* sont d'âge tardi-glaciaire et que l'existence d'une masse de glace centrée sur la baie d'Ungava, évoquée dans certaines reconstructions, s'avère impossible. La caractérisation de la mosaïque des conditions sous-glaciaires suggérent l'existence d'une couverture de glace polythermale au cours du dernier cycle glaciaire ce qui a des implications pour la préservation et/ou l'érosion des terrains. Les formes convergentes au nord du *Horseshoe Unconformity* seraient le résultats d'une succession d'événements glaciaires distincts, d'âge légèrement différent, associé à l'activité de courant de glace dans la partie ouest de la zone d'étude (entre 8-10 ka) et à l'évolution de la ligne de partage glaciaire du Labrador à l'est, au cours du dernier maximum glaciaire. Ces résultats indiquent que, ce qui est communément décrit comme la limite Est de la zone du *Horseshoe Unconformity* traduit plutôt l'activité de la ligne de partage glaciaire du Labrador au dernier maximum glaciaire dont les terrains ont été recoupés par l'activité subséquente de courants de glace convergeant vers la baie d'Ungava. La forme arquée du *Horseshoe Unconformity*, et ses similitudes en tant que position d'une ligne de partage glaciaire, ne sont que des artefacts associés à la génération/préservation des ensembles morpho-sédimentaires à travers le temps, ayant pour principal point commun d'être convergents vers la baie. La position de cette limite serait plutôt contrôlée par des aspects de configuration topographique locale tel que la limite sud du bassin versant de la baie d'Ungava. De plus amples travaux seront nécessaires afin de pleinement expliquer l'entièreté de l'organisation spatio-temporelle des terrains du Secteur Labrador, mais les résultats présentés ici soulignent que l'architecture des dépôts de surface traduit un assemblage fragmentaire d'événements asynchrones plutôt qu'un cliché instantané de l'histoire glaciaire tel que suggéré par la carte glaciaire du Canada (Prest et al., 1968). Les résultats de ce chapitre permettent en outre de renforcer le modèle de capture glaciaire afin d'expliquer l'étroitesse de la zone du *Horseshoe Unconformity*.

D'un point de vue pratique, les résultats de cette thèse renforcent l'argumentaire soulignant la nécessité de travaux de cartographie de terrain à la compréhension de l'historique glaciaire du nord québécois. Les données obtenues lors des campagnes de terrain représentent les assises sur lesquels repose le corps de cette thèse. La combinaison de données de terrain à la photo-interprétation permet l'intégration d'un plus large spectre d'information renforçant la solidité des reconstructions paléogéographiques. Finalement, l'ajout de nouvelles données géochronologiques et l'application de la datation cosmogénique à de nouveaux types de morphologie de surface, en particulier sur les rivages glaciolacustres et deltas glaciomarins, ouvrent une toute nouvelle perspective pour la compréhension du Secteur Labrador, mais aussi pour le reste du territoire couvert par l'Inlandsis laurentidien. La caractérisation des interactions entre les systèmes océaniques et la cryosphère, ainsi que des mécanismes modulant le ralentissement de la circulation océanique, passe inévitablement par l'ajout de contraintes temporelles inhérentes à l'évolution de la calotte laurentidienne. L'obtention de données chronologiques inédites combinées à de nouvelles estimations des volumes sur de tels événements de drainage permettront à terme de mieux estimer la sensibilité du système océanique face à ces épisodes de forçage climatique. Dans un contexte où, les grandes calottes continentales actuelles sont en perpétuelle régression, et que l'apport en eau de fonte ainsi généré semble vouloir s'accélérer, les modèles prédictifs du climat se doivent de se calibrer sur des données paléoclimatiques fiables afin de mieux conjecturer les impacts des changements globaux à venir.